Cover Page

Universiteit Leiden

Leiden University Repository

The handle http://hdl.handle.net/1887/29080 holds various files of this Leiden University dissertation

Author: Fan, Yuanwei
Title: The role of AGC3 kinases and calmodulins in plant growth responses to abiotic signals
Issue Date: 2014-10-15

The role of AGC3 kinases and calmodulins in plant growth responses to abiotic signals

Yuanwei Fan

The role of AGC3 kinases and calmodulins in plant growth responses to abiotic signals

Proefschrift

Ter verkrijging van
de graad van Doctor aan de Universiteit Leiden,
op gezag van Rector Magnificus prof. mr. C.J.J.M. Stolker,
volgens besluit van het College voor Promoties
te verdedigen op woensdag 15 oktober 2014
klokke 16:15 uur

door

Yuanwei Fan

Geboren te Weifang (China) in 1984

Promotiecommissie

Promotor: Prof. dr. P.J.J. Hooykaas

Co-promotor: Dr. R. Offringa

Overige leden: Prof. dr. J Kudla (Univ. Münster, Germany)
Prof. dr. J. Memelink
Prof. dr. B. van Duijn (Fytagoras, Leiden)
Prof. dr. C.J. ten Cate

Contents

Page

Chapter 1 7

Ca^{2+} signaling in the regulation of auxin transport by developmental and environmental signals

Chapter 2 39

TOUCHing PINOID: A Calmodulin – Kinase Interaction Modulates Auxin Transport Polarity during Root Gravitropism

Chapter 3 89

PINOID plasma membrane association and calmodulin binding converge on an amphipathic alpha helix/IQ-like motif

Chapter 4 125

AGC3 kinase-calmodulin signaling in phyllotaxis

Summary 151

Samenvatting 159

Curriculum vitae 166

Chapter 1

Ca^{2+} signaling in the regulation of auxin transport by developmental and environmental signals

Yuanwei Fan[1], Remko Offringa[1]

[1] Molecular and Developmental Genetics, Institute Biology Leiden, Leiden University, Sylviusweg 72, 2333 BE Leiden, The Netherlands

The signaling molecule auxin is an important regulator of plant development, instructing tissue differentiation and organ development and growth, while translating environmental stimuli into developmental responses. Here we review the role of auxin in a plant's response to developmental and environmental signals, with a focus on the interaction of auxin with the second messenger Ca^{2+}, Ca^{2+} receptors, such as calmodulins, play an important role in this interaction, as these receptors are able to translate signal-induced changes in the cytosolic Ca^{2+} concentrations into a developmental or growth response, e.g. by modulating the direction of polar auxin transport.

1. Auxin is a crucial regulator of plant development

As sessile organisms, plants respond to changes in their environment by adjusting their growth and development through a highly dynamic combination of signal perception and transduction systems. The plant hormone auxin is a central regulator of these adaptive responses to environmental cues. Already around 1880, Charles Darwin predicted the existence of some 'mobile factor' that mediates the bending of canary grass and oat coleoptiles toward a unidirectional light source (Darwin, 1880). This 'factor' was first isolated from coleoptile tips in 1926, and was later identified as the plant hormone indole-3-acetic acid (IAA), which was named auxin after the greek word 'auxein' for 'to grow' (Went and Thimann, 1937). Auxin acts as a crucial regulator of plant development and mediates different cellular responses by its differential distribution between cells, resulting from its biosynthesis and metabolism on the one hand (Zhao, 2010; Sauer et al., 2013), and its polar cell-to-cell auxin transport on the other. Polar auxin transport (PAT) results in local auxin accumulation or -depletion in tissues and organs, which instructs plant growth and development by regulating basic cellular processes such as cell division, -differentiation and -elongation (Tanaka et al., 2006).

2. Polar auxin transport

PAT involves the activity of several families of auxin transporters, of which the "long" members of the PIN auxin efflux carrier family in *Arabidopsis* (PIN1, 2, 3, 4, 7 and possibly 6) determine the direction of transport through their asymmetric localization at the plasma membrane (PM) (Petrasek et al., 2006; Tanaka et al., 2006; Wisniewska et al., 2006; Mravec et al., 2009; Sawchuk et al., 2013). This PIN-driven PAT is essential for a wide array of plant developmental processes, including apical-basal axis formation during embryogenesis (Friml et al., 2003), postembryonic organogenesis (Okada et al., 1991; Benkova et al., 2003; Reinhardt et al., 2003), root meristem organization (Sabatini et al., 1999; Friml et al., 2002b; Blilou et al., 2005), tropisms (Luschnig et al., 1998; Friml et al., 2002a; Ding et al., 2011), vascular differentiation and tissue regeneration (Sauer et al., 2006; Scarpella et al., 2006; Xu et al., 2006).

Polar PIN localization is dynamic; according to the current model, following their biosynthetic secretion to the PM PIN proteins constitutively undergo cycles of clathrin-dependent endocytosis and subsequent recycling to their correct polar domain (Geldner et al., 2001; Dhonukshe et al., 2007; Dhonukshe et al., 2008; Kleine-Vehn et al., 2011). This trafficking is mediated by ADP ribosylation factors (ARFs) GTPases and their corresponding guanine nucleotide exchange factors (GEFs), of which the brefeldin A (BFA) toxin sensitive ARF GEF GNOM mediates exocytosis to the basal (rootward) or inner-lateral polar domains (Geldner et al., 2001; Geldner et al., 2003; Kleine-Vehn et al., 2009; Ding et al., 2011). The subcellular sorting of PIN proteins is directed by post-translational modification through phosphorylation or ubiquitination (Habets and Offringa, 2014). The PINOID (PID) serine/threonine protein kinase has been identified as one of the key determinants in this process (Benjamins et al., 2001; Friml et al., 2004). *Arabidopsis pinoid* mutants share the phenotypic defects in the inflorescences of the *pin-formed* mutant, which develop pin-like structures that lack lateral organs due to defective polar auxin transport (Bennett et al., 1995; Christensen et al., 2000). Loss of *PINOID* (*PID*) function causes an apical-to-basal shift in PIN polarity, correlating with defects in embryo and shoot organogenesis. In contrast, PID gain-of-function results in an opposite basal-to-apical PIN polarity shift, which leads to auxin depletion from the root meristem, ultimately causing collapse of the meristem (Friml et al., 2004). Together with the close homologs WAG1, WAG2 and AGC3-4, PID forms the AGC3 clade of the plant-specific AGC-VIII protein kinases in *Arabidopsis*. For PID, WAG1 and WAG2 it has been shown that they phosphorylate serines in three conserved TPRXS motifs in the central hydrophilic loop (HL) of “long” PINs, thereby recruiting these PINs into the apical recycling pathway, directing cotyledon development, and regulating root meristem size and gravitropic responses (Dhonukshe et al., 2010; Huang et al., 2010; Ding et al., 2011). The three AGC3 kinases act antagonistically with trimeric PP2A-/PP6-type phosphatases on the phosphorylation state of the PIN HL (Michniewicz et al., 2007; Dai et al., 2012; Ballesteros et al., 2013). Phosphorylated PINs are sorted to the GNOM-independent recycling pathway, which is apical for epidermal cells in meristems and for pro-vascular cells, outer-lateral for endodermis cells, and lobe-polarity for leaf pavement cells (Friml et al., 2004; Kleine-Vehn et al., 2009; Ding et al., 2011).

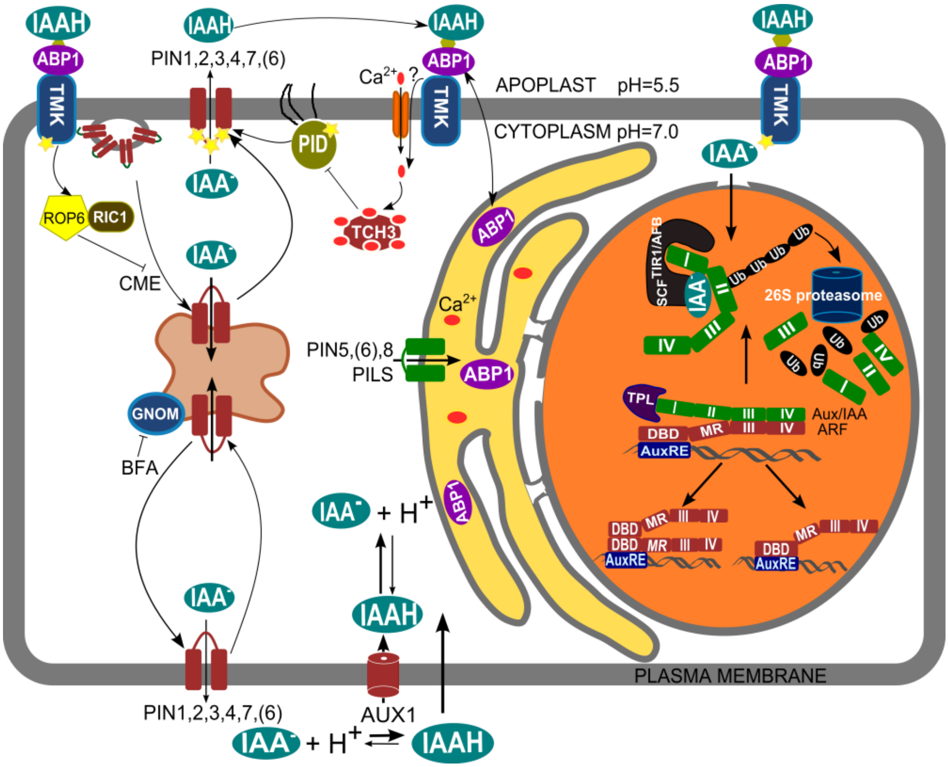
IAAH
ABP1
TMK
IAAH
PIN1,2,3,4,7,(6)
IAAH
ABP1
Ca2+ ?
TMK
APOPLAST pH=5.5
IAAH
ABP1
TMK
CYTOPLASM pH=7.0
PID
IAA-
TCH3
ROP6
RIC1
CME
IAA-
IAA-
ABP1
SCF TIR1/AFB
I
II
IAA-
Ub
Ub
Ub
Ub
26S proteasome
Ca2+
PIN5,(6),8
PILS
ABP1
IV
III
III
Ub
Ub
Ub
Ub
IV
II
I
GNOM
BFA
TPL
I
II
III
IV
Aux/IAA
DBD
MR
III
IV
ARF
AuxRE
IAA- + H+
ABP1
DBD
MR
III
IV
DBD
MR
III
IV
AuxRE
MR
III
IV
DBD
AuxRE
IAA-
IAAH
PIN1,2,3,4,7,(6)
AUX1
IAA- + H+ ⇄ IAAH
PLASMA MEMBRANE

Figure1 The auxin transport and signaling network.

Auxin, or indole-3-acetic acid, is mostly in its protonated form (IAAH) in the relatively acidic apoplast, and can pass the plasma membrane (PM) by diffusion, or can enter the cell via the AUX1/LAX influx carriers. In the more basic cytosol, auxin becomes trapped as deprotonated anion (IAA-) that requires “long” PIN auxin efflux carriers (1, 2, 3, 4, 7 and possibly 6) for its transport across the PM or short PINs (5, 6, 8) for transport across the endoplasmatic reticulum (ER, yellow) membrane. Long PINs determine the direction of polar cell-to-cell auxin transport through their asymmetric localization at the PM, which is determined by phosphorylation of their central hydrophilic loop by the PM-associated PINOID (PID) kinase. The Ca^{2+}-dependent interaction of PID with the calmodulin-like protein TOUCH3 (TCH3) negatively regulates PID activity.

Plant cells sense auxin either by the apoplastic auxin-binding protein 1 (ABP1), or by the nuclear

TRANSPORT INHIBITOR RESISTANT 1 (TIR1)/AUXIN SIGNALING F-BOX (AFB) and Aux/IAA co-receptors. Binding of apoplastic auxin to ABP1 inhibits its activity in promoting clathrin-mediated endocytosis (CME), leading to PIN stabilization at the plasma membrane, and resulting in its recruitment by the Transmembrane Kinase 1 (TMK1), which triggers the activation of the ROP2/RIC4 and ROP6/RIC1 pathways that antagonistically regulate polar cell expansion. The ABP1-TMK1 complex is might also be responsible for the auxin-induced elevation of Ca^{2+} levels by activation of Ca^{2+} channels in the PM. In the nucleus, auxin stabilizes the interaction between the TIR1/AFB and Aux/IAA co-repectors, leading to SKP1-CULLIN-F-Box (SCF)-mediated ubiquitination (Ub) and proteasome degradation of the Aux/IAA repressor proteins, In the the absence of the Aux/IAA-TOPLESS (TPL) repressor complex, the AUXIN RESPONSE FACTORs (ARFs) can dimerize at the DNA binding domain (DBD) to efficiently activate gene transcription.

The role of the fourth member of the AGC3 clade, AGC3-4, is until now unclear. Apart from the AGC3 kinases, the D6 protein kinases (D6PK) and the D6PK-like1 (D6PKL1), D6PKL2 and D6PKL3, belonging to the AGC1 clade of the *Arabidopsis* AGCVIII kinases, have been reported to promote PAT (Zourelidou et al., 2014). Two recent reports suggest that D6PK phosphorylates a partially overlapping set of serine residues in the PIN HL, leading to activation rather than changing the polarity of PAT (Barbosa et al., 2014; Zourelidou et al., 2014).

3. Auxin perception and signaling

PAT-generated differential auxin distribution is translated into developmental or growth responses by a complex signaling network. Based on our current knowledge, there are at least three types of auxin receptors. One is the family of TRANSPORT INHIBITOR RESISTANT1/AUXIN SIGNALING F-BOX (TIR1/AFB) proteins, which together with the Aux/IAA repressor proteins act as auxin co-receptors to regulate the AUXIN RESPONSE FACTOR (ARF)-mediated gene expression in the nucleus (Dharmasiri et al., 2005a; Dharmasiri et al., 2005b; Kepinski and Leyser, 2005; Tan et al., 2007). The TIR1/AFB family consists of 6 members in *Arabidopsis* that use auxin as a molecular glue to recruit Aux-IAA proteins for ubiquitination and subsequent degradation as part of the SKP1 – CULLIN1 – F-box SCF ubiquitin E3 ligase complex (Gray et al., 2001; Dharmasiri et al., 2005a; Dharmasiri et al., 2005b). Arabidopsis has 29 Aux/IAAs proteins and each Aux/IAA protein has four highly conserved domains (Liscum and Reed, 2002). The domain I has an ERF-associated amphiphilic repressor (EAR) motif which is crucial for its role in transcription repression (Tiwari et al., 2004), as it binds the TOPLESS (TPL) corepressor (Szemenyei et al., 2008). Domain II interacts with TIR1, resulting in the ubiquitination and subsequent degradation of AUX/IAAs by the 26S proteasome, thereby releasing ARFs to activate transcription (Gray et al., 2001; Dharmasiri et al., 2005a; Kepinski and Leyser, 2005; Maraschin Fdos et al., 2009). The domains III and IV are also found in Aux/IAAs and mediate dimerization between Aux/IAAs and ARFs (Liscum and Reed, 2002; Tiwari et al., 2004). The ARFs consist of a family of 23 proteins in *Arabidopsis* that depending on their middle domain act as activators or repressors (Liscum and Reed, 2002; Tiwari et al., 2004). Through their N-terminal DNA binding domain (DBD) ARFs interact with Auxin Response Elements (AuxRE) in the promoters of auxin responsive genes (Guilfoyle and Hagen, 2007). ARFs have been reported to act as monomers or dimers, but the recent resolution of the crystal structure of ARF5/MONOPTEROS(MP) and ARF1 has revealed that ARFs most likely act as homo- or heterodimers, and that dimerization occurs through their DNA binding domain (Boer et al., 2014).

The second type of auxin receptor is the plant-specific protein AUXIN BINDING PROTEIN 1 (ABP1). ABP1 is retained in the endoplasmic reticulum (ER) by a KDEL-motif, but is also secreted to the extracellular space (Jones and Herman, 1993; Henderson et al., 1997). The *abp1* null mutant is embryo lethal, showing that ABP1 plays an important role in embryogenesis (Chen et al., 2001), but conditional knock downs and weak mutant alleles show that ABP1 is also important for postembryonic shoot and root development (Braun et al., 2008; Tromas et al., 2009; Xu et al., 2010; Li et al., 2011). Recent studies show that ABP1 promotes the recruitment of clathrin to the PM, thereby promoting clathrin-mediated PIN endocytosis (Robert et al., 2010). When auxin binds to ABP1, it inhibits this action and thus prevents clathrin-mediated endocytosis (Robert et al., 2010). Auxin was found to promote binding of ABP1 to the leucine rich repeat TransMembrane Kinase (TMK) receptor-like kinases (Xu et al., 2014). One developmental process where the role of ABP1 has been demonstrated is the interdigitated pattern of leaf pavement cell expansion by coordinated activation of the antagonistic Rho of Plants 2 (ROP2) and ROP6 GTPases (Xu et al., 2010). At the position of the lobe, binding of apoplastic auxin to ABP1 leads to TMK-mediated activation of the ROP2-RIC4 pathway, promoting diffuse F-actin formation that allows PM expansion during lobe formation, whereas at the indentation the auxin-ABP1-TMK1 complex activates the ROP6-RIC1 pathway, promoting microtubules activity that suppresses cell expansion (Xu et al., 2010). This interdigitated patterning is enhanced by ROP2-RIC4-mediated PIN1 localization at the lobes, since

PIN1 loss-of-function or a shift of PIN1 localisation to the indentations by reduced PP2A phosphatase activity or *PID* overexpression led to a significant reduction in pavement cell interdigitation (Jurado et al., 2010; Li et al., 2011).

Recent studies show that ABP1 is a negative regulator of the $SCF^{TIR1/AFB}$ pathway. *ABP1* knock-down results in enhanced degradation of AUX/IAA repressors, which appears to be independent of the effect of ABP1 on endocytosis (Tromas et al., 2009).

A third potential auxin receptor is the S-PHASE KINASE-ASSOCIATED PROTEIN 2A (SKP2A), which is an F-box protein that regulates proteolysis of cell cycle transcription factors. Direct and specific binding of auxin to SKP2A induces its ubiquitin-dependent degradation, together with the proteolysis of a transcription repressor and the promotion of cell division in the root meristem. The results suggest that SKP2A is a positive regulator of cell division (Jurado et al., 2010).

4. Ca^{2+}, a general second messenger in plant signaling

Ca^{2+} is a second messenger that is involved in many developmental and stress signaling processes in plants. Developmental and stress signals can be translated into transient or oscillating changes in the cytosolic Ca^{2+} concentration ($[Ca^{2+}]_{cyt}$). These changes differ per signal and are therefore called stimulus-specific Ca^{2+} signatures that elicit specific physiological responses by altering enzyme activities, cell structures and/or gene expression profiles (Webb et al., 1996; Sanders et al., 1999; Kaplan et al., 2006; Kudla et al., 2010).

Structural changes in the cell wall as well as in membranes are maintained using Ca^{2+} as structural component (Hepler, 2005; Reddy et al., 2011). Ca^{2+} also plays an important role in the symbiosis process in legume root hair cells, where biphasic changes in the $[Ca^{2+}]_{cyt}$ can be induced by rhizobial-derived nodulation (Nod) factors that induce an initial Ca^{2+} influx and a subsequent long-term Ca^{2+} oscillation in the perinucleus (Shaw and Long, 2003; Levy et al., 2004; Kudla et al., 2010). Also during tip growth in pollen tubes and root hair cells, a high $[Ca^{2+}]_{cyt}$ is maintained at the tip by extracellular influx (Sanders et al., 1999; Hepler et al., 2001; Kudla et al., 2010).

Elevation of $[Ca^{2+}]_{cyt}$ can be induced by environmental stimuli by regulation of Ca^{2+} channels and transporters. Ca^{2+} is toxic to plants cells at high intracellular concentrations, and therefore Ca^{2+} is actively pumped from the cytosol either to the apoplast or to intracellular compartments, such as the endoplasmic reticulum and the vacuole, to maintain the $[Ca^{2+}]_{cyt}$ at 10^{-7} M. In the apoplast, Ca^{2+} concentrations are high, varying around 10^{-3} M (McCormack and Braam, 2003). Several Ca^{2+} channels and transporters have been identified so far, such as energy-dependent Ca^{2+} ATPases and transporters that pump Ca^{2+} out of the cytosol, and Ca^{2+}-permeable channels that allow Ca^{2+} influx into the cytosol based on the electrochemical potential. Rapid and dramatic (10- to 100-fold) increases in local $[Ca^{2+}]_{cyt}$ can be achieved by gating Ca^{2+} channels (McAinsh and Pittman, 2009) . Based on the activation mechanism, Ca^{2+} influx channels can be classified as voltage-dependent, voltage-independent/ligand-dependent, and stretch-activated Ca^{2+} channels (Cosgrove and Hedrich, 1991; White et al., 2002; White and Broadley, 2003; Dutta and Robinson, 2004; Nakagawa et al., 2007; Kudla et al., 2010).

5. Ca^{2+} sensors: Ca^{2+} receptors for different signaling pathways

Ca^{2+} signaling is mediated by Ca^{2+} sensors, which are proteins that can monitor the Ca^{2+} concentration changes by affinity-dependent binding of Ca^{2+} to specific receptor domains. Each Ca^{2+} binding site consists of a Ca^{2+} binding loop with negatively charged residues flanked by two helices, which are named E and F helices, and the Ca^{2+} binding pocket is named 'EF hand' after of the hand-like shape of the helix-loop-helix structure (Strynadka and James, 1989). After Ca^{2+} binding, the EF hands generally undergo a conformational change, leading to activation of the EF-hand containing protein, or to an enhanced interaction with other proteins that are in turn activated or repressed (Travé et al., 1995; Sanders et al., 1999; Luan et al., 2002). There are two groups of Ca^{2+} sensors: one is the sensor relays, including calmodulins (CaMs) and calcineurin B-like proteins (CBLs), which do not have any intrinsic activity and have to transmit the Ca^{2+} binding-induced modification to downstream target proteins. The other group comprises the sensor protein kinases, including the Ca^{2+}-dependent protein kinases (CDPKs) and the Ca^{2+} and calmodulin-dependent protein kinases (CCaMKs), which can be directly activated upon Ca^{2+} binding (Sanders et al., 2002).

CDPKs have an N-terminal protein kinase domain, connected by a junction sequence to a CaM-like domain that keeps the protein inactive through a pseudosubstrate-binding mechanism. CCaMKs have a kinase domain at the N-terminus of the protein, followed by two regulatory domains. One is a CaM-binding domain that overlaps with an auto-inhibitory region. The other is a visinin-like domain containing 3 EF-hands. This specific structure allows the protein to be regulated by both Ca^{2+} and Ca^{2+}/CaM (Sathyanarayanan and Poovaiah, 2004; A.Pareek, 2010). At basal Ca^{2+} concentrations, Ca^{2+} binding to two EF-hands keeps the CCaMK in the inactive state. Elevated $[Ca^{2+}]_{cyt}$ during Ca^{2+} spiking results in activation of the kinase by Ca^{2+} binding to the third EF hand and CaM binding to the autoinhibitory domain (Miller et al., 2013).

CBLs have two globular domains containing two conserved EF-hand motifs that are connected by a short linker (Nagae et al., 2003). There are ten members of the CBL family in *Arabidopsis* and rice (Kolukisaoglu et al., 2004). CaMs, like CBLs, have two pairs of Ca^{2+} binding sites that are connected by a linker domain. Ca^{2+} binding to the EF hands at micromolar affinity induces a conformational change that exposes the negative charges in the EF hand, allowing the CaM to bind to positively charged residues in target proteins (Lee et al., 2000; Snedden and Fromm, 2001; McCormack and Braam, 2003; Choi et al., 2005; McCormack et al., 2005; Yoo et al., 2005).

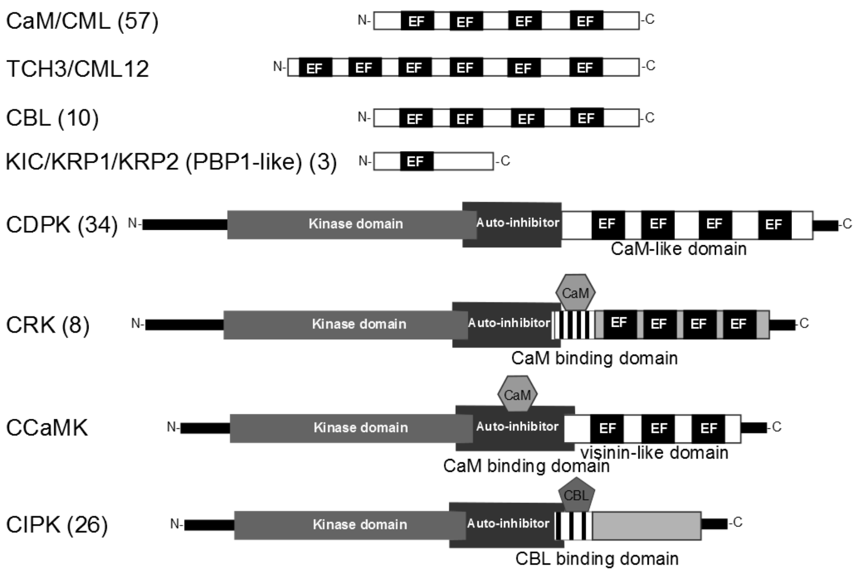
CaM/CML (57)
TCH3/CML12
CBL (10)
KIC/KRP1/KRP2 (PBP1-like) (3)
CDPK (34)
CRK (8)
CCaMK
CIPK (26)
N-
-C
EF
Kinase domain
Auto-inhibitor
CaM-like domain
CaM
CaM binding domain
visinin-like domain
CBL
CBL binding domain

Figure 2 Schematic representation of the structures of plant Ca^{2+} sensors.

Calmodulins and calmodulin-like proteins (CaM/CMLs), calcineurin B-like proteins (CBLs) and KIC/KRP1/KRP2 (PBP1-like) are Ca^{2+} sensor relay proteins that bind Ca^{2+} through their EF hands. Most CaM/CMLs have four predicted EF-hands, although some members of this family are predicted to have 1, 3 or 6 (TCH3/CML12) EF hands. Ca^{2+}-dependent protein kinases (CDPK), CDPK-related protein kinase (CRK), Ca^{2+} and CaM-dependent protein kinases (CCaMKs) and CBL-Interacting Protein Kinases (CIPKs) are sensor protein kinases. The number of family members in *Arabidopsis* is indicated between brackets.

Plants have a large family of CaM and CaM-like (CML) proteins (McCormack et al., 2005). The *Arabidopsis* genome encodes seven CAM isoforms that differ only in one to four amino acids, and 50 CMLs, which are more divergent and contain additional domains. The seven *CAM* genes share 89% identity to vertebrate CaMs and are considered to be the true type CaMs (McCormack et al., 2005). The 50 CML proteins share at least 16% amino acid identity with CaMs, most of them (31/50) are predicted to have four EF hands, and based on their apparent divergence, they have been classified into nine groups (McCormack and Braam, 2003; McCormack et al., 2005).

Several *CML* genes have been identified as touch-inducible (*TCH*) genes in *Arabidopsis*, whose mRNA levels are rapidly induced by mechanical stimuli, in some cases up to 100-fold within minutes (Braam and Davis, 1990). *TCH3/CML12* is one of these genes, encoding a unique CML with six instead of four predicted EF hands (Antosiewicz et al., 1995).

By using a protein binding microarray, several previously identified and more than 173 novel *in vitro* CaM/CML binding partners have been identified, including Receptor-like Protein Kinases (RLKs), transcription factors, CBL-Interacting Protein Kinases (CIPKs), Ca^{2+}-dependent protein kinases (CDPKs), proteins involved in the cell cycle, and F-box and RNA-binding proteins. Around 25% of the identified target proteins could interact with all CaMs/CMLs, whereas another 25% could only interact with one CaM/CML, indicating that there is both functional redundancy and also specificity among the different CaMs and CMLs (Popescu et al., 2007).

CaMs and CMLs play a significant role in plant defense, transducing the pathogen-induced Ca^{2+} increase to downstream components of defense signaling (Harding et al., 1997; Heo et al., 1999; Chiasson et al., 2005; Takabatake et al., 2007; Zhu et al., 2010; Reddy et al., 2011). CaM binding transcription factors play a role in plant responses to biotic and abiotic signals (Reddy et al., 2011).

6. Auxin transport in plant responses to abiotic signals

Abiotic environmental factors such as gravity, light, and touch play an important role in modulating plant growth via respectively gravitropic, phototropic and thigmotropic growth responses. Abundant studies on these tropic plant growth responses have uncovered a tight relationship between Ca^{2+} and auxin signaling. Below we have summarized the involvement of them in PAT.

Around 1930, Cholodny and Went hypothesized, based on their investigations on light- or gravity-induced bending of seedling coleoptiles and roots, that this bending was the result of asymmetric growth induced by the redistribution of a plant growth regulator to respectively the dark or lower side of plant tissues (Went and Thimann, 1937). Later, after the identification of auxin as the plant growth regulator, others confirmed the lateral movement of auxin to the dark or lower side of root tips, coleoptiles or hypocotyls (Briggs, 1963; Gillespie and Thimann, 1963; Filner et al., 1970; Baskin et al., 1986; Gehring et al., 1990b; Esmon et al., 2006). With the development of the *DR5::GFP* and *35S*::*DII:VENUS* auxin response reporters it became possible to follow the differential auxin response in time and to show with *Arabidopsis* mutants or inhibitor treatments that PAT is essential for both the asymmetric auxin distribution and the resulting growth response (Rashotte et al., 2000; Friml et al., 2002a; Ottenschlager et al., 2003; Ding et al., 2011; Band et al., 2012; Brunoud et al., 2012).

In *Arabidopsis* root tips, the gravitropic response is thought to be initiated in the collumella root cap cells, where the statolites sense the gravity vector by touching the cortical cytoskeleton. Via an unknown signaling pathway, this leads to a relocalization of PIN3 and PIN7 from apolar to polarized to the lower side in gravity-sensing columella root cap cells, resulting in predominant auxin transport to the lower side of the root tip (Friml et al., 2002a; Kleine-Vehn et al., 2010). This higher auxin induces calcium influx and TCH3 expression high expression at the lower side of root tip, thus PID is internalized by calmodulins and results in PIN2 apolarization, leading to higher auxin levels in the lateral root cap- and epidermis cells at the lower side of the root (Band et al., 2012; Brunoud et al., 2012; Baster et al., 2013). The higher auxin levels in these cells lead to stabilization of PIN2 at the PM by inhibition of ABP1-mediated endocytosis, whereas PIN2 is degraded due to reduced auxin levels at the upper side of the root tip (Paciorek et al., 2005; Abas et al., 2006; Robert et al., 2010; Baster et al., 2013).

Phototropic growth of the *Arabidopsis* hypocotyl is initiated by the phototropins phot1 and phot2 under respectively low and medium light fluency conditions (Liscum et al., 2014). These blue light photoreceptors trigger a signaling cascade that leads to the rapid redistribution of PIN3 to the inner lateral side of hypocotyl endodermis cells (Friml et al., 2002; Ding et al., 2011). Recent findings suggest the involvement of the PID kinase in this process. In the dark, expression and activity of the PID kinase results in PIN3 apolar targeting to all cell sides. Light represses *PID* transcription and polarizes the auxin efflux carrier PIN3 cellular localization to the lateral inner side in hypocotyls endodermis cells by GNOM ARF-GEF-dependent trafficking, resulting in auxin distribution changes and differential growth, causing hypocotyls to bend toward the light source (Ding et al., 2011). Besides PIN3, at least eight other auxin transporters (PIN1, 2, 4 and 7, ABCB19, AUX1, LAX2, LAX3) are involved in phototropism.

However, their independent roles have not been defined as clearly as for PIN3 (reviewed in (Liscum et al., 2014)).

Thigmotropism is the plant growth response to mechanical stresses, like touch or contact stimuli (thigmo means “touch” in Greek). Thigmotropism can be induced by the soil or rocks for roots or by wind, raindrops and animals passing by for the shoot. Surprisingly, the role of auxin and PAT in thigmotropic growth has not been studied in a lot of detail, possibly because the induction of the response requires a more delicate experimental set up. The research efforts have been mainly focused on the shoot part, where auxin turn-over by peroxidase-mediated decarboxylation has been proposed as major mechanism leading to touch-induced differential growth of the shoot (reviewed in (Chehab et al., 2009)). Although it is likely that differential auxin distribution plays a role in touch-induced growth responses, the role of PAT in thigmotropism remains to be clarified.

7. Auxin and Ca^{2+} in plant responses to abiotic signals

In 1956 Bennet-Clark proposed that Ca^{2+} might act antagonistically with auxin during the phototropic response in oat coleoptiles (College. et al., 1956). In 1973, dela Fuente and Leopold showed that the Ca^{2+} chelator EGTA could reduce auxin transport in sunflower stem sections, which could be restored after washing with Ca^{2+}, indicating that Ca^{2+} is an important regulator of PAT (dela Fuente and Leopold, 1973). Ten years later, Lee and coworkers showed that lateral PAT was promoted by a Ca^{2+} gradient in maize root tips (Lee et al., 1983), and that PAT inhibitors not only prevented the gravity response of these roots, but also the gravity-induced Ca^{2+} gradient (Lee et al., 1984). Detailed investigations of the effect of exogenously applied Ca^{2+} on the kinetics of gravitropism has shown that the root elongation rate could be significantly reduced by high concentrations of Ca^{2+}, similar to treatment with low auxin concentrations, suggesting that auxin induces an increase in $[Ca^{2+}]_{cyt}$, which in turn affects plant growth (Hasenstein and Evans, 1986; Mulkey and Vaughan, 1986). In 1987, Gross and Sauter published on experiments with corn coleoptiles, suggesting that Ca^{2+} ions move to lower auxin concentrations in a lateral auxin concentration gradient, whereas auxin moves to the lower Ca^{2+} concentration side when exposed to a lateral Ca^{2+} concentration gradient, proposing a link between Ca^{2+} and auxin fluxes (Gross and Sauter, 1987). Although this result suggests an antagonistic role for Ca^{2+} and auxin, later experiments have shown a more synergistic role for Ca^{2+} in auxin responses. By monitoring $[Ca^{2+}]_{cyt}$ using double-barrelled ion-sensitive microelectrodes, it was observed that 1 μM exogenously applied IAA could induce Ca^{2+} oscillations within a period of 20 to 30 minutes in epidermal cells of maize (*Zea mays* L.) coleoptiles (Felle, 1988). Similarly, by using the Ca^{2+} indicator fluo-3, it was shown that the synthetic auxin analogue 2,4-dichlorophenoxyacetic acid (2,4-D) could induce an increase in $[Ca^{2+}]_{cyt}$ within 4 minutes after application in epidermal cells of parsley hypocotyls and roots and dark-grown corn coleoptiles (Gehring et al., 1990a). IAA and Ca^{2+} could enhance adventitious root initiation on sunflower (*Helianthus annuus* L.) hypocotyls, but when a Ca^{2+} channel blocker was used instead of Ca^{2+}, the IAA-induced rooting response was inhibited, suggesting that auxin induces a net influx of Ca^{2+}, which is required for root initiation (Kalra and Bhatia, 1998).

Ca^{2+} signaling has also been reported to mediate the phototropic bending response (Harada et al., 2003; Stoelzle et al., 2003). By using a fluorescent Ca^{2+} probe fluo-3, a rapid light induced increase in $[Ca^{2+}]_{cyt}$ was observed on the shaded side of maize coleoptiles. This provided the first direct link between rapid $[Ca^{2+}]_{cyt}$ increases and the cell elongation induced by light (Gehring et al., 1990a). A rapid transient $[Ca^{2+}]_{cyt}$ increase could be induced by photostimulation of PHOT1(Baum et al., 1999).

Based on electrophysiology studies it has been reported that the $[Ca^{2+}]_{cyt}$ in epidermis cells of the elongation zone is increased upon gravistimulation and that the $[Ca^{2+}]_{cyt}$ peaks coincide with the basipetal movement of auxin from the root tip to the elongation zone at the lower side of the root tip (Lee et al., 1984; Toyota et al., 2008).

The development of the FRET-based Ca^{2+} sensor yellow cameleon YC3.6 has allowed to more accurately follow the temporal and spatial dynamics of $[Ca^{2+}]_{cyt}$ changes in whole plant tissues. By using this marker it could be demonstrated that exogenous auxin application or gravitropism-induced enhancement of auxin levels triggers a rapid Ca^{2+} influx in *Arabidopsis* root epidermal cells within seconds. These experiments further demonstratedthat Ca^{2+} acts downstream of auxin to translate local auxin levels into appropriate physiological responses (Plieth and Trewavas, 2002; Nagai et al., 2004; Monshausen et al., 2008; Monshausen et al., 2011).

Gravistimulation by rotating apo-aequorin expressing *Arabidopsis* seedlings induced a two-peaked $[Ca^{2+}]_{cyt}$-increase in root epidermis cells, which lasted for several minutes. The auxin transport inhibitor TIBA and vesicle trafficking inhibitor BFA could attenuate the increased $[Ca^{2+}]_{cyt}$ peak amplitudes, indicating that the $[Ca^{2+}]_{cyt}$ response during gravitropism is tightly coupled to auxin transport (Toyota et al., 2008). By using parabolic flight-induced microgravity conditions it could be demonstrated that gravistimulation is responsible for the second sustained increase in $[Ca^{2+}]_{cyt}$ (Toyota et al., 2013).

Mechanosensing in roots induces calcium responses leading to reactive oxygen species and pH (Monshausen et al., 2009). The mechnical stress-induced calcium channels identified in *Arabiodpsis* (Nakagawa et al., 2007) provide a likely mechanism for the rapid touch-induced elevation of $[Ca^{2+}]_{cyt}$. Based on analogy with gravitropism, it is tempting to speclate that the differential growth response induced by touch is mediated by PAT-mediated differential auxin distribution. The exact mechanism, however, remains to be established.

How auxin-induced Ca^{2+} signals are actually translated into physiological responses has remained unclear for a long time. In 1990, Janet Braam identified at least four touch-induced (*TCH*) genes of which the transcription levels were increased in ten to thirty minutes by wind, touch, water spray, subirrigation, wounding or darkness. Several of these genes appeared to encode CMLs, suggesting that Ca^{2+} ions and CaM are involved in translating touch signals into plant growth responses (Braam and Davis, 1990). The first molecular players were identified through the finding that one of the key regulators of PAT, the PID protein kinase, interacts with two Ca^{2+} binding proteins: TOUCH3 (TCH3) and PID-BINDING PROTEIN 1 (PBP1) (Benjamins et al., 2003). As discussed above, PID regulates the direction of PAT by triggering the recruitment of PIN proteins into the GNOM-independent trafficking pathway through direct phosphorylation of the PIN HL (Friml et al., 2004; Huang et al., 2010). The interaction of PID with Ca^{2+} binding proteins potentially makes this kinase responsive to changes in $[Ca^{2+}]_{cyt}$, which would induce changes in the direction of PAT. The PID-Ca^{2+} binding protein module is an important candidate in the signaling pathway that modulates the subcellular PIN localization by environmental and developmental cues, as has been observed for several developmental processes (Friml et al., 2002a; Benkova et al., 2003; Friml et al., 2003; Reinhardt et al., 2003; Scarpella et al., 2006; Michniewicz et al., 2007). Another player in Ca^{2+} signalling in animals cells is inositol 1,4,5-trisphosphate ($InsP_3$), which can trigger Ca^{2+} release into the cytoplasm from intracellular stores (Mikoshiba, 2007). In plants IP3 has also been suggested to act as a signalling molecule, even in modulating PIN polarity (Blatt et al., 1990; Gilroy et al., 1990; Krinke et al., 2007; Tang et al., 2007; Zhang et al., 2011) It is very unlikely however, that IP3 is a signaling molecule in plants, as the levels of the precursor PIP2 in plant membranes are extremely low, and also since candidate genes for the IP3 receptor and the downstream calcium-activated kinase PKC have not been identified in sequenced plant genomes (Wheeler and Brownlee, 2008; Munnik, 2014).

8. Auxin and Ca^{2+} in responses to endogenous mechanical stress

During plant development, also endogenous mechanical stresses on cells have an effect on their growth. This has been mainly studied in relation to the regular patterns of organ initiation at the shoot apical or inflorescence meristems, referred to as phyllotaxis. It is well established that PAT-generated auxin maxima form initiation points for the development of new organs (reviewed in (Sassi and Vernoux, 2013)). More recently, reports on the role of mechanical stresses in determining phyllotactic patterns have appeared, indicating an important role for the cell wall and the microtubule cytoskeleton (reviewed in (Sassi and Vernoux, 2013)).

Cellulose microfibrils which are the main component of the plant cell wall, are synthesized by hexameric complexes of cellulose synthesizing proteins called CESA at the PM. A tight association of these cellulose microfibrils with a matrix of proteins and polysaccharides, like pectins and hemicelluloses, make the cell wall extreme stiff, and by modulating these interactions the stiffness of the wall and the dynamics and mechanical properties can be varied (Cosgrove, 2005; Uyttewaal et al., 2010). Uptake of osmotic water gives the plants a strong internal pressure, which is named turgor pressure, causing the cells to swell. The extremely rigid cell wall prevents the cell from bursting (Hamant et al., 2010). In response to this turgor pressure, cells yield to it through cell wall synthesis and remodeling, resulting in an increase in cell size and shape changes. The forces produced in one cell can quickly spread to the surrounding cells. In this way mechanical forces act as a motor of growth and shape change. The feedback between cell wall expansion and turgor pressure is important for plant morphogenesis. Another mechanical stress is from the differential growth between neighboring cells in the tissues where cells adhere to each other.

Assuming that the epidermis is under tension and limiting for growth, the shoot apical meristem can be compared to a pressure vessel (Kutschera and Niklas, 2007; Uyttewaal et al., 2010). Assuming that the epidermis is stiffer than ground tissues, turgor is mainly supported by epidermal walls. Interestingly, the predicted force pattern in this system strongly correlates with the direction of microtubules. Microtubules align along the predicted stress directions in the SAM, suggesting that microtubule orientation could be controlled by mechanical stress (Uyttewaal et al., 2010). At the shoot apical meristem, cortical microtubules show characteristic patterns: dynamic at the tip, transverse arrays on the flanks, and arrays parallel to the crease at the boundary between the emerging organ and the meristem tip (Hamant et al., 2008; Hamant et al., 2010; Uyttewaal et al., 2010). Further manipulation of the meristem by compression or cell ablation induces microtubule reorientation along stress patterns, confirming that cortical microtubules tend to be parallel to the direction of maximal force (Hamant et al., 2008; Hamant et al., 2010; Uyttewaal et al., 2010). The ensuing reinforcement by cellulose microfibrils might also help delimiting the boundary between a primordium and the meristem tip (Hamant et al., 2008; Corson et al., 2009; Hamant et al., 2010; Uyttewaal et al., 2010). This mechanical feedback can be viewed as a cell-autonomous readout of the meristem shape, providing directional information (Hamant et al., 2010). Interestingly, PIN1 localisation in shoot meristem cells negative correlated with the direction of the microtubule arrays, and wounding experiments suggested that PIN1 polarity and thus auxin transport patterns are modulated by mechanical forces (Heisler et al., 2010). The mechano-sensitive calcium channels that have been identified in *Arabidopsis*, could directly translate mechanical stress into a Ca^{2+} response. The prominent role of PID in organ-initiation in the inflorescence meristem (Christensen et al., 2000; Benjamins et al., 2001; Friml et al., 2004) makes it tempting to speculate that mechanical stress induced peaks in $[Ca^{2+}]_{cyt}$ could affect PIN1 polarity through the calcium-dependent interaction between the CML12/TCH3 calcium receptor and the PIN polarity regulator PID (Benjamins et al., 2003).

9. Outline of this thesis

As described above, the protein kinase PID works as a binary switch in directing the asymmetric localization of PIN proteins at the PM, and thereby the polarity of auxin transport, by phosphorylating long PIN proteins on serines in three conserved TPRXS motifs present in the PIN HL (Friml et al., 2004; Michniewicz et al., 2007; Dhonukshe et al., 2010). Previous studies have shown that the calmodulin-like protein CML12 /TCH3 interacts with PID in a yeast two hybrid assay and *in vitro* (Benjamins et al., 2003). The research described in this thesis focused on the PID-TCH3 interaction *in vivo* and *in planta* and on the effect of this interaction on the downstream processes, including auxin transport-dependent processes in the root- (**Chapter 2**) and shoot meristem (**Chapter 4**), e.g. gravitropism or phyllotaxis, respectively. Since the *tch3-3* loss-of-function mutant did not show a strong phenotype, we investigated whether other CaMs or CMLs also interact with PID and mapped the CaM-binding site on the PID kinase (**Chapter 3**).

Chapter 2 shows that the PM-associated PID kinase interacted with TCH3 in a Ca^{2+}-dependent manner, and that this interaction resulted in dissociation of PID from the PM to the cytosol, away from its phosphorylation targets, the PIN proteins. Auxin treatment induced rapid dissociation of PID from the PM of root epidermis cells. We showed that this was mediated by Ca^{2+}-dependent interaction with TCH3 and leads, after the initial apical (shootward) PIN2 stabilization by auxin, to PIN2 apolarity. We investigated the effect of TCH3 mediated PID internalization during gravitropism, inducing a shift from apical (shootward) to apolar PIN2 localisation 3-5 hours after the start of gravistimulation. Of the other three AGC3 kinases, only WAG2 could interact with TCH3.

In **Chapter 3** we showed that CML10 and the calmodulin CAM2, two proteins closely related to TCH3, were also able to recruit PID from the PM. To overcome the redundant action between the calmodulins (CaMs) and CMLs in our functional analysis of the PID-calmodulin signaling complex, we fine-mapped the PM associated domain and the CML/CaM binding domain in PID. Our analysis revealed that PID CML/CaM binding and PM association converges on an amphipathic alpha helix/IQ-like motif in the PID insertion domain, and that the two functionalities cannot be separated. This dual interaction domain allows an elegant novel mechanism of protein kinase activity regulation, by which $[Ca^{2+}]_{cyt}$ determine whether the kinase is available to phosphorylation of substrate proteins.

In **Chapter 4** we show that PIN1 phosphorylation by the three AGC3 kinases is important for regular phyllotaxis in *Arabidopsis*, and that *pidwag1*, *pidwag2* or *pidwag1wag2* loss-of-function, or PIN1 loss-of-phosphorylation, or to a lesser extent also gain-of-phosphorylation, leads to irregular phyllotaxis, varying from absence of primordium initiation to a switch from the normal spiral (137.5° angle) to a decussate (alternating 180° and 90° angles) pattern. Auxin, mechanical stress and TCH3 overexpression trigger Ca^{2+}-dependent internalization of PID in the inflorescence meristem, probably involving the calmodulin-like protein (CML) TCH3 based on the research from Chapter 2, but also can from other calmodulins as the redundancy. The enhanced variation in the divergence angle between flowers at *TCH3* overexpression or *tch3* loss-of-function mutant inflorescences suggests that a dynamic recruitment of the kinase by TCH3 is required for a regular spiral phyllotaxis. Our results suggest the involvement of the AGC3 kinase-CML signalling complex in modulating of the phyllotactic pattern in response to auxin and mechanical stress.

References

A.Pareek, S.K.S., H.J.Bohnert and Govindjee. (2010). Abiotic stress adaptation in plants:physiological, molecular and genomic foundation**,** 75-90.

Abas, L., Benjamins, R., Malenica, N., Paciorek, T., Wisniewska, J., Moulinier-Anzola, J.C., Sieberer, T., Friml, J., and Luschnig, C. (2006). Intracellular trafficking and proteolysis of the *Arabidopsis* auxin-efflux facilitator PIN2 are involved in root gravitropism. Nat Cell Biol **8,** 249-256.

Antosiewicz, D.M., Polisensky, D.H., and Braam, J. (1995). Cellular localization of the Ca^{2+} binding TCH3 protein of *Arabidopsis*. Plant J **8,** 623-636.

Ballesteros, I., Domínguez, T., Sauer, M., Paredes, P., Duprat, A., Rojo, E., Sanmartín, M., and Sánchez-Serrano, J.J. (2013). Specialized functions of the PP2A subfamily II catalytic subunits PP2A-C3 and PP2A-C4 in the distribution of auxin fluxes and development in Arabidopsis. Plant J **73,** 862-872.

Band, L.R., Wells, D.M., Larrieu, A., Sun, J., Middleton, A.M., French, A.P., Brunoud, G., Sato, E.M., Wilson, M.H., Peret, B., Oliva, M., Swarup, R., Sairanen, I., Parry, G., Ljung, K., Beeckman, T., Garibaldi, J.M., Estelle, M., Owen, M.R., Vissenberg, K., Hodgman, T.C., Pridmore, T.P., King, J.R., Vernoux, T., and Bennett, M.J. (2012). Root gravitropism is regulated by a transient lateral auxin gradient controlled by a tipping-point mechanism. Proc Natl Acad Sci U S A **109,** 4668-4673.

Barbosa, I.C., Zourelidou, M., Willige, B.C., Weller, B., and Schwechheimer, C. (2014). D6 PROTEIN KINASE activates auxin transport-dependent growth and PIN-FORMED phosphorylation at the plasma membrane. Dev Cell **29,** 674-685.

Baskin, T.I., Briggs, W.R., and Iino, M. (1986). Can lateral redistribution of auxin account for phototropism of maize coleoptiles? Plant Physiol **81,** 306-309.

Baster, P., Robert, S., Kleine-Vehn, J., Vanneste, S., Kania, U., Grunewald, W., De Rybel, B., Beeckman, T., and Friml, J. (2013). SCF$^{TIR1/AFB}$-auxin signalling regulates PIN vacuolar trafficking and auxin fluxes during root gravitropism. EMBO J **32,** 260-274.

Baum, G., Long, J.C., Jenkins, G.I., and Trewavas, A.J. (1999). Stimulation of the blue light phototropic receptor NPH1 causes a transient increase in cytosolic Ca^{2+}. Proc Natl Acad Sci U S A **96,** 13554-13559.

Benjamins, R., Ampudia, C.S., Hooykaas, P.J., and Offringa, R. (2003). PINOID-mediated signaling involves calcium-binding proteins. Plant Physiol **132,** 1623-1630.

Benjamins, R., Quint, A., Weijers, D., Hooykaas, P., and Offringa, R. (2001). The PINOID protein kinase regulates organ development in *Arabidopsis* by enhancing polar auxin transport. Development **128,** 4057-4067.

Benkova, E., Michniewicz, M., Sauer, M., Teichmann, T., Seifertova, D., Jurgens, G., and Friml, J. (2003). Local, efflux-dependent auxin gradients as a common module for plant organ formation. Cell **115,** 591-602.

Bennett, S.R.M., Alvarez, J., Bossinger, G., and Smyth, D.R. (1995). Morphogenesis in *pinoid* mutants of *Arabidopsis thaliana*. Plant J. **8,** 505-520.

Blatt, M.R., Thiel, G., and Trentham, D.R. (1990). Reversible inactivation of K^+ channels of *Vicia* stomatal guard cells following the photolysis of caged inositol 1,4,5-trisphosphate. Nature **346,** 766-769.

Blilou, I., Xu, J., Wildwater, M., Willemsen, V., Paponov, I., Friml, J., Heidstra, R., Aida, M., Palme, K., and Scheres, B. (2005). The PIN auxin efflux facilitator network controls growth and patterning in *Arabidopsis* roots. Nature **433,** 39-44.

Boer, D.R., Freire-Rios, A., van den Berg, W.A., Saaki, T., Manfield, I.W., Kepinski, S., Lopez-Vidrieo, I., Franco-Zorrilla, J.M., de Vries, S.C., Solano, R., Weijers, D., and Coll, M. (2014). Structural basis for DNA binding specificity by the auxin-dependent ARF transcription factors. Cell **156,** 577-589.

Braam, J., and Davis, R.W. (1990). Rain-, wind-, and touch-induced expression of calmodulin and calmodulin-related genes in Arabidopsis. Cell **60,** 357-364.

Braun, N., Wyrzykowska, J., Muller, P., David, K., Couch, D., Perrot-Rechenmann, C., and Fleming, A.J. (2008). Conditional repression of AUXIN BINDING PROTEIN1 reveals that it coordinates cell division and cell expansion during postembryonic shoot development in *Arabidopsis* and tobacco. Plant Cell **20,** 2746-2762.

Briggs, W.R. (1963). Mediation of phototropic responses of corn coleoptiles by lateral transport of auxin. Plant Physiol **38,** 237-247.

Brunoud, G., Wells, D.M., Oliva, M., Larrieu, A., Mirabet, V., Burrow, A.H., Beeckman, T., Kepinski, S., Traas, J., Bennett, M.J., and Vernoux, T. (2012). A novel sensor to map auxin response and distribution at high spatio-temporal resolution. Nature **482,** 103-106.

Chehab, E.W., Eich, E., and Braam, J. (2009). Thigmomorphogenesis: a complex plant response to mechano-stimulation. J Exp Bot **60,** 43-56.

Chen, J.G., Ullah, H., Young, J.C., Sussman, M.R., and Jones, A.M. (2001). ABP1 is required for organized cell elongation and division in *Arabidopsis* embryogenesis. Genes Dev **15,** 902-911.

Chiasson, D., Ekengren, S.K., Martin, G.B., Dobney, S.L., and Snedden, W.A. (2005). Calmodulin-like proteins from *Arabidopsis* and tomato are involved in host defense against *Pseudomonas syringae* pv. *tomato*. Plant Mol Biol **58,** 887-897.

Choi, M.Y., Partridge, A.W., Daniels, C., Du, K., Lukacs, G.L., and Deber, C.M. (2005). Destabilization of the transmembrane domain induces misfolding in a phenotypic mutant of cystic fibrosis transmembrane conductance regulator. J Biol Chem **280,** 4968-4974.

Christensen, S.K., Dagenais, N., Chory, J., and Weigel, D. (2000). Regulation of auxin response by the protein kinase PINOID. Cell **100,** 469-478.

College., W., Wain, R.L., and Wightman, F. (1956). The chemistry and mode of action of plant growth substances; proceedings of a symposium held at Wye College, University of London, July 1955. Edited by R.L. Wain and F. Wightman. (London: Butterworths Scientific Publications).

Corson, F., Hamant, O., Bohn, S., Traas, J., Boudaoud, A., and Couder, Y. (2009). Turning a plant tissue into a living cell froth through isotropic growth. Proc Natl Acad Sci U S A **106,** 8453-8458.

Cosgrove, D.J. (2005). Growth of the plant cell wall. Nat Rev Mol Cell Biol **6,** 850-861.

Cosgrove, D.J., and Hedrich, R. (1991). Stretch-activated chloride, potassium, and calcium channels coexisting in plasma membranes of guard cells of Vicia faba L. Planta **186,** 143-153.

Dai, M., Zhang, C., Kania, U., Chen, F., Xue, Q., McCray, T., Li, G., Qin, G., Wakeley, M., Terzaghi, W., Wan, J., Zhao, Y., Xu, J., Friml, J., Deng, X.W., and Wang, H. (2012). A PP6-type phosphatase holoenzyme directly regulates PIN phosphorylation and auxin efflux in *Arabidopsis*. Plant Cell **24,** 2497-2514.

Darwin, C. (1880). The power of movement in plants. London: John Murray.

dela Fuente, R.K., and Leopold, A.C. (1973). A role for calcium in auxin transport. Plant Physiol **51,** 845-847.

Dharmasiri, N., Dharmasiri, S., and Estelle, M. (2005a). The F-box protein TIR1 is an auxin receptor. Nature **435,** 441-445.

Dharmasiri, N., Dharmasiri, S., Weijers, D., Lechner, E., Yamada, M., Hobbie, L., Ehrismann, J.S., Jurgens, G., and Estelle, M. (2005b). Plant development is regulated by a family of auxin receptor F box proteins. Dev Cell **9,** 109-119.

Dhonukshe, P., Aniento, F., Hwang, I., Robinson, D.G., Mravec, J., Stierhof, Y.D.,

and Friml, J. (2007). Clathrin-mediated constitutive endocytosis of PIN auxin efflux carriers in *Arabidopsis*. Curr Biol **17,** 520-527.

Dhonukshe, P., Huang, F., Galvan-Ampudia, C.S., Mahonen, A.P., Kleine-Vehn, J., Xu, J., Quint, A., Prasad, K., Friml, J., Scheres, B., and Offringa, R. (2010). Plasma membrane-bound AGC3 kinases phosphorylate PIN auxin carriers at TPRXS(N/S) motifs to direct apical PIN recycling. Development **137,** 3245-3255.

Dhonukshe, P., Grigoriev, I., Fischer, R., Tominaga, M., Robinson, D.G., Hasek, J., Paciorek, T., Petrasek, J., Seifertova, D., Tejos, R., Meisel, L.A., Zazimalova, E., Gadella, T.W., Jr., Stierhof, Y.D., Ueda, T., Oiwa, K., Akhmanova, A., Brock, R., Spang, A., and Friml, J. (2008). Auxin transport inhibitors impair vesicle motility and actin cytoskeleton dynamics in diverse eukaryotes. Proc Natl Acad Sci U S A **105,** 4489-4494.

Ding, Z., Galvan-Ampudia, C.S., Demarsy, E., Langowski, L., Kleine-Vehn, J., Fan, Y., Morita, M.T., Tasaka, M., Fankhauser, C., Offringa, R., and Friml, J. (2011). Light-mediated polarization of the PIN3 auxin transporter for the phototropic response in *Arabidopsis*. Nat Cell Biol **13,** 447-452.

Dutta, R., and Robinson, K.R. (2004). Identification and characterization of stretch-activated ion channels in pollen protoplasts. Plant Physiol **135,** 1398-1406.

Esmon, C.A., Tinsley, A.G., Ljung, K., Sandberg, G., Hearne, L.B., and Liscum, E. (2006). A gradient of auxin and auxin-dependent transcription precedes tropic growth responses. Proc Natl Acad Sci U S A **103,** 236-241.

Felle, H. (1988). Auxin causes oscillations of cytosolic free calcium and pH in *Zea mays* coleoptiles. Planta **174,** 495-499.

Filner, B., Hertel, R., Steele, C., and Fan, V. (1970). Some aspects of geotropism in coleoptiles. Planta **94,** 333-354.

Friml, J., Wisniewska, J., Benkova, E., Mendgen, K., and Palme, K. (2002a). Lateral relocation of auxin efflux regulator PIN3 mediates tropism in *Arabidopsis*. Nature **415,** 806-809.

Friml, J., Vieten, A., Sauer, M., Weijers, D., Schwarz, H., Hamann, T., Offringa, R., and Jurgens, G. (2003). Efflux-dependent auxin gradients establish the apical-basal axis of *Arabidopsis*. Nature **426,** 147-153.

Friml, J., Benkova, E., Blilou, I., Wisniewska, J., Hamann, T., Ljung, K., Woody, S., Sandberg, G., Scheres, B., Jurgens, G., and Palme, K. (2002b). AtPIN4 mediates sink-driven auxin gradients and root patterning in *Arabidopsis*. Cell **108,** 661-673.

Friml, J., Yang, X., Michniewicz, M., Weijers, D., Quint, A., Tietz, O., Benjamins, R., Ouwerkerk, P.B., Ljung, K., Sandberg, G., Hooykaas, P.J., Palme, K., and Offringa, R. (2004). A PINOID-dependent binary switch in apical-basal PIN polar targeting directs auxin efflux. Science **306,** 862-865.

Gehring, C.A., Irving, H.R., and Parish, R.W. (1990a). Effects of auxin and abscisic acid on cytosolic calcium and pH in plant cells. Proc Natl Acad Sci U S A **87,** 9645-9649.

Gehring, C.A., Williams, D.A., Cody, S.H., and Parish, R.W. (1990b). Phototropism and geotropism in maize coleoptiles are spatially correlated with increases in cytosolic free calcium. Nature **345,** 528-530.

Geldner, N., Friml, J., Stierhof, Y.D., Jurgens, G., and Palme, K. (2001). Auxin transport inhibitors block PIN1 cycling and vesicle trafficking. Nature **413,** 425-428.

Geldner, N., Anders, N., Wolters, H., Keicher, J., Kornberger, W., Muller, P., Delbarre, A., Ueda, T., Nakano, A., and Jurgens, G. (2003). The *Arabidopsis* GNOM ARF-GEF mediates endosomal recycling, auxin transport, and auxin-dependent plant growth. Cell **112,** 219-230.

Gillespie, B., and Thimann, K.V. (1963). Transport & distribution of auxin during tropistic response. I. The lateral migration of auxin in geotropism. Plant Physiol **38,** 214-225.

Gilroy, S., Read, N.D., and Trewavas, A.J. (1990). Elevation of cytoplasmic calcium by caged calcium or caged inositol triphosphate initiates stomatal closure. Nature **346,** 769-771.

Gray, W.M., Kepinski, S., Rouse, D., Leyser, O., and Estelle, M. (2001). Auxin regulates SCF^{TIR1}-dependent degradation of AUX/IAA proteins. Nature **414,** 271-276.

Gross, J., and Sauter, M. (1987). Are auxin and calcium movements in corn coleoptiles linked processes? Plant Science **49,** 189-198.

Guilfoyle, T.J., and Hagen, G. (2007). Auxin response factors. Curr. Opin. Plant Biol. **10,** 453-460.

Habets, M.E., and Offringa, R. (2014). PIN-driven polar auxin transport in plant developmental plasticity: a key target for environmental and endogenous signals. New Phytol **203,** 362-377.

Hamant, O., Traas, J., and Boudaoud, A. (2010). Regulation of shape and patterning in plant development. Curr Opin Genet Dev **20,** 454-459.

Hamant, O., Heisler, M.G., Jonsson, H., Krupinski, P., Uyttewaal, M., Bokov, P.,

Corson, F., Sahlin, P., Boudaoud, A., Meyerowitz, E.M., Couder, Y., and Traas, J. (2008). Developmental patterning by mechanical signals in *Arabidopsis*. Science **322,** 1650-1655.

Harada, A., Sakai, T., and Okada, K. (2003). phot1 and phot2 mediate blue light-induced transient increases in cytosolic Ca^{2+} differently in *Arabidopsis* leaves. Proc Natl Acad Sci U S A **100,** 8583-8588.

Harding, S.A., Oh, S.H., and Roberts, D.M. (1997). Transgenic tobacco expressing a foreign calmodulin gene shows an enhanced production of active oxygen species. EMBO J **16,** 1137-1144.

Hasenstein, K.-H., and Evans, M.L. (1986). Calcium dependence of rapid auxin action in maize roots. Plant Physiol **81,** 439-443.

Heisler, M.G., Hamant, O., Krupinski, P., Uyttewaal, M., Ohno, C., Jonsson, H., Traas, J., and Meyerowitz, E.M. (2010). Alignment between PIN1 polarity and microtubule orientation in the shoot apical meristem reveals a tight coupling between morphogenesis and auxin transport. PLoS Biol **8,** e1000516.

Henderson, J., Bauly, J.M., Ashford, D.A., Oliver, S.C., Hawes, C.R., Lazarus, C.M., Venis, M.A., and Napier, R.M. (1997). Retention of maize auxin-binding protein in the endoplasmic reticulum: quantifying escape and the role of auxin. Planta **202,** 313-323.

Heo, W.D., Lee, S.H., Kim, M.C., Kim, J.C., Chung, W.S., Chun, H.J., Lee, K.J., Park, C.Y., Park, H.C., Choi, J.Y., and Cho, M.J. (1999). Involvement of specific calmodulin isoforms in salicylic acid-independent activation of plant disease resistance responses. Proc Natl Acad Sci U S A **96,** 766-771.

Hepler, P.K. (2005). Calcium: a central regulator of plant growth and development. Plant Cell **17,** 2142-2155.

Hepler, P.K., Vidali, L., and Cheung, A.Y. (2001). Polarized cell growth in higher plants. Annu Rev Cell Dev Biol **17,** 159-187.

Huang, F., Zago, M.K., Abas, L., van Marion, A., Galvan-Ampudia, C.S., and Offringa, R. (2010). Phosphorylation of conserved PIN motifs directs *Arabidopsis* PIN1 polarity and auxin transport. Plant Cell **22,** 1129-1142.

Jones, A.M., and Herman, E.M. (1993). KDEL-Containing auxin-binding protein is secreted to the plasma membrane and cell wall. Plant Physiol **101,** 595-606.

Jurado, S., Abraham, Z., Manzano, C., Lopez-Torrejon, G., Pacios, L.F., and Del Pozo, J.C. (2010). The *Arabidopsis* cell cycle F-box protein SKP2A binds to auxin.

Plant Cell **22,** 3891-3904.

Kalra, G., and Bhatia, S. (1998). Auxin-calcium interaction in adventitious root formation in the hypocotyl explants of sunflower (*Helianthus annuus* L.). J. Plant Biochem. Biotechnol. **7,** 107-110.

Kaplan, B., Davydov, O., Knight, H., Galon, Y., Knight, M.R., Fluhr, R., and Fromm, H. (2006). Rapid transcriptome changes induced by cytosolic Ca^{2+} transients reveal ABRE-related sequences as Ca^{2+}-responsive *cis* elements in *Arabidopsis*. Plant Cell **18,** 2733-2748.

Kepinski, S., and Leyser, O. (2005). The *Arabidopsis* F-box protein TIR1 is an auxin receptor. Nature **435,** 446-451.

Kleine-Vehn, J., Ding, Z., Jones, A.R., Tasaka, M., Morita, M.T., and Friml, J. (2010). Gravity-induced PIN transcytosis for polarization of auxin fluxes in gravity-sensing root cells. Proc Natl Acad Sci U S A **107,** 22344-22349.

Kleine-Vehn, J., Huang, F., Naramoto, S., Zhang, J., Michniewicz, M., Offringa, R., and Friml, J. (2009). PIN auxin efflux carrier polarity is regulated by PINOID kinase-mediated recruitment into GNOM-independent trafficking in *Arabidopsis*. Plant Cell **21,** 3839-3849.

Kleine-Vehn, J., Wabnik, K., Martiniere, A., Langowski, L., Willig, K., Naramoto, S., Leitner, J., Tanaka, H., Jakobs, S., Robert, S., Luschnig, C., Govaerts, W., Hell, S.W., Runions, J., and Friml, J. (2011). Recycling, clustering, and endocytosis jointly maintain PIN auxin carrier polarity at the plasma membrane. Mol Syst Biol **7,** 540.

Kolukisaoglu, U., Weinl, S., Blazevic, D., Batistic, O., and Kudla, J. (2004). Calcium sensors and their interacting protein kinases: genomics of the Arabidopsis and rice CBL-CIPK signaling networks. Plant Physiol **134,** 43-58.

Krinke, O., Novotna, Z., Valentova, O., and Martinec, J. (2007). Inositol trisphosphate receptor in higher plants: is it real? J Exp Bot **58,** 361-376.

Kudla, J., Batistic, O., and Hashimoto, K. (2010). Calcium signals: the lead currency of plant information processing. Plant Cell **22,** 541-563.

Kutschera, U., and Niklas, K.J. (2007). The epidermal-growth-control theory of stem elongation: an old and a new perspective. J Plant Physiol **164,** 1395-1409.

Lee, J.S., Mulkey, T.J., and Evans, M.L. (1983). Gravity-induced polar transport of calcium across root tips of maize. Plant Physiol **73,** 874-876.

Lee, J.S., Mulkey, T.J., and Evans, M.L. (1984). Inhibition of polar calcium movement and gravitropism in roots treated with auxin-transport inhibitors. Planta **160,**

536-543.

Lee, S.H., Johnson, J.D., Walsh, M.P., Van Lierop, J.E., Sutherland, C., Xu, A., Snedden, W.A., Kosk-Kosicka, D., Fromm, H., Narayanan, N., and Cho, M.J. (2000). Differential regulation of Ca^{2+}/calmodulin-dependent enzymes by plant calmodulin isoforms and free Ca^{2+} concentration. Biochem J **350,** 299-306.

Levy, J., Bres, C., Geurts, R., Chalhoub, B., Kulikova, O., Duc, G., Journet, E.P., Ane, J.M., Lauber, E., Bisseling, T., Denarie, J., Rosenberg, C., and Debelle, F. (2004). A putative Ca^{2+} and calmodulin-dependent protein kinase required for bacterial and fungal symbioses. Science **303,** 1361-1364.

Li, H., Lin, D., Dhonukshe, P., Nagawa, S., Chen, D., Friml, J., Scheres, B., Guo, H., and Yang, Z. (2011). Phosphorylation switch modulates the interdigitated pattern of PIN1 localization and cell expansion in *Arabidopsis* leaf epidermis. Cell Res **21,** 970-978.

Liscum, E., and Reed, J.W. (2002). Genetics of Aux/IAA and ARF action in plant growth and development. Plant Mol Biol **49,** 387-400.

Liscum, E., Askinosie, S.K., Leuchtman, D.L., Morrow, J., Willenburg, K.T., and Coats, D.R. (2014). Phototropism: growing towards an understanding of plant movement. Plant Cell **26,** 38-55.

Luan, S., Kudla, J., Rodriguez-Concepcion, M., Yalovsky, S., and Gruissem, W. (2002). Calmodulins and calcineurin B-like proteins: calcium sensors for specific signal response coupling in plants. Plant Cell **14,** S389-400.

Luschnig, C., Gaxiola, R.A., Grisafi, P., and Fink, G.R. (1998). EIR1, a root-specific protein involved in auxin transport, is required for gravitropism in *Arabidopsis thaliana*. Genes Dev. **12,** 2175-2187.

Maraschin Fdos, S., Memelink, J., and Offringa, R. (2009). Auxin-induced, SCF^{TIR1}-mediated poly-ubiquitination marks AUX/IAA proteins for degradation. Plant J **59,** 100-109.

McAinsh, M.R., and Pittman, J.K. (2009). Shaping the calcium signature. New Phytol **181,** 275-294.

McCormack, E., and Braam, J. (2003). Calmodulins and related potential calcium sensors of Arabidopsis. New Phytol. **159,** 585-598.

McCormack, E., Tsai, Y.C., and Braam, J. (2005). Handling calcium signaling: *Arabidopsis* CaMs and CMLs. Trends Plant Sci **10,** 383-389.

Michniewicz, M., Zago, M.K., Abas, L., Weijers, D., Schweighofer, A., Meskiene, I.,

Heisler, M.G., Ohno, C., Zhang, J., Huang, F., Schwab, R., Weigel, D., Meyerowitz, E.M., Luschnig, C., Offringa, R., and Friml, J. (2007). Antagonistic regulation of PIN phosphorylation by PP2A and PINOID directs auxin flux. Cell **130,** 1044-1056.

Mikoshiba, K. (2007). IP3 receptor/Ca^{2+} channel: from discovery to new signaling concepts. J Neurochem **102,** 1426-1446.

Miller, J.B., Pratap, A., Miyahara, A., Zhou, L., Bornemann, S., Morris, R.J., and Oldroyd, G.E. (2013). Calcium/Calmodulin-dependent protein kinase is negatively and positively regulated by calcium, providing a mechanism for decoding calcium responses during symbiosis signaling. Plant Cell **25,** 5053-5066.

Monshausen, G.B., Messerli, M.A., and Gilroy, S. (2008). Imaging of the Yellow Cameleon 3.6 indicator reveals that elevations in cytosolic Ca^{2+} follow oscillating increases in growth in root hairs of Arabidopsis. Plant Physiol **147,** 1690-1698.

Monshausen, G.B., Bibikova, T.N., Weisenseel, M.H., and Gilroy, S. (2009). Ca^{2+} regulates reactive oxygen species production and pH during mechanosensing in *Arabidopsis* roots. Plant Cell **21,** 2341-2356.

Monshausen, G.B., Miller, N.D., Murphy, A.S., and Gilroy, S. (2011). Dynamics of auxin-dependent Ca^{2+} and pH signaling in root growth revealed by integrating high-resolution imaging with automated computer vision-based analysis. Plant J. **65,** 309-318.

Mravec, J., Skupa, P., Bailly, A., Hoyerova, K., Krecek, P., Bielach, A., Petrasek, J., Zhang, J., Gaykova, V., Stierhof, Y.D., Dobrev, P.I., Schwarzerova, K., Rolcik, J., Seifertova, D., Luschnig, C., Benkova, E., Zazimalova, E., Geisler, M., and Friml, J. (2009). Subcellular homeostasis of phytohormone auxin is mediated by the ER-localized PIN5 transporter. Nature **459,** 1136-1140.

Mulkey, T.J., and Vaughan, M.A. (1986). Auxin and root gravitropism: the state of our knowledge. In Plant Growth Substances 1985, M. Bopp, ed (Springer Berlin Heidelberg), pp. 241-246.

Munnik, T. (2014). PI-PLC: Phosphoinositide-Phospholipase C in Plant Signaling. In Phospholipases in Plant Signaling, X. Wang, ed (Springer Berlin Heidelberg), pp. 27-54.

Nagae, M., Nozawa, A., Koizumi, N., Sano, H., Hashimoto, H., Sato, M., and Shimizu, T. (2003). Crystallization and preliminary X-ray characterization of a novel calcium-binding protein AtCBL2 from *Arabidopsis thaliana*. Acta Crystallogr D Biol Crystallogr **59,** 1079-1080.

Nagai, T., Yamada, S., Tominaga, T., Ichikawa, M., and Miyawaki, A. (2004).

Expanded dynamic range of fluorescent indicators for Ca^{2+} by circularly permuted yellow fluorescent proteins. Proc Natl Acad Sci U S A **101,** 10554-10559.

Nakagawa, Y., Katagiri, T., Shinozaki, K., Qi, Z., Tatsumi, H., Furuichi, T., Kishigami, A., Sokabe, M., Kojima, I., Sato, S., Kato, T., Tabata, S., Iida, K., Terashima, A., Nakano, M., Ikeda, M., Yamanaka, T., and Iida, H. (2007). *Arabidopsis* plasma membrane protein crucial for Ca^{2+} influx and touch sensing in roots. Proc Natl Acad Sci U S A **104,** 3639-3644.

Okada, K., Ueda, J., Komaki, M.K., Bell, C.J., and Shimura, Y. (1991). Requirement of the auxin polar transport system in early stages of *Arabidopsis* floral bud formation. Plant Cell **3,** 677-684.

Ottenschlager, I., Wolff, P., Wolverton, C., Bhalerao, R.P., Sandberg, G., Ishikawa, H., Evans, M., and Palme, K. (2003). Gravity-regulated differential auxin transport from columella to lateral root cap cells. Proc Natl Acad Sci U S A **100,** 2987-2991.

Paciorek, T., Zazimalova, E., Ruthardt, N., Petrasek, J., Stierhof, Y.D., Kleine-Vehn, J., Morris, D.A., Emans, N., Jurgens, G., Geldner, N., and Friml, J. (2005). Auxin inhibits endocytosis and promotes its own efflux from cells. Nature **435,** 1251-1256.

Petrasek, J., Mravec, J., Bouchard, R., Blakeslee, J.J., Abas, M., Seifertova, D., Wisniewska, J., Tadele, Z., Kubes, M., Covanova, M., Dhonukshe, P., Skupa, P., Benkova, E., Perry, L., Krecek, P., Lee, O.R., Fink, G.R., Geisler, M., Murphy, A.S., Luschnig, C., Zazimalova, E., and Friml, J. (2006). PIN proteins perform a rate-limiting function in cellular auxin efflux. Science **312,** 914-918.

Plieth, C., and Trewavas, A.J. (2002). Reorientation of seedlings in the earth's gravitational field induces cytosolic calcium transients. Plant Physiol **129,** 786-796.

Popescu, S.C., Popescu, G.V., Bachan, S., Zhang, Z., Seay, M., Gerstein, M., Snyder, M., and Dinesh-Kumar, S.P. (2007). Differential binding of calmodulin-related proteins to their targets revealed through high-density *Arabidopsis* protein microarrays. Proc Natl Acad Sci U S A **104,** 4730-4735.

Rashotte, A.M., Brady, S.R., Reed, R.C., Ante, S.J., and Muday, G.K. (2000). Basipetal auxin transport is required for gravitropism in roots of Arabidopsis. Plant Physiol **122,** 481-490.

Reddy, A.S.N., Ali, G.S., Celesnik, H., and Day, I.S. (2011). Coping with stresses: roles of calcium- and calcium/calmodulin-regulated gene expression. Plant Cell **23,** 2010-2032.

Reinhardt, D., Pesce, E.R., Stieger, P., Mandel, T., Baltensperger, K., Bennett, M., Traas, J., Friml, J., and Kuhlemeier, C. (2003). Regulation of phyllotaxis by polar auxin transport. Nature **426,** 255-260.

Robert, S., Kleine-Vehn, J., Barbez, E., Sauer, M., Paciorek, T., Baster, P., Vanneste, S., Zhang, J., Simon, S., Covanova, M., Hayashi, K., Dhonukshe, P., Yang, Z., Bednarek, S.Y., Jones, A.M., Luschnig, C., Aniento, F., Zazimalova, E., and Friml, J. (2010). ABP1 mediates auxin inhibition of clathrin-dependent endocytosis in *Arabidopsis*. Cell **143,** 111-121.

Sabatini, S., Beis, D., Wolkenfelt, H., Murfett, J., Guilfoyle, T., Malamy, J., Benfey, P., Leyser, O., Bechtold, N., Weisbeek, P., and Scheres, B. (1999). An auxin-dependent distal organizer of pattern and polarity in the *Arabidopsis* root. Cell **99,** 463-472.

Sanders, D., Brownlee, C., and Harper, J.F. (1999). Communicating with calcium. Plant Cell **11,** 691-706.

Sanders, D., Pelloux, J., Brownlee, C., and Harper, J.F. (2002). Calcium at the crossroads of signaling. Plant Cell **14 Suppl,** S401-417.

Sassi, M., and Vernoux, T. (2013). Auxin and self-organization at the shoot apical meristem. J Exp Bot **64,** 2579-2592.

Sathyanarayanan, P.V., and Poovaiah, B.W. (2004). Decoding Ca^{2+} signals in plants. CRC Crit Rev Plant Sci **23,** 1-11.

Sauer, M., Robert, S., and Kleine-Vehn, J. (2013). Auxin: simply complicated. J Exp Bot **64,** 2565-2577.

Sauer, M., Balla, J., Luschnig, C., Wisniewska, J., Reinohl, V., Friml, J., and Benkova, E. (2006). Canalization of auxin flow by Aux/IAA-ARF-dependent feedback regulation of PIN polarity. Genes Dev **20,** 2902-2911.

Sawchuk, M.G., Edgar, A., and Scarpella, E. (2013). Patterning of leaf vein networks by convergent auxin transport pathways. PLoS Genet **9,** e1003294.

Scarpella, E., Marcos, D., Friml, J., and Berleth, T. (2006). Control of leaf vascular patterning by polar auxin transport. Genes Dev **20,** 1015-1027.

Shaw, S.L., and Long, S.R. (2003). Nod factor elicits two separable calcium responses in *Medicago truncatula* root hair cells. Plant Physiol **131,** 976-984.

Snedden, W.A., and Fromm, H. (2001). Calmodulin as a versatile calcium signal transducer in plants. New Phytol **151,** 35-66.

Stoelzle, S., Kagawa, T., Wada, M., Hedrich, R., and Dietrich, P. (2003). Blue light activates calcium-permeable channels in *Arabidopsis* mesophyll cells via the phototropin signaling pathway. Proc Natl Acad Sci U S A **100,** 1456-1461.

Strynadka, N.C., and James, M.N. (1989). Crystal structures of the helix-loop-helix calcium-binding proteins. Annu Rev Biochem **58,** 951-998.

Szemenyei, H., Hannon, M., and Long, J.A. (2008). TOPLESS mediates auxin-dependent transcriptional repression during *Arabidopsis* embryogenesis. Science **319,** 1384-1386.

Takabatake, R., Karita, E., Seo, S., Mitsuhara, I., Kuchitsu, K., and Ohashi, Y. (2007). Pathogen-induced calmodulin isoforms in basal resistance against bacterial and fungal pathogens in tobacco. Plant Cell Physiol **48,** 414-423.

Tan, X., Calderon-Villalobos, L.I., Sharon, M., Zheng, C., Robinson, C.V., Estelle, M., and Zheng, N. (2007). Mechanism of auxin perception by the TIR1 ubiquitin ligase. Nature **446,** 640-645.

Tanaka, H., Dhonukshe, P., Brewer, P.B., and Friml, J. (2006). Spatiotemporal asymmetric auxin distribution: a means to coordinate plant development. Cell Mol Life Sci **63,** 2738-2754.

Tang, R.H., Han, S., Zheng, H., Cook, C.W., Choi, C.S., Woerner, T.E., Jackson, R.B., and Pei, Z.M. (2007). Coupling diurnal cytosolic Ca^{2+} oscillations to the CAS-IP_3 pathway in *Arabidopsis*. Science **315,** 1423-1426.

Tiwari, S.B., Hagen, G., and Guilfoyle, T.J. (2004). Aux/IAA proteins contain a potent transcriptional repression domain. Plant Cell **16,** 533-543.

Toyota, M., Furuichi, T., Tatsumi, H., and Sokabe, M. (2008). Critical consideration on the relationship between auxin transport and calcium transients in gravity perception of Arabidopsis seedlings. Plant Signal Behav **3,** 521-524.

Toyota, M., Furuichi, T., Sokabe, M., and Tatsumi, H. (2013). Analyses of a gravistimulation-specific Ca^{2+} signature in Arabidopsis using parabolic flights. Plant Physiol **163,** 543-554.

Travé, G., Lacombe, P.J., Pfuhl, M., Saraste, M., and Pastore, A. (1995). Molecular mechanism of the calcium-induced conformational change in the spectrin EF-hands. EMBO J **14,** 4922-4931.

Tromas, A., Braun, N., Muller, P., Khodus, T., Paponov, I.A., Palme, K., Ljung, K., Lee, J.Y., Benfey, P., Murray, J.A., Scheres, B., and Perrot-Rechenmann, C. (2009). The AUXIN BINDING PROTEIN 1 is required for differential auxin responses mediating root growth. PLoS One **4,** e6648.

Uyttewaal, M., Traas, J., and Hamant, O. (2010). Integrating physical stress, growth, and development. Curr Opin Plant Biol **13,** 46-52.

Webb, A.A.R., McAinsh, M.R., Taylor, J.E., and Hetherington, A.M. (1996). Calcium ions as intracellular second messengers in higher plants. In Advances in Botanical Research, J.A. Callow, ed (Academic Press), pp. 45-96.

Went, F., and Thimann, K.V. (1937). Phytohormones. New York: The Macmillan Company.

Wheeler, G.L., and Brownlee, C. (2008). Ca^{2+} signalling in plants and green algae--changing channels. Trends Plant Sci **13,** 506-514.

White, P.J., and Broadley, M.R. (2003). Calcium in plants. Ann Bot **92,** 487-511.

White, P.J., Bowen, H.C., Demidchik, V., Nichols, C., and Davies, J.M. (2002). Genes for calcium-permeable channels in the plasma membrane of plant root cells. Biochim Biophys Acta **1564,** 299-309.

Wisniewska, J., Xu, J., Seifertova, D., Brewer, P.B., Ruzicka, K., Blilou, I., Rouquie, D., Benkova, E., Scheres, B., and Friml, J. (2006). Polar PIN localization directs auxin flow in plants. Science **312,** 883.

Xu, J., Hofhuis, H., Heidstra, R., Sauer, M., Friml, J., and Scheres, B. (2006). A molecular framework for plant regeneration. Science **311,** 385-388.

Xu, T., Wen, M., Nagawa, S., Fu, Y., Chen, J.G., Wu, M.J., Perrot-Rechenmann, C., Friml, J., Jones, A.M., and Yang, Z. (2010). Cell surface- and rho GTPase-based auxin signaling controls cellular interdigitation in *Arabidopsis*. Cell **143,** 99-110.

Xu, T., Dai, N., Chen, J., Nagawa, S., Cao, M., Li, H., Zhou, Z., Chen, X., De Rycke, R., Rakusova, H., Wang, W., Jones, A.M., Friml, J., Patterson, S.E., Bleecker, A.B., and Yang, Z. (2014). Cell surface ABP1-TMK auxin-sensing complex activates ROP GTPase signaling. Science **343,** 1025-1028.

Yoo, J.H., Park, C.Y., Kim, J.C., Heo, W.D., Cheong, M.S., Park, H.C., Kim, M.C., Moon, B.C., Choi, M.S., Kang, Y.H., Lee, J.H., Kim, H.S., Lee, S.M., Yoon, H.W., Lim, C.O., Yun, D.J., Lee, S.Y., Chung, W.S., and Cho, M.J. (2005). Direct interaction of a divergent CaM isoform and the transcription factor, MYB2, enhances salt tolerance in *Arabidopsis*. J Biol Chem **280,** 3697-3706.

Zhang, J., Vanneste, S., Brewer, P.B., Michniewicz, M., Grones, P., Kleine-Vehn, J., Lofke, C., Teichmann, T., Bielach, A., Cannoot, B., Hoyerova, K., Chen, X., Xue, H.W., Benkova, E., Zazimalova, E., and Friml, J. (2011). Inositol trisphosphate-induced Ca^{2+} signaling modulates auxin transport and PIN polarity. Dev

Cell **20,** 855-866.

Zhao, Y. (2010). Auxin biosynthesis and its role in plant development. Annu Rev Plant Biol **61,** 49-64.

Zhu, X., Caplan, J., Mamillapalli, P., Czymmek, K., and Dinesh-Kumar, S.P. (2010). Function of endoplasmic reticulum calcium ATPase in innate immunity-mediated programmed cell death. EMBO J **29,** 1007-1018.

Zourelidou, M., Absmanner, B., Weller, B., Barbosa, I.C., Willige, B.C., Fastner, A., Streit, V., Port, S.A., Colcombet, J., de la Fuente van Bentem, S., Hirt, H., Kuster, B., Schulze, W.X., Hammes, U.Z., and Schwechheimer, C. (2014). Auxin efflux by PIN-FORMED proteins is activated by two different protein kinases, D6 PROTEIN KINASE and PINOID. Elife **3,** e02860.

Chapter 2

TOUCHing PINOID: a calmodulin–kinase interaction modulates auxin transport polarity during root gravitropism

Yuanwei Fan[1], Carlos Samuel Galván-Ampudia[1,2,3], Hélène S. Robert[1,2,4], Karen Sap[1], Elco Backus[1], Remko Offringa[1, 5]

[1] Molecular and Developmental Genetics, Institute Biology Leiden, Leiden University, Sylviusweg 72, 2333 BE Leiden, The Netherlands

[2] These authors contributed equally to this manuscript

[3] Present address: Laboratoire de Reproduction et Développement des Plantes, CNRS, INRA, ENS Lyon, UCBL, Université de Lyon, 69364 Lyon, France

[4] Present address: Mendel Centre for Genomics and Proteomics of Plants Systems, CEITEC MU - Central European Institute of Technology, Masaryk University, CZ-625 00 Brno, Czech Republic.

[5] Author for correspondence (r.offringa@biology.leidenuniv.nl)

Summary

The plant hormone auxin is well-known to cause elevated cytosolic Ca^{2+} levels ($[Ca^{2+}]_{cyt}$), however, how Ca^{2+} signaling assists in auxin-mediated plant development and growth is not well understood. Here we show that the Arabidopsis plasma membrane (PM)-associated kinase PINOID (PID), a key-determinant in the polar subcellular targeting of PIN auxin efflux carriers, interacts in an auxin-induced, Ca^{2+}-dependent manner with the calmodulin-like protein CML12/TCH3. This interaction results in dissociation of the PID kinase from the PM to the cytosol, away from its PIN phosphorylation targets. During root gravitropism, elevated $[Ca^{2+}]_{cyt}$ and TCH3 levels act downstream of auxin to trigger PID internalization followed by PIN2 depolarization, which enhances root gravitropism by maximizing the differential auxin response in the root tip. The dynamic Ca^{2+}/CML-dependent shuttling of PID between PM and cytosol reveals a novel regulatory mechanism through which auxin modulates the direction of its own transport.

Introduction

Ca^{2+} plays an important role as intracellular second messenger in a variety of signaling pathways. In plants, rapid changes in the cytosolic Ca^{2+} concentration ($[Ca^{2+}]_{cyt}$) are required for the transduction of both abiotic signals and biotic stimuli (Bouché et al., 2005). In order to give an appropriate response, cells need to distinguish the Ca^{2+} signals produced by these different stimuli. Spatial and temporal patterns of Ca^{2+} responses, and also the presence of Ca^{2+} "receptors" or sensors in the cell, are needed to give specificity to the signal (Luan et al., 2002; Sanders et al., 2002). A major group of Ca^{2+} receptor proteins monitor changes in the $[Ca^{2+}]_{cyt}$ through helix-loop-helix Ca^{2+} binding domains called EF-hands (Strynadka and James, 1989). The conformational changes induced by binding of Ca^{2+} to these proteins either induce their activation, or enhance their interaction with other proteins that are in turn activated or repressed (Travé et al., 1995; Luan et al., 2002; Sanders et al., 2002). Two main types of EF hand proteins are known: the calmodulins (CaMs) and the Ca^{2+}-dependent protein kinases (CDPKs). CaMs are small proteins with typically four EF-hands without an effector domain that are highly conserved in all eukaryotes. Plant genomes, however, also encode a large number of CaM-like proteins (CMLs) that in most cases also have 4 EF-hands, and seem to act in a similar manner as CaMs (McCormack and Braam, 2003; Hashimoto and Kudla, 2011). The transmission of the Ca^{2+} signal occurs through the interaction with target proteins to influence their activity (Snedden and Fromm, 2001; Bouché et al., 2005). The CDPKs combine a calmodulin-like domain with a kinase domain. Binding of Ca^{2+} directly activates the protein kinase (Cheng et al., 2002).

The phytohormone auxin regulates plant development by controlling basic cellular processes such as cell division, -differentiation and -elongation (Reinhardt et al., 2000; Nakajima and Benfey, 2002; Weijers and Jurgens, 2005; Peret et al., 2009). Ever since the first observations of Darwin on the growth response of Canary grass coleoptiles to unidirectional light (Darwin, 1880), it is well-established that auxin is transported from cell to cell in a polar fashion from its sites of synthesis to its sites of action (Tanaka et al., 2006; Petrasek and Friml, 2009; Vanneste and Friml, 2009; Ljung, 2013). This polar auxin transport (PAT) generates auxin gradients and maxima that mediate photo- and gravitropic growth responses, and are instructive for embryogenesis, meristem maintenance and organ positioning (Sabatini et al., 1999; Friml et al., 2002; Benkova et al., 2003; Friml et al., 2003; Reinhardt et al., 2003). The mechanism of auxin transport has been intensely studied, and PIN transmembrane proteins have been identified as auxin efflux carriers that direct this polar cell-to-cell transport through their asymmetric subcellular localization (Petrasek et al., 2006; Wisniewska et al., 2006). The plant-specific AGC serine/threonine protein kinase PINOID (PID) was identified as a regulator of auxin transport (Benjamins et al., 2001) Together with two close homologs WAG1 and WAG2, PID directs PIN polar localization at the apical (shootward) cell membrane, by phosphorylation of the serines in three conserved TPRXS motifs of the PIN central hydrophilic loop (Friml et al., 2004; Michniewicz et al., 2007; Dhonukshe et al., 2010; Huang et al., 2010).

Several studies suggest that the auxin signaling pathway involves rapid changes in the $[Ca^{2+}]_{cyt}$. For example, in wheat protoplasts (Shishova and Lindberg, 2004), maize coleoptile cells (Felle, 1988; Gehring et al., 1990a) and parsley cells (Gehring et al., 1990a), an increase of the $[Ca^{2+}]_{cyt}$ was detected within minutes after auxin application using Ca^{2+} fluorescent dyes or ion-sensitive microelectrodes. Also, an auxin-induced Ca^{2+} pulse was observed in intact plant tissues such as maize and pea roots (Gehring et al., 1990a) and Ca^{2+} has been implied as an important signal in the regulation of PAT in sunflower hypocotyls (dela Fuente and Leopold, 1973), in gravistimulated roots (Lee and Evans, 1985; Monshausen et al., 2008; Monshausen et al., 2011) and during phototropism (Baum et al., 1999; Harada and Shimazaki, 2007). In gravitropic root growth, the gravity vector is perceived by the interaction between statoliths and the cytoskeleton in the columella root cap cells, leading to a local Ca^{2+} response. Initial experiments by Lee et al. (Lee et al., 1984; Lee and Evans, 1985) suggested that Ca^{2+} transport across the root tip plays an important role and that Ca^{2+} in the elongation zone enhances auxin transport in horizontally placed root tips. Although the exact order of events is still unknown, the use of the Yellow Cameleon Ca^{2+} reporter YC3.6 has shown that gravitropic growth and auxin induce elevated $[Ca^{2+}]_{cyt}$ in epidermis cells at the lower side of the root (Monshausen et al., 2011). For phototropic growth, the blue light signal perceived by the phototropin receptor kinases phot1 and phot2 induces a rapid increase in $[Ca^{2+}]_{cyt}$ (Baum et al., 1999; Harada et al., 2003; Zhao et al., 2013) and triggers PIN-dependent auxin accumulation at the shaded side, leading to shoot bending toward the light source (Friml et al., 2002; Esmon et al., 2006; Ding et al., 2011). Although the Ca^{2+} response does not seem to be required for phot1-mediated phototropic response to low fluence rate blue light (Folta et al., 2003), it seems to be essential for the phot1- and phot2-mediated phototropic response to higher fluence rate blue light (Zhao et al., 2013). The PHYTOCHROME KINASE SUBSTRATE 1 protein (PKS1) was found to interact with phot1 (Lariguet et al., 2006) and to act redundantly with PKS2 and PKS4, which is downstream of Ca^{2+} signaling, possibly through its interaction with CAM4 (Zhao et al., 2013).

Our previous finding found that PID interacts in a Ca^{2+}-dependent manner with the EF-hand protein PINOID BINDING PROTEIN1 (PBP1) and the CML TOUCH3 (TCH3/CML12) provided the first molecular evidence for Ca^{2+} as a signal transducer in the regulation of PAT (Benjamins et al., 2003). In *Arabidopsis*, TCH3 is unique in that it has 6 instead of the 4 EF-hand motifs generally predicted in CaMs and CMLs. Its corresponding gene was initially identified as a touch-responsive gene (Braam and Davis, 1990; Sistrunk et al., 1994). Here we present a detailed study of the *in vivo* interaction between PID and TCH3. Using loss- and gain-of-function mutant lines, we confirm *in vitro* observations that TCH3 is a negative regulator of the PINOID kinase activity. This regulation occurs directly by inhibition of the kinase activity, as shown in phosphorylation assays, and by sequestration of PID from the plasma membrane (PM) where its phospho-targets the PIN proteins are located (Michniewicz et al., 2007; Huang et al., 2010). We also show that the PID-TCH3 signaling complex plays a role in fine-tuning root growth, e.g. during root gravitropism where PID internalization triggered by the auxin-induced Ca^{2+} response at the lower side of the root leads to PIN2 apolarity, which is needed for maximization of the differential auxin distribution, and thus the gravitropic response.

Results

TCH3 reduces kinase activity by binding to the PID catalytic domain

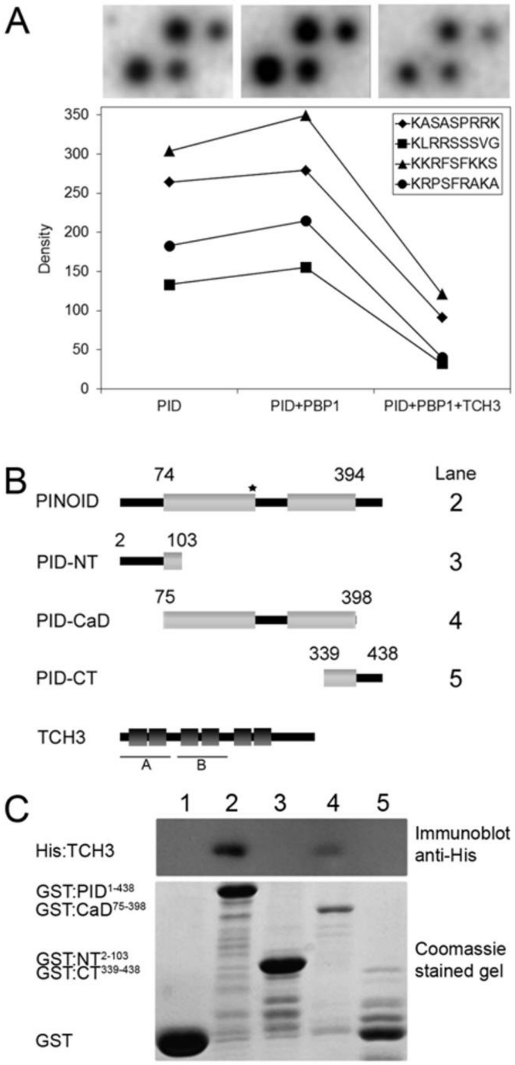

Figure 1 TCH3 reduces PID activity by interacting with its catalytic kinase domain.

(A) Detail of a phospho-peptide chip incubated with radiolabelled ATP and either PID alone, PID and the positive regulator PBP1, or PID, PBP1 and TCH3. Densitometry analysis of the four spots in the upper images is provided in the graph below. The density value indicates the number of black grains in the measured circle.

(B, C) Mapping the TCH3 interaction domain in PID with *in vitro* pull downs (B) Schematic representation of PID (498 aa), or its N-terminal portion (PID-NT, aa 2-103), the catalytic domain (PID-CaD, aa 75-398), or the C-terminal portion (PID-CT, aa 339-438), and TCH3 (324 aa). The light grey boxes in PID represent the kinase catalytic core (aa 74-394), which in PID has an amino acid insertion between sub-domain VII and VIII (aa 226-281). The star indicates the position of the DFG to DFD mutation characteristic for the plant-specific AGCVIII protein kinases. The six EF-hand domains in TCH3 (aa 11-38, 50-74, 101-127, 139-163, 191-217, 228-253) are depicted as dark grey boxes. A and B indicate an exact duplication of two EF-hand domains in TCH3.

(C) Western blot analysis (top panel) following pull-down with GST-tagged PID or deletion versions thereof. Lane 1 is the pull down with GST alone. Other lane numbers refer to the GST-PID versions depicted in (B). Coomassie stained gel (bottom panel) showing the input of proteins used in the pull-down assay.

Previous *in vitro* pull-down assays showed that the PID kinase-TCH3 CML interaction is Ca^{2+}-dependent (Benjamins et al., 2003). Moreover, a traditional kinase assay with Myelin Basic Protein (MBP) as substrate showed that TCH3 reduces the *in vitro* phosphorylation activity of PID (Benjamins et al., 2003). To confirm the effect of TCH3 on PID activity with a wider array of substrates, we incubated a commercial phospho-peptide chip with radiolabelled ATP and PID. For a quantitative comparison of differences in PID activity, we focused on the phosphorylation intensity of four peptides, including a phospho-target in MBP. PID efficiently phosphorylated all four peptides (Figure 1A). In the presence of the single EF-hand protein PBP1, a positive regulator of PID activity (Benjamins et al., 2003), the phosphorylation intensity was significantly increased (Figure 1A). Addition of TCH3 to the PID and PBP1 containing mix reduced the phosphorylation intensity significantly reduced to even below the basal phosphorylation level by PID alone (Figure 1A). These data corroborate the conclusions of our previous analysis that TCH3 is a negative regulator of PID kinase activity *in vitro*, and indicate that TCH3 binding to PID is able to overrule the positive effect of PBP1.

In order to roughly map the TCH3 interaction site in PID, *in vitro* pull-down assays were performed using GST-tagged isolates of the N-terminal domain (aa 2-103), the catalytic domain (aa 75-398) or the C-terminal domain (aa 339-438) of PID, along with its full-length version to test their interaction with crude *E. coli* extracts containing histidine (His)-tagged TCH3 (Figure 1B, C). Immuno-detection of His-TCH3 after GST pull-down indicated that TCH3 interacts with full-length PID or its catalytic domain (Figure 1C, lanes 2 and 4) but not with the N- or C-terminal domains (Figure 1C, lanes 3 and 5). Binding of TCH3 to the PID catalytic domain provided an explanation why this interaction affected PID kinase activity in the phosphorylation assays (Figure 1A).

TCH3 mediates auxin-dependent sequestration of PID from the PM

Transfection of *Arabidopsis* protoplasts with a *35S::TCH3-YFP* construct showed that the fusion protein, like soluble CFP, is cytoplasmic, but unlike CFP it is excluded from the nucleus (Figure 2A, upper panel). A similar localization was observed for the TCH3-mRFP fusion protein in root epidermis cells of *TCH3::TCH3-mRFP* seedlings (Figure 2B, right panel). In contrast, PID showed predominant membrane-association and partial cytosolic localization both in protoplasts (Figure 2B, left panel) and *in planta* (Figure 2B, middle panel), in accordance with previously published data (Lee and Cho, 2006; Michniewicz et al., 2007).

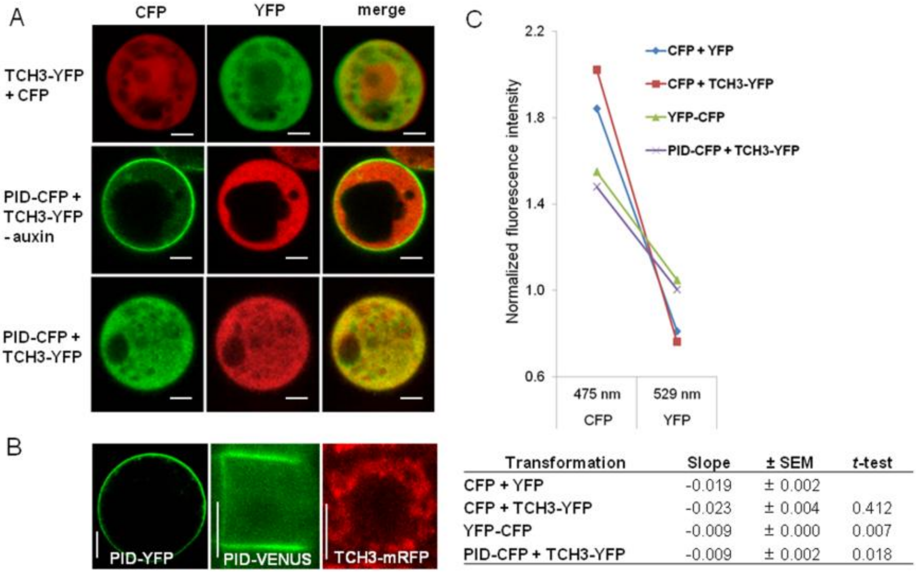
A
CFP
YFP
merge
TCH3-YFP + CFP
PID-CFP + TCH3-YFP - auxin
PID-CFP + TCH3-YFP
C
Normalized fluorescence intensity
2.2
1.8
1.4
1.0
0.6
475 nm CFP
529 nm YFP
CFP + YFP
CFP + TCH3-YFP
YFP-CFP
PID-CFP + TCH3-YFP
B
PID-YFP
PID-VENUS
TCH3-mRFP

Transformation	Slope	± SEM	*t*-test
CFP + YFP	-0.019	± 0.002	
CFP + TCH3-YFP	-0.023	± 0.004	0.412
YFP-CFP	-0.009	± 0.000	0.007
PID-CFP + TCH3-YFP	-0.009	± 0.002	0.018

Figure 2 Auxin-dependent interaction with TCH3 sequesters PID from the PM to the cytosol in *Arabidopsis* protoplasts.

(A) The indicated YFP and CFP fusion proteins were (co-)expressed from *35S* promoter-driven constructs, and CFP channel-, YFP channel-, and merged images of representative protoplasts are shown per transfection. TCH3-YFP is cytoplasmic and unlike CFP excluded from the nucleus (1st row). In auxin-starved protoplasts, PID-CFP localizes to the plasma membrane (PM) and TCH3-YFP to the cytosol (2nd row), however, when protoplasts are cultured in the presence of NAA, PID co-localizes with TCH3 in the cytosol (3rd row).

(B) PID-YFP expressed in auxin-cultured cells shows clear PM localization (left image). In root epidermis cells PID-VENUS also shows predominant PM localization (middle image), whereas TCH3-mRFP is localized in the cytosol (right image).

(C) Fluorescence resonance energy transfer (FRET) analysis by lambda scanning of 3 separate locations in 3 different representative protoplasts. The graph shows the average normalized fluorescence intensities (see materials and methods) at 475 nm (CFP emission peak) and 529 nm (YFP emission peak) using an excitation wavelength of 457 nm (donor, CFP) in *Arabidopsis* protoplasts co-expressing CFP and YFP (diamond, blue line, negative control), CFP and TCH3-YFP (square, red line, negative control), a translational fusion between YFP and CFP (triangle, green line, positive control), or PID-CFP and TCH3-YFP (cross, purple line). The significant decrease in the slopes of the lines representing the PID-CFP and TCH3-YFP co-expressing and the YFP-CFP expressing protoplasts compared to those of the negative controls (Table, Student's *t*-test, $p < 0.05$) is indicative for the occurrence of FRET. Size bars in A and B are 10 µm.

When the *35S::PID-CFP* and *35S::TCH3-YFP* constructs were cotransfected in auxin-starved *Arabidopsis* protoplasts, PID-CFP and TCH3-YFP remained at their respective subcellular location, showing only weak overlap in the cytosol (Figures 2A, middle panel). However, when cells were cultured in normal auxin-containing medium, PID-CFP showed predominant cytosolic localization in the presence of TCH3-YFP (Figures 2A, lower panel), suggesting that an auxin-dependent interaction with TCH3 sequestered PID from the PM.

To confirm the *in vivo* interaction between the two proteins, we checked for Förster (Fluorescence) Resonance Energy Transfer (FRET) between the CFP and YFP moieties of the co-expressed fusion proteins using confocal lambda scanning (Siegel et al., 2000). No acceptor spectral bleed-through occurred in control protoplasts co-expressing cytosolic CFP and YFP, meaning that YFP (excitation of 514 nm) was not excited by the CFP excitation wavelength (457 nm) and vice versa (data not shown). However, excitation with 457 nm led to a significant CFP-derived signal at the YFP emission wavelength (529 nm) in the samples where *35S::PID-CFP* and *35S::TCH3-YFP* were co-transfected (Figure 2C). The significant FRET signal in these samples was characterized by a quenched signal at the CFP emission wavelength (475 nm) and an enhanced signal at the YFP emission wavelength (527 nm), as compared to control transfections with non-interacting versions of CFP and YFP (*35S::CFP* co-transfected either with *35S::TCH3-YFP* or with *35S::YFP*). The lambda scanning profile matched that of protoplasts expressing a YFP-CFP fusion protein for which FRET is expected (Figures 2C). These data corroborate our earlier hypothesis that TCH3 sequesters PID from the PM to the cytoplasm upon interacting with the protein kinase.

The PID homolog WAG2 also interacts with TCH3

In view of the functional redundancy between PID and its close homologs (Dhonukshe et al., 2010), we analyzed whether the AGC3 kinases WAG1, WAG2 and AGC3-4 interact with TCH3 by *in vitro* pull-down assays. A His-tagged version of TCH3 was pulled down with GST-PID and -WAG2, but not with GST-WAG1 or GST alone. A very weak band could be observed in the pull down with AGC3-4, suggesting a weak interaction between this kinase and TCH3 (Supplementary Figure S1A).

To confirm these findings *in vivo*, we performed FRET and sequestration analysis on auxin-cultured *Arabidopsis* protoplasts co-expressing the kinase-CFP and TCH3-YFP fusion proteins. A significant relative FRET signal could be detected in protoplasts that co-expressed TCH3-YFP and PID-CFP or WAG2-CFP, whereas co-expression of TCH3-YFP with WAG1-CFP or AGC3-4-CFP resulted in background FRET levels (Supplementary Figure S1B). As observed before (Figure 2A), PID-CFP was sequestered by TCH3-YFP from the PM to the cytoplasm, and the same was observed for WAG2-CFP (Supplementary Figure S1C). In contrast, WAG1-CFP remained at the PM, corroborating the previous *in vitro* pull down and FRET results that WAG1 does not interact with TCH3. Also for AGC3-4-CFP no clear change in subcellular localization could be observed (Supplementary Figure S1C). This latter kinase, however, already showed strong cytosolic and nuclear localization (Supplementary Figure S1C), so it is difficult to draw any conclusion for this kinase from this specific experiment. These data indicate that TCH3 interacts significantly with PID and WAG2 to regulate the activity of these AGC3 kinases in response to changes in $[Ca^{2+}]_{cyt}$.

Auxin-induced sequestration of PID in root epidermis cells is Ca^{2+}- and TCH3-dependent

Previous studies already indicated that expression patterns of *PID* and *TCH3* overlap (Sistrunk et al., 1994; Antosiewicz et al., 1997; Benjamins et al., 2001; Michniewicz et al., 2007). As shown by a *TCH3::TCH3-GUS* translational fusion, *TCH3* is expressed in epidermis cells of the root elongation zone (Supplementary Figure S2A). Upon IAA or NAA treatment for 1 hour, *TCH3* expression was strongly induced in the root tip, and extended to the vasculature and the epidermis of the complete root (Supplementary Figures S2B, G). Also the *PID* gene is auxin responsive and expressed in epidermis cells in the elongation zone of the root tip ((Benjamins et al., 2001; Michniewicz et al., 2007); Figure 3A, 7A) implying the possibility of a functional *in vivo* interaction between the two proteins in these cells. Interestingly, in the same cells auxin treatment triggers a rise in $[Ca^{2+}]_{cyt}$ within seconds and pre-treatment with the Ca^{2+} channel blocker lanthanum chloride ($LaCl_3$) completely inhibits these auxin-induced Ca^{2+} transients (Monshausen et al., 2011). Based on these data we hypothesized that the auxin-induced, TCH3-dependent sequestration of PID observed in protoplasts should also occur in root epidermis cells. To test our hypothesis we used the *PID::PID-VENUS* line (Michniewicz et al., 2007). Without any treatment PID-VENUS localized both at the PM and in the cytoplasm (Figure 3A and Supplementary Figure S3A). IAA treatment, however, resulted in a release of PID-VENUS from the PM to the cytoplasm within 5 minutes, and PM localization was restored 10 minutes after IAA addition (Supplementary Figure S3B-F). Pre-treatment of seedlings with $LaCl_3$ did not influence PID localization by itself (Supplementary Figure S3G), but did inhibit IAA-induced dissociation of PID-VENUS from the PM (Supplementary Figure S3H). In contrast to protoplasts, the IAA induced dissociation of PID-VENUS from the PM in root epidermis cells occurred only transiently. As it has been experimentally established that IAA is very unstable under tissue culture conditions (Paciorek et al., 2005; Korasick et al., 2013), and the stable auxin analog naphthalene-1-acetic acid (NAA) was used in protoplast experiments, we repeated the treatments of *PID::PID-VENUS* roots with NAA. Like with IAA, PID internalization was observed after 5 minutes of NAA treatment (Figure 3B and Supplementary Figure S3I-L). This time, however, PID localization at the PM was not restored, and the kinase remained internalized after prolonged treatment (Figure 3C, D). Quantification showed that PID internalization gradually became stronger in time (Figure 3M). This data indicated that the restoration of PM localization after IAA treatment was due to IAA instability. Pre-treatment of seedlings with $LaCl_3$ again inhibited NAA-induced dissociation of PID from the PM (Figures 3F-H, M), confirming that also the NAA-triggered response is dependent on the activity of PM-localized Ca^{2+} channels.

To analyze the involvement of TCH3 in auxin–triggered PID internalization, we selected the *Arabidopsis tch3-3* allele, with a T-DNA insertion at position -71 of the *TCH3* gene. This allele, was reported to be a complete loss-of-function mutant, based on Northern- and Western blot analysis (J. Braam, pers. com.), but did not display any obvious phenotypes, suggesting that TCH3 is functionally redundant with other CML proteins (McCormack and Braam, 2003). In the *tch3-3* background, NAA-induced PID-VENUS internalization was delayed but not abolished (Figure 3M).

These data corroborated our hypothesis that, like in protoplasts, auxin-triggered PM dissociation of PID occurs in root epidermis cells, and that this response involves $LaCl_3$-sensitive Ca^{2+} channels and the Ca^{2+}-dependent binding of TCH3 or other redundantly acting CaMs or CMLs.

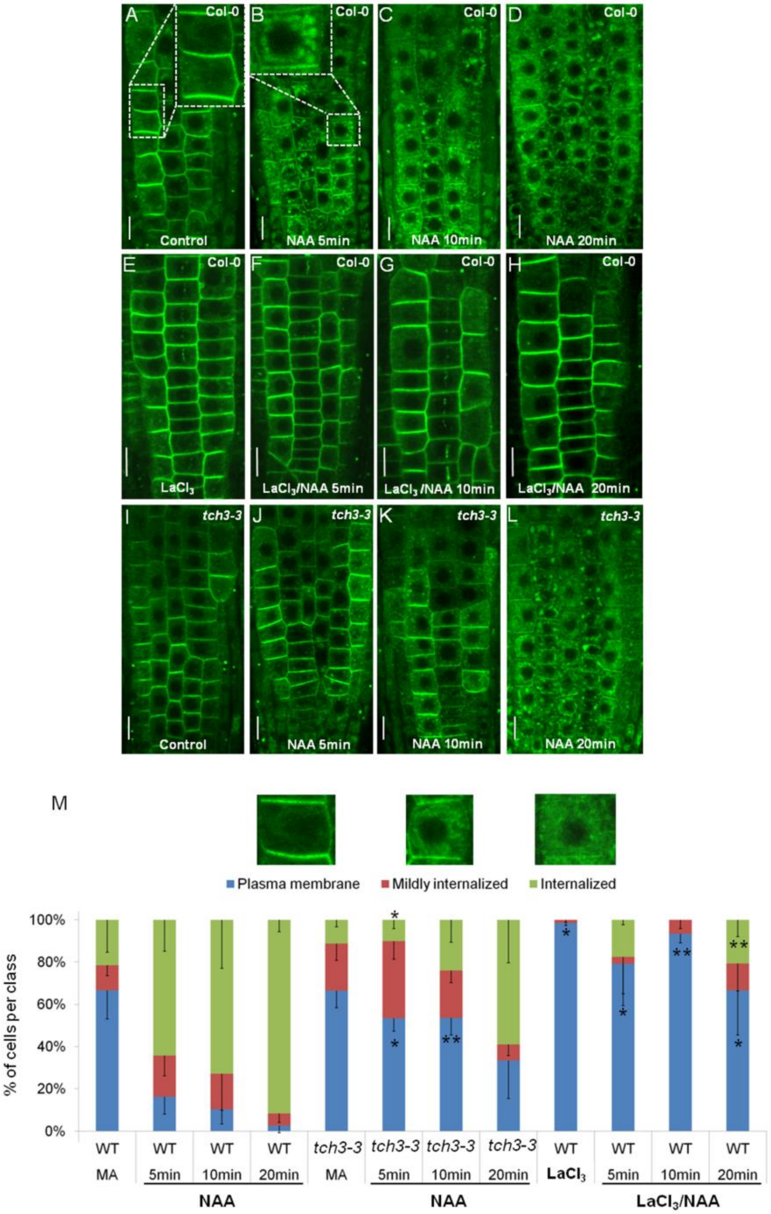
A
Col-0
Control
B
Col-0
NAA 5min
C
Col-0
NAA 10min
D
Col-0
NAA 20min
E
Col-0
LaCl3
F
Col-0
LaCl3/NAA 5min
G
Col-0
LaCl3 /NAA 10min
H
Col-0
LaCl3/NAA 20min
I
tch3-3
Control
J
tch3-3
NAA 5min
K
tch3-3
NAA 10min
L
tch3-3
NAA 20min
M
Plasma membrane
Mildly internalized
Internalized
% of cells per class
100%
80%
60%
40%
20%
0%
WT MA
WT 5min
WT 10min
WT 20min
tch3-3 MA
tch3-3 5min
tch3-3 10min
tch3-3 20min
WT LaCl3
WT 5min
WT 10min
WT 20min
NAA
NAA
LaCl3/NAA
*
**

Figure 3 Auxin-induced internalization of PID:VENUS in *Arabidopsis* root epidermis cells is Ca^{2+}- and

TCH3-dependent.

(A-L) Auxin treatment (5 µM NAA) induces rapid internalization of PID-VENUS in *Arabidopsis* root epidermis cells of four days-old seedlings (A-D), but not after 30 minutes pre-treatment with 1.25 mM of the Ca^{2+} channel blocker $LaCl_3$ (E-H). Auxin-induced PID-VENUS internalization is delayed in the *tch3-3* mutant background (I-L). Scale bars represent 10 µm.

(M) Quantification of the results exemplified in A-L as percentage of cells displaying PM (mainly PM-localized PID, blue), mildly internalized (still some PM-localized PID visible, red), or completely internalized (no visible PM-localized PID, green) PID-VENUS signal in wild-type or *tch3-3* mutant seedlings. Values are based on 125 to 335 root epidermal cells in 4 to 9 seedlings. MA = MA medium (untreated). Error bars represent standard error of the mean. Asterisks indicate values from *tch3-3* and $LaCl_3$-treated seedlings that are significantly different from WT at the same time point: *$p<0.05$; **$p<0.01$ (*t*-test).

TCH3 expression affects PID activity by reducing its PM localization

In contrast to the *tch3-3* loss-of-function mutant, which did not show obvious phenotypes, *35S::TCH3* overexpression seedlings showed a significant reduction in root length (Figure 4A, B). The *pidwag1wag2* triple loss-of-function mutant also showed a reduced root length (Dhonukshe et al., 2010), and this together with the observed negative effect of TCH3 on the *in vitro* activity of PID (Figure 1A) suggested that *TCH3* overexpression resulted in reduced AGC3 kinase activity. To test this, we combined *TCH3* overexpression with the *PID::PID-VENUS* reporter or with *PID* overexpression. PID-VENUS showed a significantly increased internalization in the *TCH3* overexpression background compared to wild-type. Even without any auxin treatment, only 5% (39/758) of the *TCH3* overexpressing cells showed PM-localized PID-VENUS, whereas this was 69% (546/790) in wild-type cells (Figure 4C). In the strong *35S::PID-21* line, a basal-to-apical PIN polarity switch triggers a reduction in the root tip auxin maximum, causing the main root meristem to differentiate and collapse (Benjamins et al., 2001; Friml et al., 2004). This phenotype is observed in only 5 % of the seedlings at 3 days after germination (DAG), but occurs in up to 97 % of the seedlings at 6 DAG (Figure 4D). Overexpression of *TCH3* significantly reduced the *PID* overexpression-induced root meristem collapse (Figure 4D) from 75 % to 31 % at 4 DAG (Student's *t*-test, $p < 0.05$) and from 97 % to 81 % at 6 DAG (Student's *t*-test, $p = 0.06$). The levels of *PID* and *TCH3* expression were more or less comparable in 5 days old *35S::PID-21*, *35S::TCH3-4*, or *35S::PID-21/35S::TCH3-4* seedlings (Figure 4D). These observations corroborate the proposed role of TCH3 as negative regulator of

PID kinase activity (above, and (Benjamins et al., 2003)), and make it tempting to speculate that the delay in the *35S::PID-21* root meristem collapse in the *TCH3* overexpression background would be due to TCH3 binding, leading to inhibition of PID kinase activity and strong PID internalization away from its phosphorylation targets.

Previously we have shown that the *PID* overexpression induced root collapse could be rescued by genetic backgrounds or treatments that increased the auxin maximum in the root tip (Benjamins et al., 2001). For *TCH3* overexpression seedlings we found that the auxin maximum in the root tip was enhanced, as visualized by the enhanced expression of the *DR5::GFP* reporter in the columella root cap (Figure 4E) and the reduced expression of the *35S::DII-VENUS* reporter in the root epidermis (Figure 4G). This explains the reduced root length of *TCH3* overexpression seedlings (Figure 4B) as well as the delay in *PID* overexpression-induced root meristem collapse observed in the *35S::TCH3* background (Figure 4D).

The enhanced auxin maximum in *35S::TCH3-2* roots pointed toward changes in PIN polarity, especially in epidermis cells of the root tip where constitutive PID internalization was observed (Figure 4C). In these cells, PID partially colocalizes with PIN2 at the apical PM (Michniewicz et al., 2007), and PID-mediated phosphorylation of the PIN2 hydrophilic loop (PIN2HL) is required for apical PIN2 localization in the distal epidermis- and lateral root cap cells (Dhonukshe et al., 2010). In *35S::TCH3-2* root epidermis cells, PIN2-GFP showed increased localization to the lateral membranes compared to wild-type roots, as demonstrated by a significant decrease of the apical/lateral PIN2-GFP ratio in the *TCH3* overexpression background (Figures 4F).

Previously we showed that *in vitro* binding of TCH3 to PID is Ca^{2+} dependent (Benjamins et al., 2003), which is in line with the observed Ca^{2+}- and TCH3-dependency on auxin-induced PID internalization in the wild type background. However, the enhanced PID internalization observed in the *TCH3* overexpression background occurs in the absence of exogenous auxin, suggesting that the sensitivity of PID for Ca^{2+}-dependent internalization is regulated by the *TCH3* expression levels, and thus by the TCH3 protein abundance.

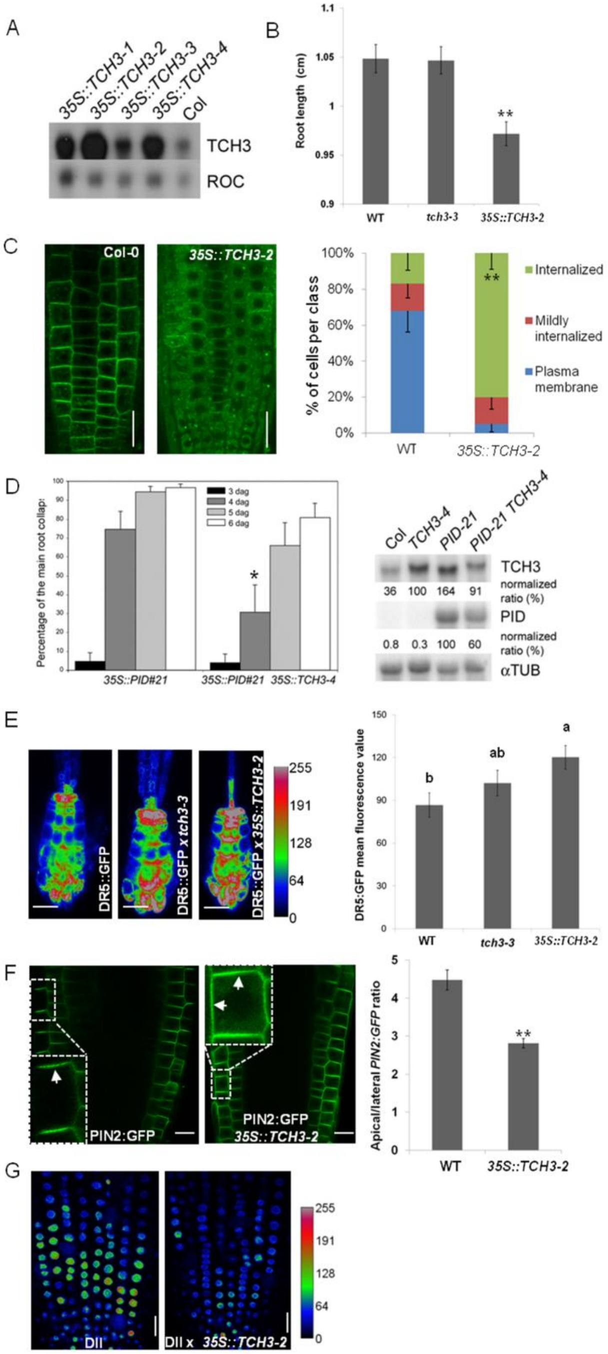

Figure 4 ***TCH3*** **overexpression reduces PID PM localization and activity.**

(A) Northern blot analysis showing the level of *TCH3* overexpression in four independent *35S::TCH3* lines (top). Hybridization with the *ROC* cDNA was used as loading control (bottom).

(B) Roots of 5-days old *35S::TCH3-2* seedlings are significantly shorter than those of wild-type (WT) and *tch3-3* seedlings (n=108 - 120).

(C) Confocal images (left, size bar indicates 10 µm) and quantification of these images (right panel) showing PID-VENUS internalization in root epidermis cells (n=790 and 758, respectively) of 15 *PID*::*PID-VENUS* or *35S::TCH3-2*/*PID*::*PID-VENUS* roots. Internalization is expressed as percentage of cells displaying PM (blue), mildly internalized (red), or completely internalized (green) PID-VENUS signal.

(D) *PID* overexpression-induced collapse of the main root meristem is significantly delayed in the *35S::TCH3-4* background (left panel). Northern blot analysis shows the expression level of *TCH3* (top), *PID* (middle) and *α-Tubulin* (bottom) in seedlings of the lines used in (left panel). The same blot was successively hybridized with the *PID*, *TCH3* or *α-Tubulin* cDNA as probe. Intensities were quantified using ImageQuant and normalized to the corresponding *α-Tubulin* sample to compensate for loading differences. The sample with *TCH3* or *PID* overexpression alone was put at 100%.

(E) *DR5::GFP* signal in WT, *tch3-3* and *35S::TCH3-2* root columella cells (images on the left), and quantification of these GFP signals (graph on the right). The significantly different classes are indicated with a to b ($p<0.05$, *t* test). The DR5::GFP signal intensity is color-coded (from blue to red indicates low to high expression).

(F) Confocal images of PIN2-GFP localization in WT and *35S::TCH3-2* root epidermis cells (images on the left). Quantification of the apical/lateral PIN2-GFP ratio (graph on the right, the mean fluorescence intensity of apical versus outer lateral membrane) shows that PIN2-GFP is significantly more apolar in the *35S::TCH3-2* background.

(G) *35S::DII-Venus* signal in WT (left) and *35S::TCH3-2* root tip epidermis cells (right).

Error bars in B, C, E and G represent the standard error of the mean, and significant differences are indicated with asterisks: $^{*}p<0.05$; $^{**}p<0.01$ (*t* test). The DII-Venus signal intensity is color-coded (from blue to red indicates low to high expression).

Ca^{2+} acts downstream of auxin during root gravitropism

It is well-established that root gravitropic growth is mediated by the PIN-driven asymmetric distribution of auxin over the root tip, resulting in differential elongation of cells at the upper and lower site of the root (Friml et al., 2002; Friml, 2003; Tanaka et al., 2006). At the same time, Ca^{2+} signaling has been reported to be important during root gravitropism (Poovaiah et al., 1987; Roux and Serlin, 1987). Concentration peaks of cytoplasmic Ca^{2+} have been found to coincide with the basipetal movement of auxin at the lower side of the root from the root tip toward the elongation zone, and auxin treatment was shown to trigger a rise in cytosolic Ca^{2+} within seconds, indicating that Ca^{2+} acts downstream of auxin (Monshausen et al., 2011). Despite these investigations, however, it is still unclear whether Ca^{2+} only acts downstream of auxin, especially since Ca^{2+} signaling in the columella root cap has been suggested to be important for the onset of root gravitropism (Moore, 1985; Poovaiah et al., 1987). To investigate the timing of Ca^{2+}- and auxin signaling during the root gravitropic response, we gravity-stimulated roots in the presence of the Ca^{2+} channel inhibitor $LaCl_3$ or the PAT inhibitor NPA. Global application of 1.25 mM $LaCl_3$ blocked the root gravitropic response (Figure 5G), but not the *DR5::GFP* (Ottenschlager et al., 2003) or *35S::DII-VENUS* (Brunoud et al., 2012) reported asymmetric auxin distribution (Figure 5B, 5D, Supplementary Figure S4). In contrast, global application of 10 µM NPA blocked gravity response (Figure 5H), as well as the establishment of an asymmetric *DR5::GFP* signal after gravity-stimulation (Figure 5C, D). These two experiments indicate that Ca^{2+} acts downstream of auxin redistribution during root gravitropism. Quantification of the asymmetric *DR5* signal 5.5 hours after gravistimulation showed that the intensity of the signal at the lower side of $LaCl_3$ treated root tips was reduced compared to untreated root tips (Figure 5E). This indicates that PIN-dependent auxin transport might be impaired in $LaCl_3$-treated gravity-stimulated seedling roots. Because 1.25 mM $LaCl_3$ might affect root gravitropism due to its inhibitory effect on root growth (Figure 5K), we performed the same tests on seedlings grown on a lower concentration (0.63 mM) that did not perturb root growth (Figure 5K), but did significantly delay gravity-dependent root bending (Figure 5I and J). From the effects of the drug treatments on the auxin response reporters and the root growth response we concluded that Ca^{2+} signaling is needed in the root gravitropic response, downstream of the asymmetric auxin redistribution, to maximize the asymmetric auxin response in the root tip, and thereby the speed of root bending.

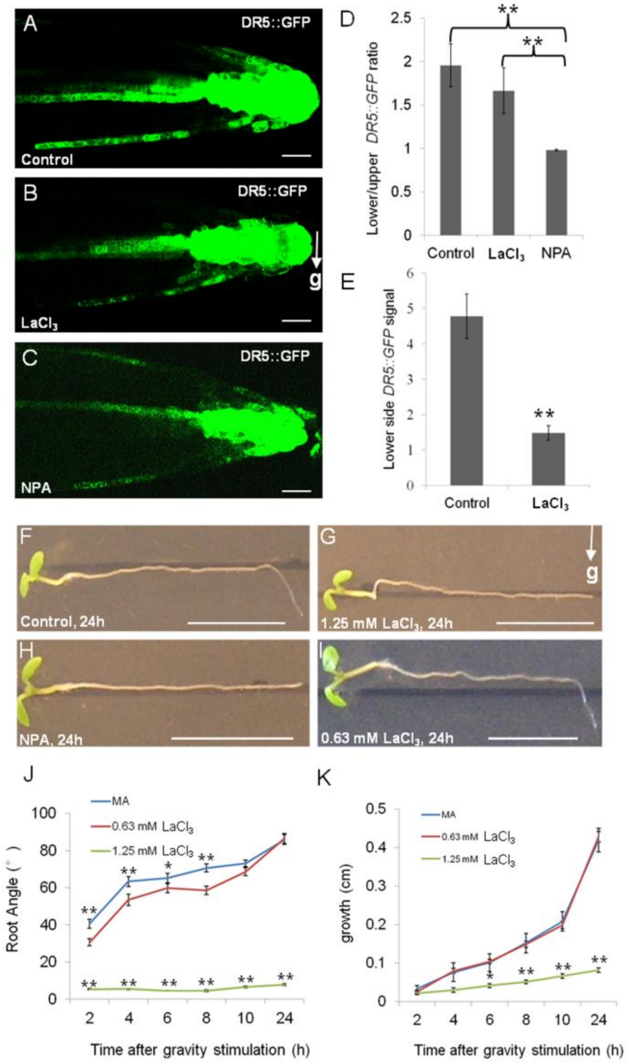

Figure 5 Ca^{2+} acts downstream of PIN-driven differential auxin responses during gravitropic root growth.

(A-E) Auxin response in *Arabidopsis* root tips 5.5 hours after gravity-stimulation, as indicated by the auxin responsive *DR5::GFP* reporter. Both untreated (A, D) and 1.25 mM $LaCl_3$ treated (B, D) roots show a clear asymmetric auxin response, whereas blocking polar auxin transport (10 µM NPA) results in a symmetric response (C, D). The mean intensity per pixel of the *DR5::GFP* signal at the lower side of $LaCl_3$–treated root tips is significantly reduced compared to untreated gravistimulated control roots (E).

(F-I) Growth response of 5-days old seedling roots after 24 hours gravistimulation, on control medium (F), or medium with 1.25 mM $LaCl_3$ (G), 10 μM NPA (H) or 0.63 mM $LaCl_3$ (I).

(J) Quantification of the gravitropic response of roots of 5-days old *Arabidopsis* seedlings on MA medium without or with 0.63 mM or 1.25 mM $LaCl_3$.

(K) Quantification of the root growth (in cm) of seedlings in J from the start of the experiment.

Error bars in D, E, J and K represent the standard error of the mean, and significant differences are indicated with asterisks: $*p<0.05$; $**p<0.01$ (*t*-test). A white arrow (g) in B and G indicates the gravity direction. Scale bars in A to C = 20 μm. Scale bars in F to I = 0.5 cm.

TCH3-mediated control of PIN2 polarity maximizes the root gravitropic response

In order for the auxin-induced Ca^{2+} signaling in the epidermis cells at the lower side of the root to have an effect on the root gravitropic response, the Ca^{2+} transients need to be translated by Ca^{2+} sensors, such as TCH3. Both *tch3-3* loss-of-function and *35S::TCH3-2* gain-of-function seedlings showed a delay in root bending upon gravity-stimulation (Figure 6A), indicating a role for TCH3 in root gravitropism, and also suggesting that asymmetric expression of *TCH3* is important. Indeed, *TCH3::TCH3-GUS* seedlings showed asymmetric GUS staining at the lower side of root tips after 2-6 hours of gravistimulation (Figure 6B), which corresponds to the timing of the asymmetric auxin response in gravity stimulated root tips (Band et al., 2012), and is in line with *TCH3* being an auxin responsive gene (Antosiewicz et al., 1995; Benjamins et al., 2003). The reduced gravitropic response correlated with a significantly reduced lower/upper *DR5::GFP* ratio in *tch3-3* root tips (1.25) compared to that in wild-type (1.60) (Figure 6C). This again confirmed a role for TCH3 in optimizing root gravitropism by maximizing the differential auxin response in the root tip. In line with the previously observed enhanced auxin response in *35S::TCH3-2* root epidermis cells (Figure 4G), the mean lower/upper *DR5* ratio of gravity stimulated *35S::TCH3-2* root tips was slightly reduced, but the difference with wild-type roots was not significant (Figure 6C).

The clear involvement of TCH3 in root gravitropism suggested that auxin-induced TCH3-mediated PID internalization forms an integral part of the root gravitropic response. Indeed, when root tips of *PID::PID-VENUS* seedlings were gravity stimulated for 3 hours, PID-VENUS showed enhanced internalization in epidermis cells at the lower side of the root tip, whereas the kinase still showed predominant PM localization in epidermis cells at the upper side of root tip (Figure 6D). In roots incubated on medium supplemented with $LaCl_3$, no enhanced PID internalization was observed following gravistimulation (Figure 6D), confirming that auxin-triggered Ca^{2+} signaling is required for PID internalization.

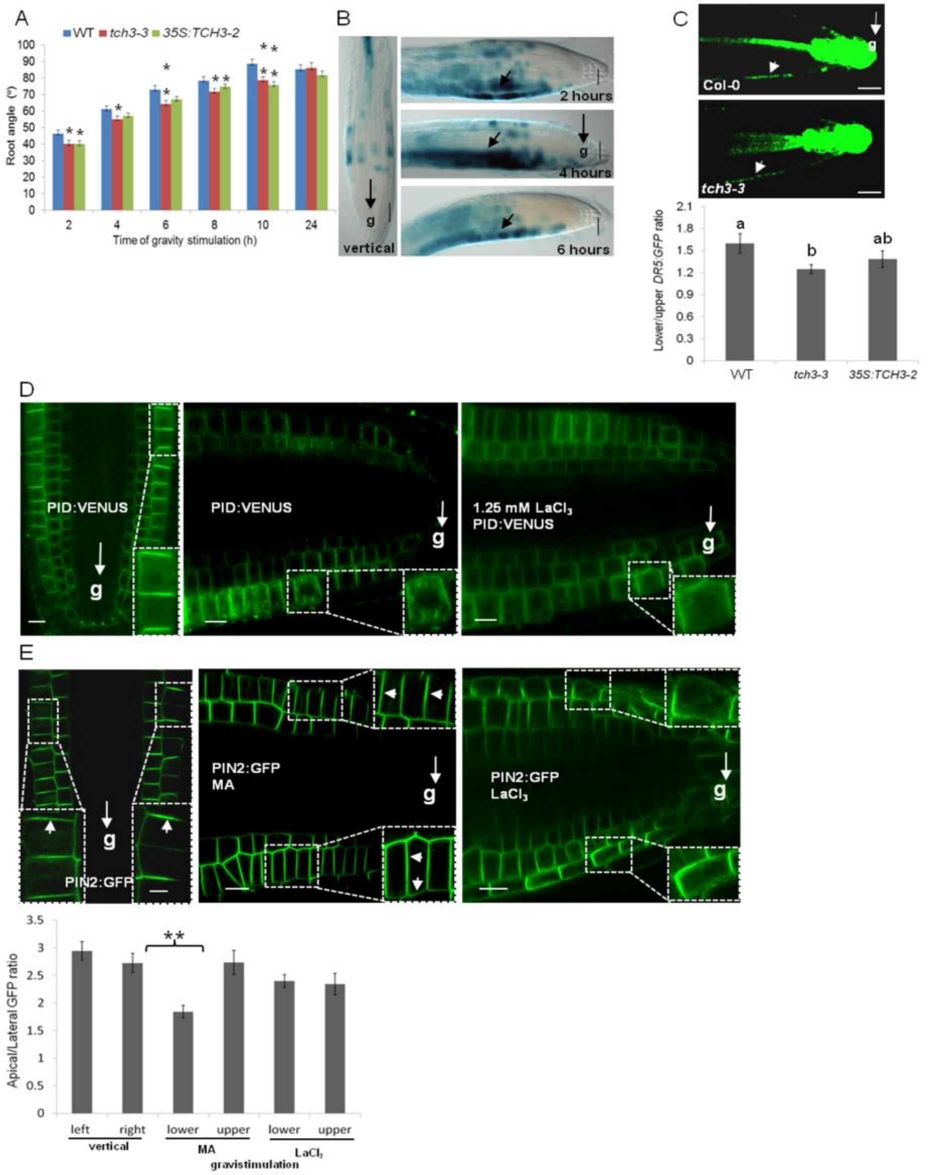

Figure 6 TCH3-mediated PID internalization and PIN2 depolarization maximizes the root gravitropic response.

(A) Five-days old *tch3-3* loss-of-function mutant and *35S::TCH3-2* overexpression seedlings show a delayed root gravitropic response compared to wild-type (WT) seedlings.

(B) DIC images of GUS stained root tips of vertically grown *TCH3::TCH3-GUS* seedlings, or at 2, 4, or 6 hours after gravistimulation. Positions of enhanced GUS expression are marked by white arrows.

(C) Confocal images of root tips of five-days old *DR5::GFP* (WT) and *tch3*-3/*DR5::GFP* seedlings at 5.5 hours after gravistimulation. The graph shows the the ratio of the *DR5::GFP* signal in the upper and lower lateral root cap cells of wild-type (WT), *tch3*-3 *and 35S::TCH3-2* roots.

(D) In root epidermis cells of four-days old vertically grown *PID::PID-VENUS* seedlings, PID-VENUS is predominantly PM-localized (left image). Three hours of gravistimulation induces dissociation of PID-VENUS from the PM in cells at the lower side of the root tip (middle image), and this is inhibited by 1.25 mM $LaCl_3$ (right image).

(E) At 3.5-5 hours after gravistimulation, the polarity of PIN2-GFP (*PIN2::PIN2-GFP*) in the lower epidermis cells shifts from predominantly apical (rootward) in untreated root tips (left image and graph) to a more apolar localization in gravistimulated root tips (middle image and graph). $LaCL_3$ treatment prevents PIN2 apolarization (right image and graph). MA indicates MA medium without $LaCL_3$.

A white arrow (g) in B, C, D and E indicates the gravity direction. Arrow heads in E mark PIN2-GFP polarity. Scale bars indicate 20 μm in B and C, and 10 μm in D and E. Error bars in A, C and E represent the standard error of the mean, and significant differences in A and E are indicated with asterisks: *$p<0.05$; **$p<0.01$ (*t*-test). Significantly different values in the graph in C are classified with a and b ($p<0.05$, *t*-test).

As was shown for *TCH3* overexpression roots (Figure 4G), we expected the enhanced PID internalization at the lower side of the gravity stimulated roots to lead to PIN2 depolarization. Indeed, PIN2-GFP showed a reduced apical-lateral polarity ratio in epidermis cells at the lower side of roots 3.5 hours after gravistimulation, whereas in epidermis cells at the upper side of the root this ratio was comparable to that in epidermis cells of unstimulated roots (Figure 6E). No significant difference in the apical-lateral PIN2 ratio between the upper side and lower side of gravistimulated root tips was observed after $LaCl_3$ treatment (Figure 6E).

In conclusion, upon gravistimulation, auxin accumulation in the lower root epidermal cells induces PID internalization, by the increase in *TCH3* expression and at the same time by enhancing the TCH3-PID interaction through an increase in cytosolic

Ca^{2+}. This internalization leads to PIN2 apolarity, which is necessary to maximize the auxin response at the lower side of the root tip. This is in line with the observation that inhibition of Ca^{2+} influx leads to a reduced differential auxin response (Figure 5B, E), whereas kinase loss-of-function or PIN2 loss-of-phosphorylation leads to an increased auxin response in the lateral root cap (Dhonukshe et al., 2010).

Discussion

Ca^{2+} is a common second messenger in signaling pathways, and has been found as one of the early signals in response to the plant hormone auxin. Experiments on plant cells have shown that the $[Ca^{2+}]_{cyt}$ is increased within a few minutes after auxin application (Felle, 1988; Gehring et al., 1990b; Shishova and Lindberg, 2004; Monshausen et al., 2011). Furthermore, Ca^{2+} has also been reported as an important second messenger in the regulation of PAT (dela Fuente and Leopold, 1973). Here we investigated a previously identified molecular link between Ca^{2+} and the regulation of PAT, being the interaction of the CML TCH3 with the PID kinase (Benjamins et al., 2003). Surprisingly, our research uncovered a new role for the Ca^{2+}-dependent binding of CaM/CML to substrate proteins, being the recruitment of a PM-associated kinase from the PM to the cytosol, away from its PIN phosphorylation targets. Our results further clarify the molecular link between Ca^{2+} signaling and auxin transport, and suggest that beside its role in optimizing the root gravitropic response through regulation of PIN2 localization and auxin redistribution, the CML-kinase complex might be a generic signaling route through which auxin or other (environmental) signals that trigger a Ca^{2+} response can modulate PAT.

Ca^{2+}/calmodulin-regulated PM association: a novel mechanism to regulate kinase activity

Previously, we used *in vitro* pull down assays to show that TCH3 interacts with PID in a Ca^{2+}-dependent manner (Benjamins et al., 2003). Here, a similar assay was used in combination with PID deletion constructs to show that TCH3 interacts with the PID catalytic domain. Moreover, co-expression of TCH3-YFP and PID-CFP in *Arabidopsis* protoplasts and subsequent FRET measurements demonstrated the *in vivo* interaction between the two proteins, and showed that TCH3-YFP sequesters the active PM-associated PID-CFP kinase fusion protein to the cytoplasm. This suggests that interaction between TCH3 and PID provokes the release of the kinase from the PM. This sequestration of PID is auxin-dependent, as auxin-starved protoplasts do not show internalization of PID. In addition, in root epidermis cells we observed that minutes after auxin treatment PID-VENUS is sequestered from the PM to the cytosol. Our data indicate that TCH3 is at least partially responsible for this process, and that most likely other CaMs/CMLs act redundantly with TCH3. As in the protoplast system, treatment with the auxin analog NAA resulted in rapid and more long term cytosolic localization of PID-VENUS (within 5 minutes for up to at least 1 hour), whereas, PM localisation of PID-VENUS was restored after 20 minutes when the natural auxin IAA was used. Previously, it was shown that the natural auxin is unstable in tissue culture, and is rapidly turned over, whereas NAA is not (Paciorek et al., 2005), and this is likely to explain the difference observed. In fact, a very transient increase in $[Ca^{2+}]_{cyt}$ (from few to 60 seconds, with a peak around 30 seconds) was detected in *Arabidopsis* root epidermis cell after application of 100 nM IAA (Monshausen et al., 2011), whereas the NAA-induced increase in $[Ca^{2+}]_{cyt}$ in wheat protoplasts lasted for at least 500 seconds (Shishova and Lindberg, 2004; Shishova et al., 2007). As long term elevation of $[Ca^{2+}]_{cyt}$ is toxic to cells (Swanson et al., 2011), the prolonged auxin-induced internalization of PID might be achieved by two parallel mechanisms: the rapid internalization is achieved by a rapid increase in $[Ca^{2+}]_{cyt}$, after which the internalization is maintained by auxin-induced *TCH3* expression, which enhances the sensitivity of the system to Ca^{2+}, thereby lowering the $[Ca^{2+}]_{cyt}$ required for prolonged PID internalization to sub-lethal levels. The observed oscillations in $[Ca^{2+}]_{cyt}$ might further reduce the toxicity of Ca^{2+} in the cytosol (Shishova and Lindberg, 2004; Shishova et al., 2007). During root gravitropism, PID internalization can only be observed several hours after the start of gravistimulation. Since the peak in $[Ca^{2+}]_{cyt}$ is already observed 6 minutes after gravistimulation, followed by moderately elevated $[Ca^{2+}]_{cyt}$ (Monshausen et al., 2011), PID internalization probably requires the induction of *TCH3* expression by auxin.

Data by Zegzouti and co-workers indicate that PID binds to phosphorylated inositides and phosphatidic acid, and that a specific amino acid sequence inside the PID catalytic domain (insertion domain) is the key determinant for its membrane association (Zegzouti et al., 2006). We therefore hypothesize that PID co-localizes at the PM with its phosphorylation targets, the PIN auxin efflux carriers (Michniewicz et al., 2007), through the interaction of the insertion domain with membrane components. An increase in $[Ca^{2+}]_{cyt}$, e.g. induced by auxin, facilitates binding of TCH3 to the catalytic domain of PID, thereby preventing the kinase-lipid interaction and resulting in sequestration of the kinase away from its phospho-targets to the cytoplasm (Figure 7A).

Based on this model, it would be interesting to test whether TCH3 and phosphoinositides are competing for the interaction with the PID catalytic domain.

PKC, one of the animal orthologs of the plant specific AGCVIII kinases to which PID belongs (Galván-Ampudia and Offringa, 2007; Rademacher and Offringa, 2012), directly binds Ca^{2+} through a C2 domain. Ca^{2+} binding to this domain promotes a change in PKC subcellular localization from cytosol to PM and enhances affinity of the C2 domain for phosphorylated inositides (Corbalan-Garcia et al., 2007). This PM translocation activates the PKC kinase. PID is also thought to be active at the PM. However, in this case, the (auxin-induced) increase in $[Ca^{2+}]_{cyt}$ results in the opposite effect and removes the kinase from the PM. PID does not have typical Ca^{2+} binding domains, and instead the kinase interacts in a Ca^{2+}-dependent manner with the Ca^{2+} receptor TCH3. An analogous system exists in animal cells, where a CaM competes with PM localized phosphatidylinositol 4,5 bisphosphate (PIP_2) for binding to a cluster of basic amino acid residues in peripheral- or transmembrane proteins, thereby pulling the cluster from the PM. In animal cells this system is used to regulate the levels of free PIP_2, or the activity of transmembrane receptors (McLaughlin and Murray, 2005). To our knowledge, the Ca^{2+}- and CaM-dependent release of the PID kinase from the PM is a new form of regulating the activity of a kinase that is designed to phosphorylate PM proteins.

TOUCHing PID: a regulatory loop that translates cellular Ca^{2+} levels to PIN polarity

Our findings on TCH3-mediated PID internalization can be integrated into the current *Arabidopsis*-based model for gravitropic root growth (Band et al., 2012; Baster et al., 2013). Gravistimulation of roots leads to rapid lateral relocation of PIN3 and PIN7 to the lower side of columella root cap cells (Friml et al., 2002; Kleine-Vehn et al., 2010), resulting in auxin transport from the auxin maximum at the root tip to the lateral root cap- and epidermis cells at the lower side of the root tip (Figure 7B: 5 minutes) (Band et al., 2012; Brunoud et al., 2012; Baster et al., 2013). The higher auxin levels in these cells lead to stabilization of PIN2 at the PM by inhibition of ABP1-mediated endocytosis, whereas PIN2 is degraded due to reduced auxin levels at the upper side of the root tip (Figure 7B: between 5 and 90 minutes) (Paciorek et al., 2005; Abas et al., 2006; Robert et al., 2010; Baster et al., 2013). The enhanced auxin levels at the lower side of the root tip also lead to a rapid increase in $[Ca^{2+}]_{cyt}$ and to an induction of *TCH3* expression (Antosiewicz et al., 1995; Monshausen et al., 2011). The elevated TCH3 levels together with the higher $[Ca^{2+}]_{cyt}$ result in sequestration of PID from the PM to the cytosol (Figure 7 A and B: between 1,5 to 5 hours). Consequently, a reduction of PM-associated PID levels eventually results in PIN2 apolar localization at the lower side of root tip, leading to enhancement of the asymmetric auxin distribution (Figure 7B: between 1.5-5 hours). This proposed model implies that a Ca^{2+} release negatively and transiently regulates PID activity through its TCH3-induced dissociation from the PM, away from its PIN phosphorylation-targets. The TCH3-dependent inactivation of PID may be part of a regulatory loop that allows fast and possibly subtle alterations in PIN polarity in response to signals that lead to rapid changes in cytosolic Ca^{2+} levels, such as auxin (Felle, 1988; Gehring et al., 1990b; Shishova and Lindberg, 2004) and unidirectional blue light or mechanical stress (Lee et al., 1984; Gehring et al., 1990b; Baum et al., 1999; Harada et al., 2003; Monshausen et al., 2009).

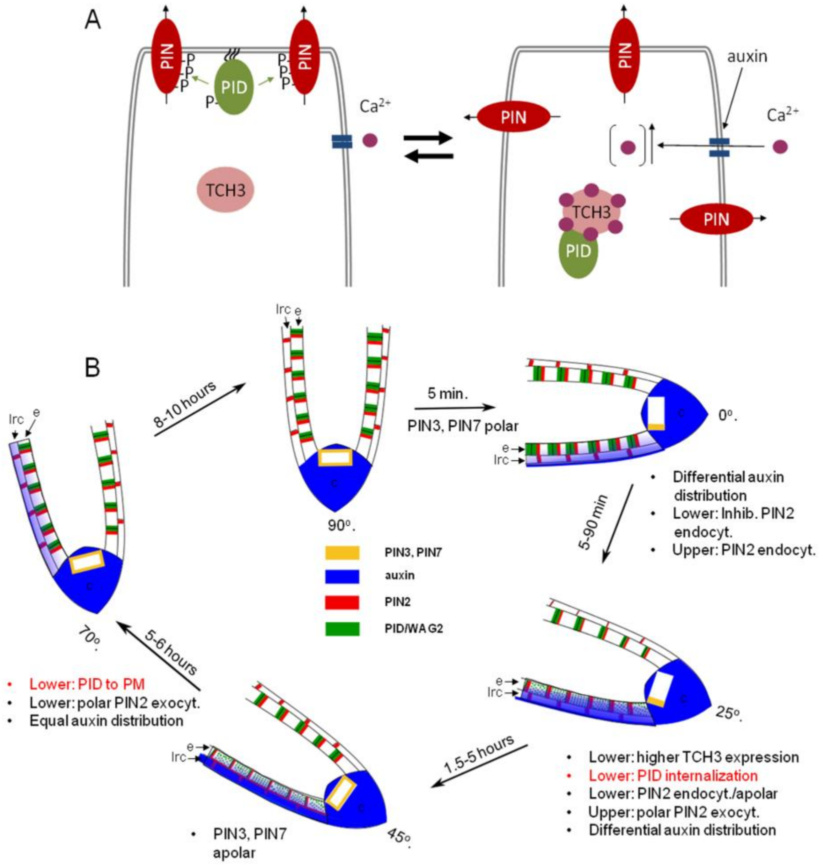
A
PIN
P
PID
Ca2+
TCH3
auxin
B
lrc
e
8-10 hours
5 min.
PIN3, PIN7 polar
0°.
90°.
PIN3, PIN7
auxin
PIN2
PID/WAG2
5-90 min
Differential auxin distribution
Lower: Inhib. PIN2 endocyt.
Upper: PIN2 endocyt.
25°.
1.5-5 hours
Lower: higher TCH3 expression
Lower: PID internalization
Lower: PIN2 endocyt./apolar
Upper: polar PIN2 exocyt.
Differential auxin distribution
45°.
PIN3, PIN7 apolar
5-6 hours
70°.
Lower: PID to PM
Lower: polar PIN2 exocyt.
Equal auxin distribution

Figure 7 TCH3-mediated PID sequestration and its role in auxin-directed PIN polarity regulation during root gravitropism

(A) Model for auxin-induced sequestration of PID from the PM to the cytoplasm. Elevated auxin levels increase the $[Ca^{2+}]_{cyt}$, by activating PM-localized Ca^{2+} channels. Binding of Ca^{2+} to the EF-hands of the calmodulin-like protein TCH3 enhances its affinity for PID, whereby TCH3 is able to compete for PID binding to PM components. This leads to sequestration of PID from the PM to the cytosol, away from its PIN phosphorylation targets, resulting in PIN dephosphorylation and apolarity.

(B) Model for the involvement of TCH3-mediated PID and /WAG2 sequestration in root gravitropism. In vertically oriented roots (90^o), PIN3 (yellow) is symmetrically distributed at the PM of columella cells, resulting in a uniform distribution of auxin (blue) from the columella to the lateral root cap and epidermis, where PID and WAG2, localized mainly at apical (shootward) and basal (rootward) PM (green), maintain an apical flow of auxin by directing apical localization of PIN2 (Red). Minutes after gravistimulation, PIN3 relocates to the lower side of columella cells (5 min), redirecting the auxin stream, and resulting in stabilization of PIN2 at the PM and in an enhanced auxin response at the lower side of the gravistimulated root (5-90 minutes). This auxin response on the one hand triggers Ca^{2+} channels, and on the other hand induces *TCH3* expression, causing gradual PID internalization at the lower epidermis of the root tip. The resulting reduction in PIN2 phosphorylation induces PIN2 apolar localization, thereby reducing the apical auxin flow and enhancing the auxin response at the lower lateral root cap and epidermis of the root tip. This mechanism maximizes the gravitropic growth response (1.5 – 5 hours), and provides feed back to the asymmetric root growth,at a later time point (5-6 hours)by normalizing PIN localization and restoring the auxin distribution to that of a vertically growing root (8-10 hours). lrc: lateral root cap; e, epidermis; c: columella.

By *in vitro* pull down assays and co-expression in *Arabidopsis* protoplasts we showed that not only PID, but also WAG2 interacts with and is sequestered by TCH3 from the PM. In view of the expression of WAG2 in epidermis cells of the root tip, it is likely that the TCH3-WAG2 interaction plays a role in root gravitropism. No clear interaction was observed between TCH3 and WAG1 or AGC3-4, indicating that the AGC3 kinases do not function completely redundant, and also that the amino acid sequence requirement for the interaction with TCH3 is only present in two of the four AGC3 kinases. Auxin is known to regulate its own transport, firstly by inhibiting ABP1-dependent PIN endocytosis (Paciorek et al., 2005; Robert et al., 2010), and secondly by regulating E3 ubiquitin ligase SKP-Cullin-F-box$^{TIR1/AFB}$ (SCF$^{TIR1/AFB}$)-dependent processes, such as canalization of the auxin flow in response to increased cellular auxin concentrations (Sauer et al., 2006), or enhanced PIN turnover by sub-optimal auxin levels (Baster et al., 2013). Sauer and co-workers still observed PIN lateralization in auxin-treated *35S::PID* seedlings, suggesting that PID is not involved in this SCF$^{TIR1/AFB}$-dependent process (Sauer et al., 2006). It will be interesting to test, however, whether the TCH3-mediated PID sequestration plays a role in SCF$^{TIR1/AFB}$-dependent PIN turnover. This would imply that a reduction in PM-associated PID, besides PIN2 depolarization, would also lead to enhanced PIN degradation, thereby providing a mechanism to normalize PIN2 levels to the situation before gravistimulation. Our results suggest that elevated cellular auxin levels may transiently alter PID kinase activity by subcellular localization changes and inhibition of its kinase activity via the interaction with TCH3. This sets the stage for a different type of auxin-dependent PIN lateralization, and leads to a subtle modulation of PIN polar targeting, e.g during tropic growth responses.

In conclusion, we show that during gravitropism asymmetric auxin transport and subsequently Ca^{2+} influx into epidermis cells at the lower side of the root tip stimulate TCH3-mediated sequestration of PID from the PM to the cytosol. As a consequence of PID inactivation PIN2 is dephosphorylated, causing apolar localization and possibly enhanced degradation of PIN2 at the lower side of the root tip. The reduced PAT results in enhanced auxin accumulation at this side. Hence accentuating the growth response mediated by the asymmetric auxin distribution (Figure 7).

Is ABP1 signaling involved in auxin-induced PID-TCH3 interaction?

The auxin-induced interaction between PID (or WAG2) and TCH3 can be observed already 5 minutes after auxin treatment. This rapid response suggests that the required increase in Ca^{2+} levels does not involve *de novo* gene transcription, but is rather mediated by rapid activation of Ca^{2+} channels at the PM. The ABP1 auxin receptor is known to be secreted to the extracellular space where it regulates cell elongation and cell division (Steffens et al., 2001; David et al., 2007; Braun et al., 2008; Dahlke et al., 2010), and its action has been linked to the promotion of clathrin-mediated endocytosis (Robert et al., 2010). Recent data indicate that auxin-induced ABP1 signaling to downstream non-transcriptional responses requires its interaction with a small subfamily of four Trans Membrane receptor-like Kinases (TMKs) (Xu et al., 2014). Being the only known auxin receptor at the PM, ABP1 is a likely candidate for mediating the auxin effects on cytosolic Ca^{2+} levels. We tested this possibility, by combining the *PID::PID-VENUS* reporter with the ethanol-inducible anti-ABP1 lines *SS12K9* and *SS12S6* or with the *abp1-5* allele containing a point mutation (His94->Tyr) in the auxin-binding pocket that is predicted to reduce auxin binding affinity (Woo et al., 2002; Braun et al., 2008; Xu et al., 2010). Unfortunately, ethanol treatment already led to complete PID-internalization in wild-type background, which prevented the use of the SS12K9 and SS12S6 lines for these experiments (data not shown). Moreover, in the *abp1-5* background we did not observed a significant reduction in auxin-induced PID-VENUS internalization (data not shown), mostly because PID-VENUS was already more internalized in this background. Interestingly, the abp1-5 mutant protein already shows some background interaction with TMK (Xu et al., 2014), suggesting that the observed enhanced PID-VENUS internalization is caused by a low level of constitutive TMK activation by the abp1-5 protein. In view of the strong effects of complete loss-of-function *abp1* mutations (Chen et al., 2001), and the sensitivity of PID-VENUS for internalization, it might be difficult to show unequivocally whether or not ABP1 is involved in triggering the Ca^{2+} signaling that leads to PID internalization.

Experimental procedures

Molecular cloning and constructs

Molecular cloning was performed following standard procedures (Sambrook, 1989). Bacteria were grown on LC medium containing 100 μg/ml carbenicillin (Cb, all high copy plasmids), 50 μg/ml kanamycin (Km, pGreen) or 250 μg/ml spectinomycin (Spc, pART 27) for *E.coli* strains DH5α or 20 µg/ml rifampicin (Rif) and 50 µg/ml Km, or 250 μg/ml Spc for *Agrobacterium* strain LBA1115 (Hood et al., 1993). The constructs *pSDM6008* (*pET16H:TCH3*), *pSDM6004* (*pGEX:PID*), *pSDM6005* (*pBluescript SK-PID*) and *pET16H:PBP1* were described previously (Benjamins et al., 2003). Primers used in this study are listed in Table 1. To obtain a plasmid encoding the GST-tagged first 100 amino acids of PID, the *Sal*I-*Sac*I (blunted) fragment from *pSDM6005* was cloned into the *Xho*I and *Hin*dIII (blunted) sites of *pGEX-KG* (Guan and Dixon, 1991). Fragments encoding the PID catalytic domain (aa 75-398) and the C-terminal part of PID (aa 339-438) were obtained by PCR amplification using the primer pairs PID PK CaD F-PID PK CaD R and PID PK CT F-PID PK CT R, respectively, and cloned into *pGEX-KG* using *Xho*I-*Hin*dIII (blunted) and *Eco*RI-*Hin*dIII (blunted), respectively.

Expression vectors *p35S::YFP* and *p35S::CFP* were obtained by inserting the *YFP-HA* and *FLAG-CFP* coding regions with appropriate restriction enzymes between the *CaMV 35S* promoter and the *CaMV 35S* terminator of *pART7*. Expression vectors *pGEX-PID*, *pGEX-WAG1*, *pGEX-WAG2*, *pGEX-AGC3-4*, *p35S::YFP-CFP*, *p35S::PID-CFP*, *p35S::WAG1-CFP*, *p35S::WAG2-CFP*, *p35S::AGC3-4-CFP*, *35S::TCH3-YFP and pET16H-PID* were constructed using the Gateway Technology (Invitrogen). BP reactions were performed in *pDONR207* according to manufacturer’s instructions (Invitrogen). LR reactions were performed in either the pGEX-based destination vector for N terminal fusions with the Glutathione-S-transferase (GST), or the *pART7*-based destination vectors. The *pART7*-based destination vectors were obtained by inserting the recombination cassette in frame with the *YFP-HA*, *FLAG-CFP* or *mRFP1* coding region between the *CaMV 35S* promoter and the *CaMV 35S* terminator. The *pGEX*-based destination vector was obtained by inserting the recombination cassette in frame with the *GST* coding region. For the *pGreenII-0229mRFP* destination vector, the recombination cassette in frame with the *mRFP1* coding region was excised from the *pART7*-based destination vector and cloned into *pGreenII0229* (Hellens et al., 2000). The coding region of *YFP-HA* was amplified from *pART7 Gateway YFP-HA* using primer pair YFP attB F-YFP attB R. The coding regions of *PID* and *AGC3-4* were amplified from *Arabidopsis thaliana* ecotype Columbia (Col-0) cDNA from siliques using respectively primer sets PID attB F-PID attB R, and AT2 attB F-AT2-Stop attB R. Coding regions for *WAG* genes were PCR amplified from *Arabidopsis thaliana* Col-0 genomic DNA using respectively primer sets WAG1 attB F-WAG1-Stop attB R, and WAG2 attB F-WAG2-Stop attB R.

Table 1 Primer list. The attB recombination sites in the primer sequence are underlined.

PID PK CaD F	5’TTC-*Xho*I-TTTCGCCTCAT3’
PID PK CaD R	5’GCGCTCAGTTTAGACCTTTGA3’
CT F	5’TAATGACG-*Eco*RI-TCCGTAACAT3’
CT R	5’AAGCTCGTTCAAAAGTAATCGAAC3’
TCH3 attB F1	5’GGGGACAAGTTTGTACAAAAAAGCAGGCTTAATGGCGGATAAGCTCACT3’
TCH3 attB R1	5’GGGGACCACTTTGTACAAGAAAGCTGGGTAAGATAACAGCGCTTCGAACA3’
gTCH3 attB F	5’GGGGACAAGTTTGTACAAAAAAGCAGGCTTAAAGACTCTTATAAGGACTC3’
gTCH3 attB R	5’GGGGACCACTTTGTACAAGAAAGCTGGGTAAGATAACAGCGCTTCGAACA3’
YFP attB F	5’GGGGACAAGTTTGTACAAAAAAGCAGGCTTCAGGGTGAGCAAGGGCGAGG3’
YFP attB R	5’GGGGACCACTTTGTACAAGAAAGCTGGGTCGATCCGGTGGATCCCGGGC3’
PID attB F1	5’GGGGACAAGTTTGTACAAAAAAGCAGGCTTCAGCATGTTACGAGAATCAGACGGT3’
PID attB R1	5’GGGGACCACTTTGTACAAGAAAGCTGGGTCAAAGTAATCGAACGCCGCTGG3’
PID exon1 F1	5’TCTCTTCCGCCAGGTAAAAA3’
PID exon2 R1	5’CGCAAGACTCGTTGGAAAAG3’
TCH3pr F1	5’AAATGTCCACTCACCCATCC3’
TCH3pr R1	5’GGGAATTCTGAAGATCAGCTTTTGTCG3’
LBaI	5’TGGTTCACGTAGTGGGCCATCG3’
AtROC5 F	5’CGGGAAGGATCGTGATGGA3’
AtROC5 R	5’CCAACCTTCTCGATGGCCT3’
αTUB F	5’CGGAATTCATGAGAGAGATCCTTCATATC3’
αTUB R	5’CCCTCGAGTTAAGTCTCGTACTCCTCTTC3’
AT2 attB F	5’GGGGACAAGTTTGTACAAAAAAGCAGGCTTCAGCATGGCTAATTCTAGTATCTTT3’
AT2-Stop attB R	5’GGGGACCACTTTGTACAAGAAAGCTGGGTCAAAATAATCAAAATAATTAGA3’
WAG1 attB F	5’GGGGACAAGTTTGTACAAAAAAGCAGGCTTCAGCATGGAAGACGACGGTTATTAC3’

WAG1-Stop attB R	5’GGGGACCACTTTGTACAAGAAAGCTGGGTCTAGCTTTTTACCCACATAATG3’
WAG2 attB F	5’GGGGACAAGTTTGTACAAAAAAGCAGGCTTAGGATGTGTTTGTGTCCCTTTGT3’
WAG2-Stop attB R	5’GGGGACCACTTTGTACAAGAAAGCTGGGTCAACGCGTTTGCGACTCGCGTA3’

To overexpress *TCH3* in *Arabidopsis thaliana*, its complete coding region was cloned from *pSDM6008* as a *Bam*HI fragment into *pART7* and the expression cassette was inserted as a *Not*I fragment into the *pART27* binary vector. To construct *35S::TCH3:YFP*, *35S::PID:CFP and pET16H:PID*, the coding regions were amplified by PCR from *pSDM6008* and *pSDM6004* with respectively primer pairs TCH3 attB F1-TCH3 attB R1, and PID attB F1 - PID attB R1 and the resulting PCR fragments were recombined into *pDONR207* (BP reaction) and subsequently into *pART7*-drived or *pET16H* destination vectors (LR reaction), containing either the *CFP* (PID), the *YFP* (TCH3) or His (PID) coding region in frame with the Gateway cassette (Invitrogen).

The binary vector *TCH3::TCH3-mRFP* was obtained by PCR amplification of a genomic fragment (from 1125 bp upstream until the stop codon) from *Arabidopsis thaliana* Col-0 genomic DNA using primer pairs gTCH3 attB F – gTCH3 attB R, recombining the resulting PCR fragment into *pDONR207* (BP reaction) and subsequently into the *pGreenII-0229-mRFP* destination vector (LR reaction). Design of cloning strategies, DNA sequence analysis and DNA and protein sequence alignments were performed using the Vector NTI 10 software (Invitrogen).

Arabidopsis lines, plant transformation and protoplast transfections

Arabidopsis seeds were germinated and plants were grown as described (Benjamins et al., 2001). The lines *35S::PID-21* (Benjamins et al., 2001), *TCH3::TCH3-GUS* (Sistrunk et al., 1994), *PID::PID-VENUS* (Michniewicz et al., 2007), *DR5rev::GFP* (Benkova et al., 2003), *PIN2::PIN2-GFP* (Xu and Scheres, 2005), *abp1-5* (Xu et al., 2010) and *35S::DII-VENUS* (Brunoud et al., 2012) were described previously. *tch3-3* was kindly provided by J.Braam. For all experiments, *Arabidopsis thaliana* Col-0 ecotype was used as wild-type control.

Double loss- or gain-of-function lines were generated by crossing parental lines, and selected using either resistance markers or by genotyping. To genotype for the presence of the different T-DNA insertions, the T-DNA-specific LBa1 primer was combined in a PCR reaction with the gene-specific PCR primers TCH3pr F1 or TCH3pr R1 for *tch3-3*

(Table 1). Sequencing of the junction fragment was used to confirm the insertion position.

Arabidopsis thaliana ecotype Columbia wild type was transformed by the floral dip method as described (Clough and Bent, 1998) using Agrobacterium LBA1115 strain. T1 transformants were selected on medium supplemented with 50 µg/ml kanamycin (Km) for *35S::TCH3*, with 30 µg/ml phosphinotricin (PPT) for *TCH3::TCH3-mRFP* and with 100 µg/ml timentin to inhibit the *Agrobacterium* growth. For further analysis, single locus insertion lines were selected by germination on 25 µg/ml Km or 15 µg/ml PPT.

Protoplasts were obtained from *Arabidopsis thaliana* Columbia cell suspension cultures that were propagated as described (Schirawski et al., 2000). Protoplast isolation and PEG-mediated transfections with 10 µg plasmid DNA were performed as described (Maraschin et al., 2009). To obtain auxin-starved protoplasts, auxin (NAA) was removed from the media during protoplast isolation. Following transfection, the protoplasts were incubated for at least 16h in the dark prior to observation.

Phenotypic and microscopy analysis

For gravitropism experiments, plants were grown on vertically placed plates containing a 3-mm layer of MA medium (Masson and Paszkowski, 1992) solidified with 1% agar (Daichin). For gravistimulation, 5 days old seedlings were transferred to fresh medium, where indicated supplemented with $LaCl_3$ (125 mM stock in H_2O; Sigma), or N-1-Naphthylphthalamic acid (NPA, 20 mM stock in DMSO; Pfaltz&Bauer). Roots were straightened and plates were incubated vertically and subsequently turned 90^o to start the gravistimulation. Plates were imaged using a digital camera and root lengths and bending angles were measured with the Image J software (http://rsb.info.nih.gov/ij/).

For the root collapse assay, about 200 seedlings per line were grown in triplicate on vertical plates containing solid MA medium. During 8 days the seedlings were monitored and scored daily for collapse of the primary root meristem.

For β-glucuronidase (GUS) expression analysis, seeds of *TCH3::TCH3-GUS* were germinated for 5 days on solid MA medium, then transferred to liquid medium supplemented with 5 µM IAA (Indole-3-acetic acid, 8.6 mM stock in DMSO) or 5 µM NAA (1-Naphthylacetic acid, BDH, 10 mM stock in DMSO) for auxin induction or to MA medium and gravistimulated for 2, 4, 6 hours. Seedlings were stained for GUS activity as described (Benjamins et al., 2001) and analyzed and imaged using a Zeiss Axioplan II microscope with differential interference contrast (DIC) optics and camera.

For the subcellular localization of PID in *Arabidopsis* roots, vertically grown 4-days old *PID::PID-VENUS* seedlings were treated for 5, 10 or 20 minutes with 5 µM IAA or NAA. For control treatments an equal amount of solvent (DMSO) was added to the medium. For pre-treatment with Ca^{2+} channel blocker, seedlings were incubated for 30 min on medium containing 1.25 mM $LaCl_3$ (Sigma), after which the seedlings were transferred to medium with 1.25 mM $LaCl_3$ together with 5 µM IAA or NAA.

Confocal microscopy on *PID::PID*-VENUS, *PIN2::PIN2-GFP* and *TCH3::TCH3-mRFP* seedlings was done using the Zeiss LSM 5 Exciter 2C/1F Imager M1 (Zeiss, Oberkochen, Germany) confocal microscope, using a 40x oil objective. The YFP fluorescence was monitored with a 530-600 nm band pass emission filter (514 nm excitation). The GFP fluorescence was monitored with a 505-530 nm band pass emission filter (488 nm excitation). The RFP fluorescence was monitored with a 560 nm long pass filter (543 nm excitation). The images were analysed and processed in Image J (http://rsb.info.nih.gov/ij/) and assembled in Adobe Photoshop.

To quantify the ratios of PIN2-GFP between outer lateral and apical PM, signals were measured using median optical sections by drawing a freehand line in Image J, and calculating the mean fluorescence intensity per pixel. *DR5::GFP* and *35S::DII:Venus* signals were quantified after gravistimulation, by measuring the lower and upper fluorescent signals in freehand boxed lateral root cap cells using median optical sections in ImageJ. *DR5:GFP* signals in QC and columella cells where measured by freehand boxing the fluorescent signal using median optical sections in Image J. For all these quantitative analysis, results were presented as mean fluorescence intensity per pixel with standard error of mean. Statistical analysis was done using the Student's *t*-test. For each independent experiment images were taken using the same microscopy settings, and to compare the pixel intensities between wild type and mutants. The same root region was imaged .

Förster (Fluorescence) Resonance Energy Transfer (FRET)

For the initial FRET analysis on the interaction between PID and TCH3, protoplasts were prepared and their fluorescence monitored using a Leica DM IRBE confocal laser scanning microscope with a 63x water objective. The fluorescence was visualized with an Argon laser for excitation at 514 nm (YFP) and 457 nm (CFP) with 522-532 nm (for the YFP) and 471-481 nm (for the CFP) emission filters. FRET studies on the interaction between PID and TCH3 were done by excitation at 457 nm (donor, CFP) and by measuring emission at 475 and 529 nm using a RSP 465 filter. The intensity of three fixed areas (regions of interest, ROIs) was quantified using the Leica confocal laser scanning software. The fluorescence intensities of these three ROIs was averaged and normalized, and used to calculate the slope of the line from 475 to 529 nm. Per sample three protoplasts were analysed, and the obtained slope values for the three protoplasts was averaged and used to calculate the standard deviation. The Student's *t*-test was used to test for significant differences in slope value between the test sample and the negative control. A significantly reduced slope value (because of a quenched donor emission wavelength intensity, combined with an increased acceptor emission wavelength intensity) was considered indicative for protein-protein interaction-dependent FRET. Similar results were obtained for three independent transfections.

Later FRET studies on the interaction between TCH3 and other AGC3 kinases were done using a sensitized emission FRET approach. Protoplasts were prepared by PEG-mediated transfection. All microscopic analyses were done with confocal laser scanning microscopy (CLSM) using a Zeiss LSM5 Exciter (Zeiss, Oberkochen, Germany) using a 63x magnifying objective. CFP signal was detected using an argon 458 nm laser and 475-525 nm band pass filter. YFP signal was detected using an argon 514 nm laser and a 530-600 nm band pass filter. To detect FRET signal a 458 nm laser and a 530 nm long pass filter were used. To quantify FRET by sensitized emission, the Image J plugin 'FRET and Colocalization Analyzer' was used. This plugin allows calculation of a FRET index on a pixel by pixel basis and corrects for donor bleed through, acceptor bleed through and false FRET (by associating FRET with colocalization of the two fluophores). A "donor only" protoplast expressing *35S:CFP* and an "acceptor only" protoplast expressing *35S:YFP* were used to determine donor bleed through and acceptor bleed through, respectively. The *35S::CFP-YFP* fusion construct was used a positive control. The plugin was used to calculate the FRET index image, and the relative FRET image was obtained by dividing the FRET index image by the YFP channel image. Three regions of interest (ROIs) were quantified using the ImageJ software. Per sample scanning was performed on ten protoplasts. The obtained intensity of all protoplasts was averaged and used to calculate the standard deviation. The Student's *t*-test was used to test for significant differences in relative FRET ($p<0.05$).

Protein biochemistry

In vitro pull-down analysis was performed as previously described (Benjamins et al., 2003).

For PepChip phosphorylation assays, His-tagged proteins were purified by immobilized-metal affinity chromatography. Bacterial pellets were resuspended in 2 ml of Lysis Buffer (LB: 25 mM Tris pH 8.0, 500 mM NaCl, 20 mM imidazole, 0.05 % Tween-20, 10 % glycerol) and incubated 5 min on ice. After sonication for 2 min, 100 µl of 20 % Triton X-100 was added and the mixture was incubated 5 min on ice, followed by centrifugation at 10000 g for 15 min at 4 ^{o}C. The soluble fraction was added with 400 µl of pre-equilibrated 50 % NTA-agarose matrix (Qiagen) and mixed gently for 1.5 h at 4 ^{o}C. Beads were washed three times with 2 ml of LB, 2 ml of Washing Buffer 3 (25 mM Tris pH 7.5, 500 mM NaCl, 40 mM imidazole, 0.01 % Tween-20, 10 % glycerol), and 2 ml of Wash Buffer 4 (25 mM Tris pH 7.0, 500 mM NaCl, 80 mM imidazole and 10 % glycerol). Elution was performed by incubating the beads on 600 µl Elution Buffer 2 (25 mM Tris pH 7.0, 300 mM NaCl, 300 mM imidazole, 10 % glycerol) for 30 min at 4 ^{o}C. Samples were analyzed by SDS-PAGE and quantified.

The Pepchip Kinase Slide A (Pepscan) was used for *in vitro* phosphorylation assays for PID in the presence of TCH3. Thirty ng of His:PID, His:TCH3 and His:PBP1 were mixed with Kinase Mastermix (50 mM HEPES pH 7.4, 20 mM $MgCl_2$, 20 % v/v glycerol, 0.01 mg/ml BSA, 0.01 % v/v Brij-35, 2 mM $CaCl_2$), 10 µM ATP and 300 µCi/ml γ-33P-ATP (specific activity ~ 3000 Ci/mmol, Amersham). Fifty µl of the reaction mix was incubated with the Pepchip Kinase Slide A for 4 h at 30 ^{o}C in a humid chamber. Slides were washed twice with 2 M NaCl, twice with water and dried for 30 min. Slides were exposed to X-ray film FUJI Super RX for 12 and 24 h. The intensity of the signal was quantified by densitometry analysis within uniform circles placed on the peptide spots using ImageQuant software (Molecular Dynamics)

RNA extraction and Northern Blots

Total RNA was purified using the RNeasy Plant Mini kit (Qiagen). Subsequent RNA blot analysis was performed as described (Memelink et al., 1994) using 10 µg of total RNA per sample. The following modifications were made: pre-hybridizations and hybridizations were conducted at 65 ^{o}C in 2xSSPE 0.5% SDS, and for 20 min at 42 ^{o}C in respectively 0.2x SSPE 0.5% SDS, 0.1xSSPE 0.5% SDS and 0.1x SSPE. Blots were exposed to X-ray film FUJI Super RX. The probes for *AtROC5*, for *αTubulin* and *PID* were PCR amplified from *Arabidopsis thaliana* Col-0 genomic DNA and column purified (Qiagen). Probes were radioactively labeled using a Prime-a-gene kit (Promega).

Accession numbers

The *Arabidopsis* Genome Initiative locus identifiers for the genes mentioned are as follows: *PBP1* (At5g54490), *PID* (At2g34650), *WAG1* (At1g5700), *WAG2* (At3g14370), *AGC3-4* (At2g26700), *TCH3* (At2g41100), *ROC* (At4g38740), *PIN2* (At5g57090), α*Tubulin (At5g44340)*.

Acknowledgments

The authors would like to thank Marcus Heisler for kindly providing the *PID::PID-VENUS* line, Janet Braam for sharing her unpublished data on the *tch3-3* allele, Teva Vernoux for providing the *35S::DII:VENUS* line, Jiri Friml for sharing the *abp1-5* mutant, and Katherine Perrot-Rechenmann for sharing the ethanol inducible SS12S6, SS12K9 lines. Also, we thank Jos Joore for support with the Pepchip Kinase experiments. We are indebted to Gerda Lamers, Ward de Winter and Jan Vink for their help with the microscopy, tissue culture and plant caretaking, respectively.

The project was supported by a grant to R.O. from the Research Council of Chemical Sciences (NWO-CW TOP 700.58.301) with financial support from the Netherlands Organisation for Scientific Research (NWO); C.G.A. was supported by a grant to RO from the Research Council for Earth and Life Sciences (ALW 813.06.004) with financial support from the Netherlands Organisation for Scientific Research (NWO).

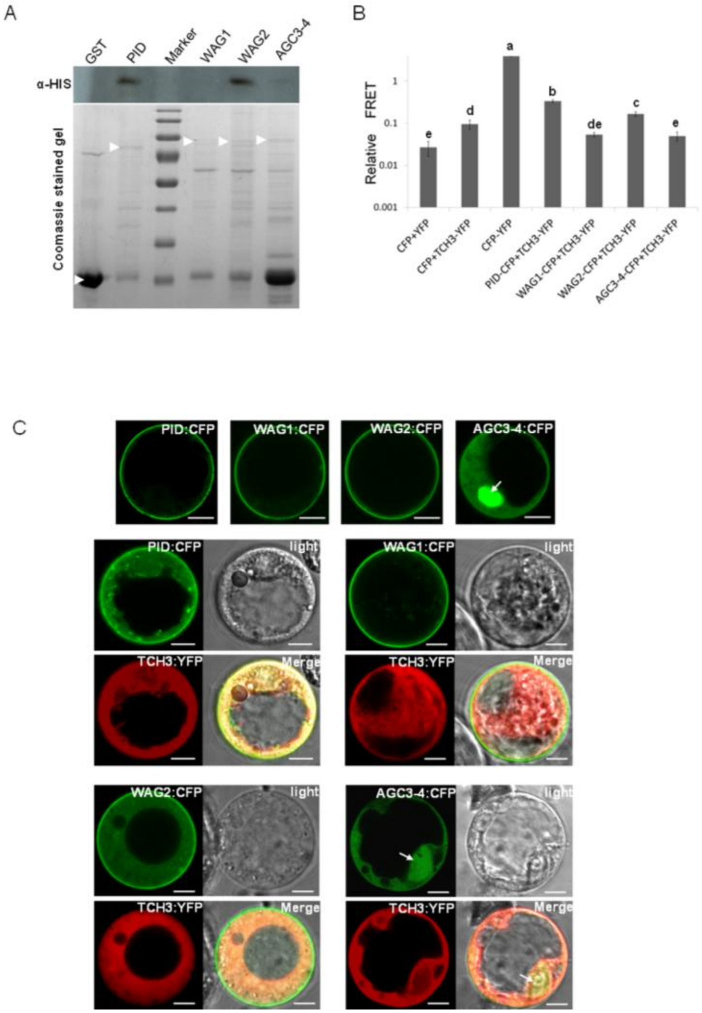

Supplementary Figure S1 TCH3 interacts with PID and WAG2, but not with the other two AGC3 kinases.

(A) Western blot analysis of an *in vitro* pull down of His-tagged TCH3 with GST-tagged PID, WAG1, WAG2 or AGC3-4 using anti-His antibodies (upper panel). The lower panel shows the coomassie stained gel used for the Western blot.

(B, C) Sensitized emission FRET analysis on protoplasts co-expressing TCH3:YFP and PID:CFP, WAG1:CFP, WAG2:CFP or AGC3-4:CFP. The relative FRET index was determined by three measurements in ten co-expressing protoplasts. (B). A $\log^{10}$ scale is used for the Y axis. Error bars represent the standard error of the mean. The significantly different classes are indicated with a to e ($p<0.05$, *t*-test). (C) Confocal images of protoplasts showing the CFP channel image for single transfected protoplasts and the CFP-, YFP- and transmitted light channel images and a merged picture of these three images for the double transfected protoplasts. Scale bar indicates 10 µm. CFP and FRET signals were collected simultaneously, and the YFP signal was collected separately.

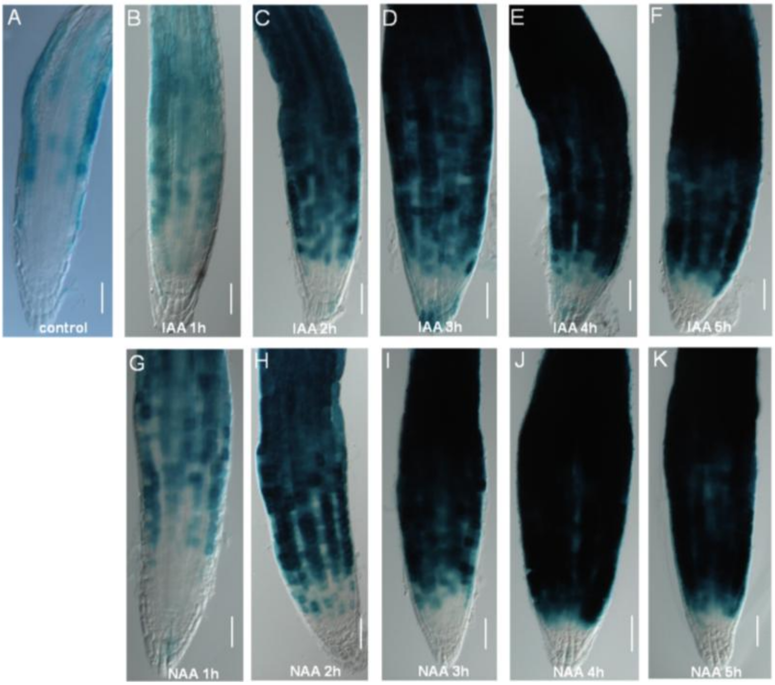

Supplementary Figure S2 Auxin-induced *TCH3* expression in the root tip

(A-K) Images of histochemically stained *TCH3:TCH3-GUS* seedling root tips that were mock treated (A), or treated for 1 to 5 hours with 5 µM IAA (B-F) or 5 µM NAA (G-K).

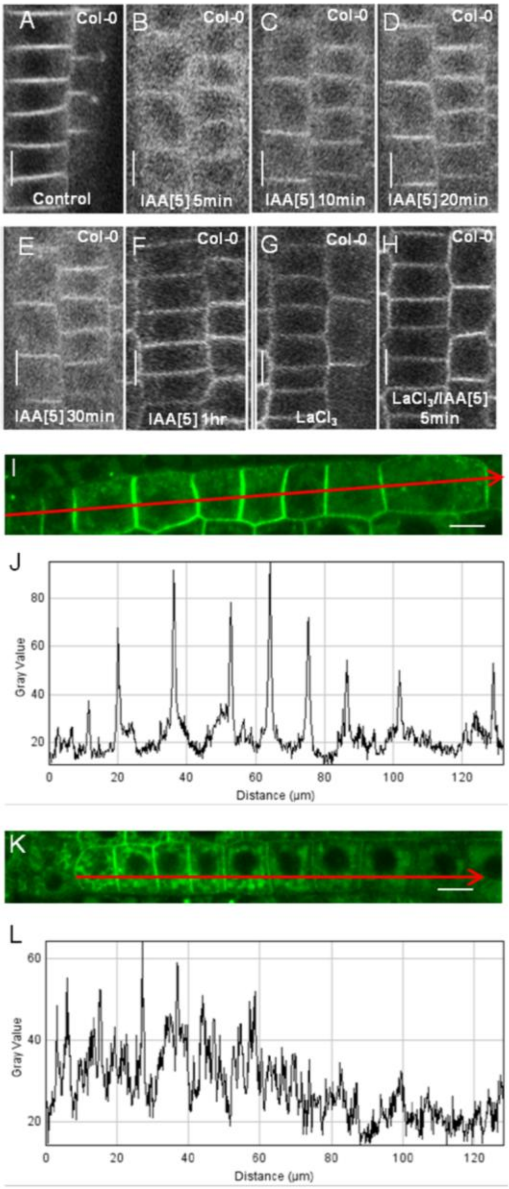
A
Col-0
Control
B
Col-0
IAA[5] 5min
C
Col-0
IAA[5] 10min
D
Col-0
IAA[5] 20min
E
Col-0
IAA[5] 30min
F
Col-0
IAA[5] 1hr
G
Col-0
LaCl₃
H
Col-0
LaCl₃/IAA[5] 5min
I
J
Gray Value
20
40
60
80
0
20
40
60
80
100
120
Distance (µm)
K
L
Gray Value
20
40
60
0
20
40
60
80
100
120
Distance (µm)

Supplementary Figure S3 The natural auxin indole-3-acetic acid (IAA) induces transient PID dissociation from the plasma membrane (PM).

(A-H) PID dissociates from the PM after 5 minutes treatment with 5 µM IAA (B), but gradually returns to the PM between 10 to 60 minutes after IAA treatment (C to F). Pretreatment for 30 minutes with $LaCl_3$ (G) does not influence PID localization, but blocks the auxin-induced dissociation of PID from the PM (5 minutes with 5 µM IAA, H). (I-L) Quantification of the PID-VENUS signal in a root epidermis cell file of untreated (I,J,) or 5 µM IAA treated (K,L) root tips using Image J software (J,L).

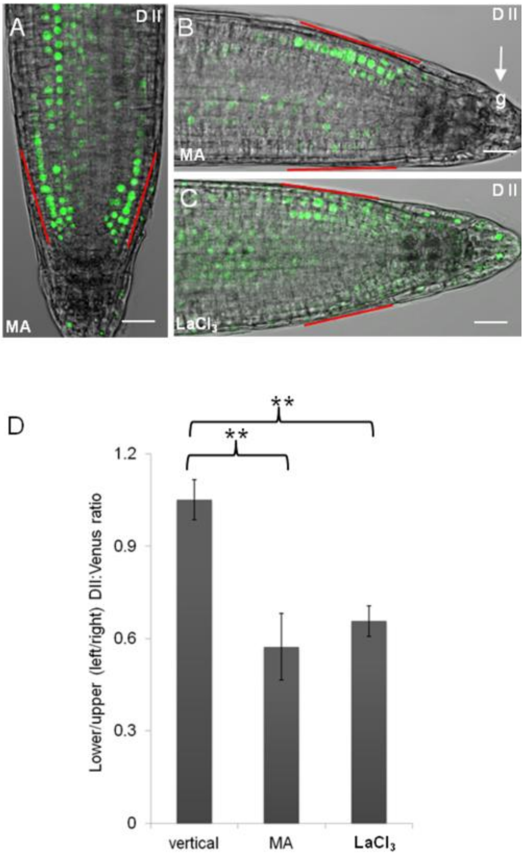

Supplementary Figure S4 Ca^{2+} acts downstream of the differential auxin distribution during gravitropic root growth.

(A-D) Auxin distribution in *Arabidopsis* root tips, as indicated by the auxin response reporter *35S::DII-VENUS*. Roots were grown vertically (A) or gravistimulated for 1 hour on control MA medium (B) or on MA medium supplemented with 1.25 mM $LaCl_3$ (C). Quantification of the DII-VENUS signal in the lateral root cap on the upper and lower side of the root tip (D). Red lines in A to C indicate the measured area.

Error bars in D represents the standard error of the mean, $^{*}p<0.05$; $^{**}p<0.01$ (*t* test). Scale bar in A to C is 20 µm.

Reference

Abas, L., Benjamins, R., Malenica, N., Paciorek, T., Wisniewska, J., Moulinier-Anzola, J.C., Sieberer, T., Friml, J., and Luschnig, C. (2006). Intracellular trafficking and proteolysis of the *Arabidopsis* auxin-efflux facilitator PIN2 are involved in root gravitropism. Nat Cell Biol **8,** 249-256.

Antosiewicz, D.M., Polisensky, D.H., and Braam, J. (1995). Cellular localization of the Ca^{2+} binding TCH3 protein of *Arabidopsis*. Plant J **8,** 623-636.

Antosiewicz, D.M., Purugganan, M.M., Polisensky, D.H., and Braam, J. (1997). Cellular localization of Arabidopsis xyloglucan endotransglycosylase-related proteins during development and after wind stimulation. Plant Physiol **115,** 1319-1328.

Band, L.R., Wells, D.M., Larrieu, A., Sun, J., Middleton, A.M., French, A.P., Brunoud, G., Sato, E.M., Wilson, M.H., Peret, B., Oliva, M., Swarup, R., Sairanen, I., Parry, G., Ljung, K., Beeckman, T., Garibaldi, J.M., Estelle, M., Owen, M.R., Vissenberg, K., Hodgman, T.C., Pridmore, T.P., King, J.R., Vernoux, T., and Bennett, M.J. (2012). Root gravitropism is regulated by a transient lateral auxin gradient controlled by a tipping-point mechanism. Proc Natl Acad Sci U S A **109,** 4668-4673.

Baster, P., Robert, S., Kleine-Vehn, J., Vanneste, S., Kania, U., Grunewald, W., De Rybel, B., Beeckman, T., and Friml, J. (2013). $SCF^{TIR1/AFB}$-auxin signalling regulates PIN vacuolar trafficking and auxin fluxes during root gravitropism. EMBO J **32,** 260-274.

Baum, G., Long, J.C., Jenkins, G.I., and Trewavas, A.J. (1999). Stimulation of the blue light phototropic receptor NPH1 causes a transient increase in cytosolic Ca^{2+}. Proc Natl Acad Sci U S A **96,** 13554-13559.

Benjamins, R., Ampudia, C.S., Hooykaas, P.J., and Offringa, R. (2003). PINOID-mediated signaling involves calcium-binding proteins. Plant Physiol **132,** 1623-1630.

Benjamins, R., Quint, A., Weijers, D., Hooykaas, P., and Offringa, R. (2001). The PINOID protein kinase regulates organ development in *Arabidopsis* by enhancing polar auxin transport. Development **128,** 4057-4067.

Benkova, E., Michniewicz, M., Sauer, M., Teichmann, T., Seifertova, D., Jurgens, G., and Friml, J. (2003). Local, efflux-dependent auxin gradients as a common module for plant organ formation. Cell **115,** 591-602.

Bouché, N., Yellin, A., Snedden, W.A., and Fromm, H. (2005). Plant-specific calmodulin-binding proteins. Annu Rev Plant Biol **56,** 435-466.

Braam, J., and Davis, R.W. (1990). Rain-, wind-, and touch-induced expression of calmodulin and calmodulin-related genes in Arabidopsis. Cell **60,** 357-364.

Braun, N., Wyrzykowska, J., Muller, P., David, K., Couch, D., Perrot-Rechenmann, C., and Fleming, A.J. (2008). Conditional repression of AUXIN BINDING PROTEIN1 reveals that it coordinates cell division and cell expansion during postembryonic shoot development in *Arabidopsis* and tobacco. Plant Cell **20,** 2746-2762.

Brunoud, G., Wells, D.M., Oliva, M., Larrieu, A., Mirabet, V., Burrow, A.H., Beeckman, T., Kepinski, S., Traas, J., Bennett, M.J., and Vernoux, T. (2012). A novel sensor to map auxin response and distribution at high spatio-temporal resolution. Nature **482,** 103-106.

Chen, J.G., Ullah, H., Young, J.C., Sussman, M.R., and Jones, A.M. (2001). ABP1 is required for organized cell elongation and division in *Arabidopsis* embryogenesis. Genes Dev **15,** 902-911.

Cheng, S.H., Willmann, M.R., Chen, H.C., and Sheen, J. (2002). Calcium signaling through protein kinases. The *Arabidopsis* calcium-dependent protein kinase gene family. Plant Physiol. **129,** 469-485.

Clough, S.J., and Bent, A.F. (1998). Floral dip: a simplified method for *Agrobacterium*-mediated transformation of *Arabidopsis thaliana*. Plant J **16,** 735-743.

Corbalan-Garcia, S., Guerrero-Valero, M., Marin-Vicente, C., and Gomez-Fernandez, J.C. (2007). The C2 domains of classical/conventional PKCs are specific PtdIns(4,5)P(2)-sensing domains. Biochem Soc Trans **35,** 1046-1048.

Dahlke, R.I., Luethen, H., and Steffens, B. (2010). ABP1: an auxin receptor for fast responses at the plasma membrane. Plant Signal Behav **5,** 1-3.

Darwin, C. (1880). The power of movement in plants. London: John Murray.

David, K.M., Couch, D., Braun, N., Brown, S., Grosclaude, J., and Perrot-Rechenmann, C. (2007). The auxin-binding protein 1 is essential for the control of cell cycle. Plant J **50,** 197-206.

dela Fuente, R.K., and Leopold, A.C. (1973). A role for calcium in auxin transport. Plant Physiol **51,** 845-847.

Dhonukshe, P., Huang, F., Galvan-Ampudia, C.S., Mahonen, A.P., Kleine-Vehn, J., Xu, J., Quint, A., Prasad, K., Friml, J., Scheres, B., and Offringa, R. (2010). Plasma membrane-bound AGC3 kinases phosphorylate PIN auxin carriers at TPRXS(N/S) motifs to direct apical PIN recycling. Development **137,** 3245-3255.

Ding, Z., Galvan-Ampudia, C.S., Demarsy, E., Langowski, L., Kleine-Vehn, J., Fan, Y., Morita, M.T., Tasaka, M., Fankhauser, C., Offringa, R., and Friml, J. (2011). Light-mediated polarization of the PIN3 auxin transporter for the phototropic response in *Arabidopsis*. Nat Cell Biol **13,** 447-452.

Esmon, C.A., Tinsley, A.G., Ljung, K., Sandberg, G., Hearne, L.B., and Liscum, E. (2006). A gradient of auxin and auxin-dependent transcription precedes tropic growth responses. Proc Natl Acad Sci U S A **103,** 236-241.

Felle, H. (1988). Auxin causes oscillations of cytosolic free calcium and pH in *Zea mays* coleoptiles. Planta **174,** 495-499.

Folta, K.M., Lieg, E.J., Durham, T., and Spalding, E.P. (2003). Primary inhibition of hypocotyl growth and phototropism depend differently on phototropin-mediated increases in cytoplasmic calcium induced by blue light. Plant Physiol **133,** 1464-1470.

Friml, J. (2003). Auxin transport - shaping the plant. Curr Opin Plant Biol **6,** 7-12.

Friml, J., Wisniewska, J., Benkova, E., Mendgen, K., and Palme, K. (2002). Lateral relocation of auxin efflux regulator PIN3 mediates tropism in *Arabidopsis*. Nature **415,** 806-809.

Friml, J., Vieten, A., Sauer, M., Weijers, D., Schwarz, H., Hamann, T., Offringa, R., and Jurgens, G. (2003). Efflux-dependent auxin gradients establish the apical-basal axis of *Arabidopsis*. Nature **426,** 147-153.

Friml, J., Yang, X., Michniewicz, M., Weijers, D., Quint, A., Tietz, O., Benjamins, R., Ouwerkerk, P.B., Ljung, K., Sandberg, G., Hooykaas, P.J., Palme, K., and Offringa, R. (2004). A PINOID-dependent binary switch in apical-basal PIN polar targeting directs auxin efflux. Science **306,** 862-865.

Galván-Ampudia, C.S., and Offringa, R. (2007). Plant evolution: AGC kinases tell the auxin tale. Trends Plant Sci. **12,** 541-547.

Gehring, C.A., Irving, H.R., and Parish, R.W. (1990a). Effects of auxin and abscisic acid on cytosolic calcium and pH in plant cells. Proc Natl Acad Sci U S A **87,** 9645-9649.

Gehring, C.A., Williams, D.A., Cody, S.H., and Parish, R.W. (1990b). Phototropism and geotropism in maize coleoptiles are spatially correlated with increases in cytosolic free calcium. Nature **345,** 528-530.

Guan, K.L., and Dixon, J.E. (1991). Eukaryotic proteins expressed in Escherichia coli: an improved thrombin cleavage and purification procedure of fusion proteins with glutathione S-transferase. Anal Biochem **192,** 262-267.

Harada, A., and Shimazaki, K. (2007). Phototropins and blue light-dependent calcium signaling in higher plants. Photochem Photobiol **83,** 102-111.

Harada, A., Sakai, T., and Okada, K. (2003). phot1 and phot2 mediate blue light-induced transient increases in cytosolic Ca^{2+} differently in *Arabidopsis* leaves. Proc Natl Acad Sci U S A **100,** 8583-8588.

Hashimoto, K., and Kudla, J. (2011). Calcium decoding mechanisms in plants. Biochimie **93,** 2054-2059.

Hellens, R.P., Edwards, E.A., Leyland, N.R., Bean, S., and Mullineaux, P.M. (2000). pGreen: a versatile and flexible binary Ti vector for *Agrobacterium*-mediated plant transformation. Plant Mol Biol **42,** 819-832.

Hood, E., Gelvin, S., Melchers, L., and Hoekema, A. (1993). New Agrobacterium helper plasmids for gene transfer to plants. Transgenic Research **2,** 208-218.

Huang, F., Zago, M.K., Abas, L., van Marion, A., Galvan-Ampudia, C.S., and Offringa, R. (2010). Phosphorylation of conserved PIN motifs directs *Arabidopsis* PIN1 polarity and auxin transport. Plant Cell **22,** 1129-1142.

Kleine-Vehn, J., Ding, Z., Jones, A.R., Tasaka, M., Morita, M.T., and Friml, J. (2010). Gravity-induced PIN transcytosis for polarization of auxin fluxes in gravity-sensing root cells. Proc Natl Acad Sci U S A **107,** 22344-22349.

Korasick, D.A., Enders, T.A., and Strader, L.C. (2013). Auxin biosynthesis and storage forms. J Exp Bot **64,** 2541-2555.

Lariguet, P., Schepens, I., Hodgson, D., Pedmale, U.V., Trevisan, M., Kami, C., de Carbonnel, M., Alonso, J.M., Ecker, J.R., Liscum, E., and Fankhauser, C. (2006). PHYTOCHROME KINASE SUBSTRATE 1 is a phototropin 1 binding protein required for phototropism. Proc Natl Acad Sci U S A **103,** 10134-10139.

Lee, J.S., and Evans, M.L. (1985). Polar transport of auxin across gravistimulated roots of maize and its enhancement by calcium. Plant Physiol **77,** 824-827.

Lee, J.S., Mulkey, T.J., and Evans, M.L. (1984). Inhibition of polar calcium movement and gravitropism in roots treated with auxin-transport inhibitors. Planta **160,** 536-543.

Lee, S.H., and Cho, H.T. (2006). PINOID positively regulates auxin efflux in *Arabidopsis* root hair cells and tobacco cells. Plant Cell **18,** 1604-1616.

Ljung, K. (2013). Auxin metabolism and homeostasis during plant development. Development **140,** 943-950.

Luan, S., Kudla, J., Rodriguez-Concepcion, M., Yalovsky, S., and Gruissem, W. (2002). Calmodulins and calcineurin B-like proteins: calcium sensors for specific signal response coupling in plants. Plant Cell **14,** S389-400.

Masson, J., and Paszkowski, J. (1992). The culture response of *Arabidopsis thaliana* protoplasts is determined by the growth conditions of donor plants. The Plant Journal **2,** 829-833.

McCormack, E., and Braam, J. (2003). Calmodulins and related potential calcium sensors of Arabidopsis. New Phytol. **159,** 585-598.

McLaughlin, S., and Murray, D. (2005). Plasma membrane phosphoinositide organization by protein electrostatics. Nature **438,** 605-611.

Memelink, J., Swords, K.M., Staehelin, L.A., and Hoge, J.H. (1994). Southern, Northern and Western blot analysis. In Plant Molecular Biology Manual, S. Gelvin and R. Schilperoort, eds (Springer Netherlands), pp. 273-295.

Michniewicz, M., Zago, M.K., Abas, L., Weijers, D., Schweighofer, A., Meskiene, I., Heisler, M.G., Ohno, C., Zhang, J., Huang, F., Schwab, R., Weigel, D., Meyerowitz, E.M., Luschnig, C., Offringa, R., and Friml, J. (2007). Antagonistic regulation of PIN phosphorylation by PP2A and PINOID directs auxin flux. Cell **130,** 1044-1056.

Monshausen, G.B., Messerli, M.A., and Gilroy, S. (2008). Imaging of the Yellow Cameleon 3.6 indicator reveals that elevations in cytosolic Ca^{2+} follow oscillating increases in growth in root hairs of Arabidopsis. Plant Physiol **147,** 1690-1698.

Monshausen, G.B., Bibikova, T.N., Weisenseel, M.H., and Gilroy, S. (2009). Ca^{2+} regulates reactive oxygen species production and pH during mechanosensing in *Arabidopsis* roots. Plant Cell **21,** 2341-2356.

Monshausen, G.B., Miller, N.D., Murphy, A.S., and Gilroy, S. (2011). Dynamics of auxin-dependent Ca^{2+} and pH signaling in root growth revealed by integrating high-resolution imaging with automated computer vision-based analysis. Plant J. **65,** 309-318.

Moore, R. (1985). Calcium movement, graviresponsiveness and the structure of columella cells and columella tissues in roots of *Allium cepa* L. Annals of Botany **56,** 173-187.

Nakajima, K., and Benfey, P.N. (2002). Signaling in and out: control of cell division and differentiation in the shoot and root. Plant Cell **14 Suppl,** S265-276.

Ottenschlager, I., Wolff, P., Wolverton, C., Bhalerao, R.P., Sandberg, G., Ishikawa, H., Evans, M., and Palme, K. (2003). Gravity-regulated differential auxin transport from columella to lateral root cap cells. Proc Natl Acad Sci U S A **100,** 2987-2991.

Paciorek, T., Zazimalova, E., Ruthardt, N., Petrasek, J., Stierhof, Y.D., Kleine-Vehn, J., Morris, D.A., Emans, N., Jurgens, G., Geldner, N., and Friml, J. (2005). Auxin inhibits endocytosis and promotes its own efflux from cells. Nature **435,** 1251-1256.

Peret, B., De Rybel, B., Casimiro, I., Benkova, E., Swarup, R., Laplaze, L., Beeckman, T., and Bennett, M.J. (2009). *Arabidopsis* lateral root development: an emerging story. Trends Plant Sci. **14,** 399-408.

Petrasek, J., and Friml, J. (2009). Auxin transport routes in plant development. Development **136,** 2675-2688.

Petrasek, J., Mravec, J., Bouchard, R., Blakeslee, J.J., Abas, M., Seifertova, D., Wisniewska, J., Tadele, Z., Kubes, M., Covanova, M., Dhonukshe, P., Skupa, P., Benkova, E., Perry, L., Krecek, P., Lee, O.R., Fink, G.R., Geisler, M., Murphy, A.S., Luschnig, C., Zazimalova, E., and Friml, J. (2006). PIN proteins perform a rate-limiting function in cellular auxin efflux. Science **312,** 914-918.

Poovaiah, B.W., McFadden, J.J., and Reddy, A.S. (1987). The role of calcium ions in gravity signal perception and transduction. Physiol Plant **71,** 401-407.

Rademacher, E.H., and Offringa, R. (2012). Evolutionary adaptations of plant AGC Kinases: from light signaling to cell polarity regulation. Front Plant Sci **3,** 250.

Reinhardt, D., Mandel, T., and Kuhlemeier, C. (2000). Auxin regulates the initiation and radial position of plant lateral organs. Plant Cell **12,** 507-518.

Reinhardt, D., Pesce, E.R., Stieger, P., Mandel, T., Baltensperger, K., Bennett, M., Traas, J., Friml, J., and Kuhlemeier, C. (2003). Regulation of phyllotaxis by polar auxin transport. Nature **426,** 255-260.

Robert, S., Kleine-Vehn, J., Barbez, E., Sauer, M., Paciorek, T., Baster, P., Vanneste, S., Zhang, J., Simon, S., Covanova, M., Hayashi, K., Dhonukshe, P., Yang, Z., Bednarek, S.Y., Jones, A.M., Luschnig, C., Aniento, F., Zazimalova, E., and Friml, J. (2010). ABP1 mediates auxin inhibition of clathrin-dependent endocytosis in *Arabidopsis*. Cell **143,** 111-121.

Roux, S.J., and Serlin, B.S. (1987). Cellular mechanisms controlling light-stimulated gravitropism: role of calcium. CRC Crit Rev Plant Sci **5,** 205-236.

Sabatini, S., Beis, D., Wolkenfelt, H., Murfett, J., Guilfoyle, T., Malamy, J., Benfey, P., Leyser, O., Bechtold, N., Weisbeek, P., and Scheres, B. (1999). An auxin-dependent distal organizer of pattern and polarity in the *Arabidopsis* root. Cell **99,**

463-472.

Sambrook, J., Fritsch F. and Maniatis, T. (1989). Molecular cloning-A laboratory mannual. Cold Spring Harbor Laboratory press, NY, USA.

Sanders, D., Pelloux, J., Brownlee, C., and Harper, J.F. (2002). Calcium at the crossroads of signaling. Plant Cell **14 Suppl,** S401-417.

Sauer, M., Balla, J., Luschnig, C., Wisniewska, J., Reinohl, V., Friml, J., and Benkova, E. (2006). Canalization of auxin flow by Aux/IAA-ARF-dependent feedback regulation of PIN polarity. Genes Dev **20,** 2902-2911.

Schirawski, J., Planchais, S., and Haenni, A.L. (2000). An improved protocol for the preparation of protoplasts from an established *Arabidopsis thaliana* cell suspension culture and infection with RNA of turnip yellow mosaic tymovirus: a simple and reliable method. J Virol Methods **86,** 85-94.

Shishova, M., and Lindberg, S. (2004). Auxin induces an increase of Ca^{2+} concentration in the cytosol of wheat leaf protoplasts. J Plant Physiol **161,** 937-945.

Shishova, M., Yemelyanov, V., Rudashevskaya, E., and Lindberg, S. (2007). A shift in sensitivity to auxin within development of maize seedlings. J Plant Physiol **164,** 1323-1330.

Siegel, R.M., Chan, F.K., Zacharias, D.A., Swofford, R., Holmes, K.L., Tsien, R.Y., and Lenardo, M.J. (2000). Measurement of molecular interactions in living cells by fluorescence resonance energy transfer between variants of the green fluorescent protein. Sci STKE **2000,** pl1.

Sistrunk, M.L., Antosiewicz, D.M., Purugganan, M.M., and Braam, J. (1994). Arabidopsis *TCH3* encodes a novel Ca^{2+} binding protein and shows environmentally induced and tissue-specific regulation. Plant Cell **6,** 1553-1565.

Snedden, W.A., and Fromm, H. (2001). Calmodulin as a versatile calcium signal transducer in plants. New Phytol **151,** 35-66.

Steffens, B., Feckler, C., Palme, K., Christian, M., Bottger, M., and Luthen, H. (2001). The auxin signal for protoplast swelling is perceived by extracellular ABP1. Plant J **27,** 591-599.

Strynadka, N.C., and James, M.N. (1989). Crystal structures of the helix-loop-helix calcium-binding proteins. Annu Rev Biochem **58,** 951-998.

Swanson, S.J., Choi, W.G., Chanoca, A., and Gilroy, S. (2011). In vivo imaging of Ca^{2+}, pH, and reactive oxygen species using fluorescent probes in plants. Annu Rev Plant Biol **62,** 273-297.

Tanaka, H., Dhonukshe, P., Brewer, P.B., and Friml, J. (2006). Spatiotemporal asymmetric auxin distribution: a means to coordinate plant development. Cell Mol Life Sci **63,** 2738-2754.

Travé, G., Lacombe, P.J., Pfuhl, M., Saraste, M., and Pastore, A. (1995). Molecular mechanism of the calcium-induced conformational change in the spectrin EF-hands. EMBO J **14,** 4922-4931.

Vanneste, S., and Friml, J. (2009). Auxin: a trigger for change in plant development. Cell **136,** 1005-1016.

Weijers, D., and Jurgens, G. (2005). Auxin and embryo axis formation: the ends in sight? Curr Opin Plant Biol **8,** 32-37.

Wisniewska, J., Xu, J., Seifertova, D., Brewer, P.B., Ruzicka, K., Blilou, I., Rouquie, D., Benkova, E., Scheres, B., and Friml, J. (2006). Polar PIN localization directs auxin flow in plants. Science **312,** 883.

Woo, E.J., Marshall, J., Bauly, J., Chen, J.G., Venis, M., Napier, R.M., and Pickersgill, R.W. (2002). Crystal structure of auxin-binding protein 1 in complex with auxin. EMBO J **21,** 2877-2885.

Xu, J., and Scheres, B. (2005). Dissection of Arabidopsis ADP-RIBOSYLATION FACTOR 1 function in epidermal cell polarity. Plant Cell **17,** 525-536.

Xu, T., Wen, M., Nagawa, S., Fu, Y., Chen, J.G., Wu, M.J., Perrot-Rechenmann, C., Friml, J., Jones, A.M., and Yang, Z. (2010). Cell surface- and rho GTPase-based auxin signaling controls cellular interdigitation in *Arabidopsis*. Cell **143,** 99-110.

Xu, T., Dai, N., Chen, J., Nagawa, S., Cao, M., Li, H., Zhou, Z., Chen, X., De Rycke, R., Rakusova, H., Wang, W., Jones, A.M., Friml, J., Patterson, S.E., Bleecker, A.B., and Yang, Z. (2014). Cell surface ABP1-TMK auxin-sensing complex activates ROP GTPase signaling. Science **343,** 1025-1028.

Zegzouti, H., Anthony, R.G., Jahchan, N., Bogre, L., and Christensen, S.K. (2006). Phosphorylation and activation of PINOID by the phospholipid signaling kinase 3-phosphoinositide-dependent protein kinase 1 (PDK1) in *Arabidopsis*. Proc Natl Acad Sci U S A **103,** 6404-6409.

Zhao, X., Wang, Y.L., Qiao, X.R., Wang, J., Wang, L.D., Xu, C.S., and Zhang, X. (2013). Phototropins function in high-intensity blue light-induced hypocotyl phototropism in Arabidopsis by altering cytosolic calcium. Plant Physiol **162,** 1539-1551.

Chapter 3

PINOID plasma membrane association and calmodulin binding converge on an amphipathic alpha helix/IQ-like motif

Yuanwei Fan, Eike.H.Rademacher[1], Elco Backus[2], Martinus Schneijderberg, Ser van der Burght, Remko Offringa

Molecular and Developmental Genetics, Institute Biology Leiden, Leiden University, Sylviusweg 72, 2333 BE Leiden, The Netherlands

[1] Current affiliation: Rijk Zwaan Breeding B.V., Burgemeester Crezéelaan 40, 2678 ZG De Lier, The Netherlands

[2] Current affiliation: Crucell, P.O.Box 248, 2301CA Leiden, The Netherlands

Summary

The *Arabidopsis* AGC protein kinase PINOID (PID) is a key regulator of plant adaptive responses to environmental signals. PID determines the direction of polar transport of the plant hormone auxin, a central regulator of plant development and growth, by directing the asymmetric subcellular distribution of PIN proteins through phosphorylation of these auxin efflux carriers. By affecting the activity of the PID protein kinase, environmental signals can change the polarity of auxin transport, and thereby the direction of plant growth. In chapter 2 we showed that PID kinase activity is repressed through Ca^{2+}-dependent binding of the calmodulin-like protein CML12/TCH3/, which sequesters PID from the plasma membrane (PM) to the cytosol, away from its PIN phosphorylation targets. Here we show that CML10 and the calmodulin CAM2, two proteins closely related to TCH3, are also able to recruit PID from the PM. In view of the redundant role of the calmodulins (CaMs) and CMLs in regulating PID activity , we fine-mapped the PM associated domain and the CML/CaM binding domain in PID with the final aim to identify amino acid substitutions that would allow to functionally analyse the role of CML/CaM recruitment throughout plant development. Our analysis revealed that PID CML/CaM binding and PM association sites converge on an amphipathic alpha helix/IQ-like motif in the PID insertion domain, and that the two functionalities cannot be separated. This dual interaction domain allows an elegant novel mechanism of protein kinase activity regulation, by which cytosolic Ca^{2+} concentrations determine whether the kinase is available to phosphorylate substrate proteins.

Introduction

As sessile organisms, plants continuously monitor their environment in order to accurately respond to changes with adaptive growth or defense mechanisms. To do this, plants have acquired a complex network of signal perception and -transduction systems, where cross talk between signaling pathways is for an important part mediated by plant hormones. The central regulator in plant adaptive development and growth is the plant hormone auxin, or indole-3-acetic acid (IAA), that orchestrates growth and positions of new organ initiation sites through local biosynthesis- and polar transport-generated maxima and minima (Tanaka et al., 2006).

PIN auxin efflux carriers have been identified as important drivers of polar auxin transport, as they determine the direction of this cell-to-cell transport through their asymmetric subcellular localization (Petrasek et al., 2006; Wisniewska et al., 2006). PIN polar localization is responsive to internal and external signals, and is regulated by post-translational modification, such as phosphorylation and ubiquitination, leading to changes in PIN trafficking and turn over (Geldner et al., 2001; Friml et al., 2004; Abas et al., 2006; Sauer et al., 2006). The AGC protein serine/threonine kinase PINOID (PID), and its close homologs WAG1 and WAG2 are key determinants in the polar localization of PIN proteins, as they can cause transcytosis-mediated switches in PIN polarity by phosphorylating PIN proteins in their central hydrophilic loop (Friml et al., 2004; Dhonukshe et al., 2010; Huang et al., 2010). One way for environmental signals to regulate endogenous auxin levels would be by regulating the activity of the AGC3 kinases and thereby altering the direction of auxin transport. In fact, light was shown to down-regulate *PID* gene expression and this has been proposed to redirect PIN3 polarity in hypocotyl endodermis cells during the phototropic response in *Arabidopsis* seedlings (Ding et al., 2011). In Chapter 2 of this thesis we showed that elevated auxin levels induced Ca^{2+}-dependent sequestration of PID by the calmodulin-like protein TCH3 from the PM to the cytosol, and that this leads to PIN2 depolarization, which is needed to maximize the gravitropic response of *Arabidopsis* roots. Interestingly, both auxin and mechanical stress induce elevation of Ca^{2+} levels (Monshausen et al., 2009; Monshausen et al., 2011), making it likely that the PID-TCH3 signaling complex also acts in regulating PIN polarity in response to mechanical signals.

There are seven almost identical CaMs in *Arabidopsis* and 50 CaM-like proteins (CMLs). The CMLs are predicted to be the potential Ca^{2+} sensors and share at least 16% amino acid identity with CaMs. The members of the CaM/CML family are separated into nine groups based on amino acid sequence divergence (McCormack et al., 2005).

CaMs use a linker domain to connect two pairs of Ca^{2+} binding pockets called ‘EF hands’. EF hands have micromolar affinity with Ca^{2+} and upon Ca^{2+} binding their conformation is changed. TCH3 is closely related to CaM, but has six EF hands instead of the four EF hands in CaMs or CMLs, because of an exact duplication of EF hands 1 and 2 in the N-terminus of the protein (McCormack et al., 2005).

Previous analysis showed that *tch3* loss-of-function mutants only show mild phenotypes, such as a slight delay in root gravitropism (Chapter 2), suggesting that other members of the CaM/CML protein family act redundantly with TCH3. Here we show that, indeed, CML10, CAM2, and most likely also the other 6 CAMs are able to interact with PID and to sequester PID from the PM. As this complicated investigating the role of the PID-CML signaling complex by looking at the function of the CaM/CMLs in plant development, we decided to map the PM association and CaM binding domains in PID, with the objective to generate a fully functional mutant PID protein, except for its interaction with the CaM/CMLs (untouchable PID).

One characteristic of PID and the other 22 plant-specific AGCVIII kinases in *Arabidopsis* is that they have a stretch of 36 to 90 additional amino acids between subdomain VII and VIII of the catalytic kinase domain, which we named the insertion domain (ID, (Rademacher and Offringa, 2012)). Previously, it was shown for PID that the PM association domain localizes to this ID (Zegzouti et al., 2006b). As our own analysis already showed that TCH3 binds to the catalytic kinase domain of PID (Chapter 2), and this interaction is able to shield off the PM association domain, we focused our search for the TCH3 binding domain to the ID of PID. Through protein modelling and extensive deletion and amino acid substitution mapping we were able to pinpoint both the PM association domain and the TCH3 binding domain to the same amino acid stretch comprising an amphipathic alpha helix/IQ-like domain. Although we were not able to generate the desired untouchable PID version, this research revealed a dual interaction domain that allows an elegant novel mechanism of regulation of the activity of PID kinase activity, through the Ca^{2+}-dependent removal of the kinase from the PM, away from its phosphorylation targets, the PIN proteins.

Results

PID interacts with TCH3 and closely-related CMLs

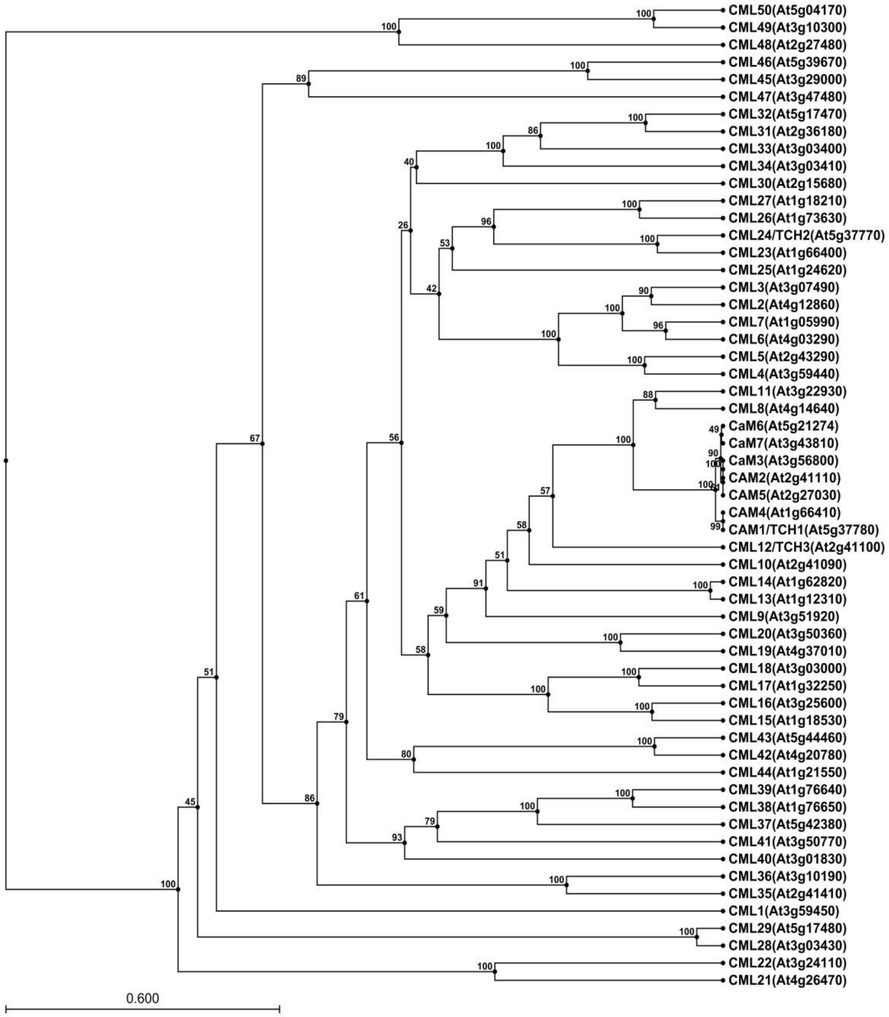
CML50(At5g04170)
CML49(At3g10300)
CML48(At2g27480)
CML46(At5g39670)
CML45(At3g29000)
CML47(At3g47480)
CML32(At5g17470)
CML31(At2g36180)
CML33(At3g03400)
CML34(At3g03410)
CML30(At2g15680)
CML27(At1g18210)
CML26(At1g73630)
CML24/TCH2(At5g37770)
CML23(At1g66400)
CML25(At1g24620)
CML3(At3g07490)
CML2(At4g12860)
CML7(At1g05990)
CML6(At4g03290)
CML5(At2g43290)
CML4(At3g59440)
CML11(At3g22930)
CML8(At4g14640)
CaM6(At5g21274)
CaM7(At3g43810)
CaM3(At3g56800)
CAM2(At2g41110)
CAM5(At2g27030)
CAM4(At1g66410)
CAM1/TCH1(At5g37780)
CML12/TCH3(At2g41100)
CML10(At2g41090)
CML14(At1g62820)
CML13(At1g12310)
CML9(At3g51920)
CML20(At3g50360)
CML19(At4g37010)
CML18(At3g03000)
CML17(At1g32250)
CML16(At3g25600)
CML15(At1g18530)
CML43(At5g44460)
CML42(At4g20780)
CML44(At1g21550)
CML39(At1g76640)
CML38(At1g76650)
CML37(At5g42380)
CML41(At3g50770)
CML40(At3g01830)
CML36(At3g10190)
CML35(At2g41410)
CML1(At3g59450)
CML29(At5g17480)
CML28(At3g03430)
CML22(At3g24110)
CML21(At4g26470)
0.600

Figure 1. Phylogenetic tree of the *Arabidopsis* calmodulins (CaMs) and calmodulin-like proteins (CMLs).

The phylogenetic tree was constructed by the UPGMA method. CaM and CML amino acid sequences were obtained from the TAIR database (http://www.Arabidopsis.org/). The TCH3 amino acid sequence used for constructing the phylogenetic tree comprises EF hands 3 to 6 (101-255 aa). For all other CAMs and CMLs the full amino acid sequence was used. The bootstrap values are given on the nodes as percentages. The scale depicts 0.6 substitutions per position.

In Chapter 2 we showed that auxin triggers sequestration of the protein kinase PINOID (PID) from the PM to the cytosol through a Ca^{2+}-dependent interaction with the CML TCH3. Internalization of PID-VENUS was significantly reduced in the *tch3-3* mutant a few minutes after auxin treatment, but after 20 minutes full internalization could be observed in this mutant background, suggesting that other CMLs or even the closely related CaMs act redundantly with TCH3 in this process. A recent protein interaction study using seven more divergent *Arabidopsis* CaM/CMLs identified 173 CaM/CMLs interacting proteins, of which 25% interact with all seven CaM/CMLs (Popescu et al., 2007). In view of these data, we tested the interaction of PID with other CaM/CMLs. Based on a phylogenetic tree of the CaMs and CMLs (Figure 1), we selected the most closely related to CML12/TCH3, CML10 (At2g41090) and one more distantly related CML24/TCH2 (At5g37770) and tested these proteins for binding with PID. Interestingly, like *TCH3*, also the *TCH2* gene has been identified in a screen for touch-inducible genes (Braam and Davis, 1990).

Co-transfection of *Arabidopsis* protoplasts with *35S:CFP* and *35S::TCH2-YFP* or *35S::CML10-YFP* showed that, like TCH3-YFP, both TCH2-YFP and CML10-YFP localize to the cytoplasm, and that in contrast to CFP these fusion proteins are excluded from the nucleus (Figures 2A,D). This localization differed significantly from that of PID-CFP, which is predominantly PM-associated both in protoplasts and *in planta* (Chapter 2 and Figure 2B).

When *35S::PID-CFP* and *35S::CML10-YFP* were co-transfected in auxin-starved *Arabidopsis* protoplasts, the subcellular location of PID-CFP did not change (Figure 2B). However, when the cotransfected cells were cultured in normal auxin-containing medium, PID-CFP subcellular localization became cytoplasmic (Figure 2C), suggesting that the auxin-dependent interaction with CML10 sequesters PID from the PM. In contrast, when *35S::PID-CFP* and *35S::TCH2-YFP* were co-transfected, either in auxin-starved or in auxin-cultured *Arabidopsis* protoplasts, PID-CFP remained at the PM (Figure 2E, F). This data suggests that PID interacts with CML10, but not with the more distantly related TCH2.

In order to confirm these results, we analyzed the interaction by cotransfecting protoplasts with *35S::PID-CFP* and *35S::TCH3-YFP*, *35S::CML10-YFP* or *35S::TCH2-YFP* and using the sensitized emission approach to detect Fluorescent Resonance Energy Transfer (FRET) between the two fluorophores. While strong FRET was detected in protoplasts transfected with the positive control construct *35S::CFP-YFP*, a much lower but significant FRET signal was detected in protoplasts co-expressing PID-CFP and one of the CML-YFP fusion proteins, relative to their corresponding negative control (protoplasts co-expressing CFP and the corresponding CML-YFP (Figure 2G). In protoplasts co-expressing PID-CFP and TCH2-YFP, the FRET index was lower than for the other two combinations, suggesting that PID and TCH2 interact only with low affinity.

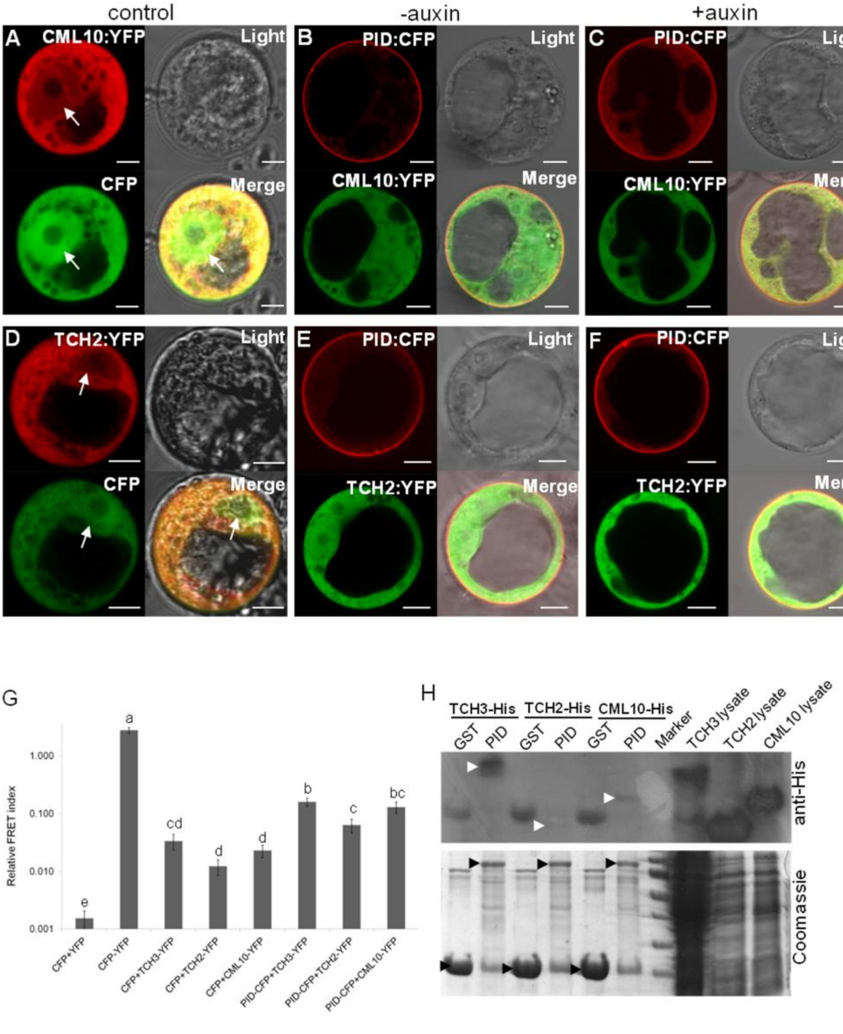
control
-auxin
+auxin
A
CML10:YFP
Light
CFP
Merge
B
PID:CFP
Light
CML10:YFP
Merge
C
PID:CFP
Light
CML10:YFP
Merge
D
TCH2:YFP
Light
CFP
Merge
E
PID:CFP
Light
TCH2:YFP
Merge
F
PID:CFP
Light
TCH2:YFP
Merge
G
Relative FRET index
1.000
0.100
0.010
0.001
a
cd
d
d
b
c
bc
e
CFP+YFP
CFP-YFP
CFP+TCH3-YFP
CFP+TCH2-YFP
CFP+CML10-YFP
PID-CFP+TCH3-YFP
PID-CFP+TCH2-YFP
PID-CFP+CML10-YFP
H
TCH3-His
TCH2-His
CML10-His
GST
PID
GST
PID
GST
PID
Marker
TCH3 lysate
TCH2 lysate
CML10 lysate
anti-His
Coomassie

Figure 2. PID is efficiently sequestered from the PM through binding with TCH3 and the closely related calmodulin-like protein CML10, but not with the more distantly related CML24/TCH2.

(A-F) *Arabidopsis* control protoplasts co-transfected with *35S::CML10-YFP* and *35S::CFP* (A) or

35S::TCH2-YFP and *35S::CFP* (D), showing that CML10-YFP and TCH2-YFP are cytoplasmic and excluded from the nucleus (white arrows). Auxin-starved (B,E) or auxin-cultured (C,F) *Arabidopsis* protoplasts co-transfected with *35S::PID-CFP* and *35S::CML10-YFP* (B,C) or with *35S::PID-CFP* and *35S::TCH2-YFP* (E,F). PID sequestration to the cytoplasm can be observed in auxin-cultured protoplasts co-expressing CML10, but not TCH2. For each protoplast in A-F confocal images are shown of the individual CFP-, YFP- and transmitted light channels and of the three channels merged. The scale bar indicates 10 μm. (G) Sensitized emission analysis of Fluorescent Resonance Energy Transfer (FRET) between PID-CFP and TCH3-YFP, TCH2-YFP or CML10-YFP. Protoplasts co-expressing CFP with YFP, TCH3-YFP, TCH2-YFP or CML10-YFP are used a negative control, and protoplasts expressing a CFP-YFP fusion as positive control. The graph shows the relative FRET index on a logarithmic ($\log^{10}$) scale. The values are compared and classified (a to e) using the Student's *t*-test ($P<0.05$). (H) *In vitro* pull down assay using GST or GST-PID bound to glutathione beads as bait. His-tagged fusions of TCH3 and CML10 show a significant interaction, whereas only a very weak interaction is observed for TCH2. Upper panel: Western blot detecting His-tagged CML proteins using anti-His antibodies. White arrowheads indicate the positions of the His-tagged CML proteins. The anti-His antibody shows cross-reaction with the dominant GST band. Lower panel: Coomassie stained gel showing the protein input in the pull-down assay. Black arrowheads indicate the band representing GST (lower) or GST-PID (upper).

In order to further confirm the interaction, GST-tagged isolates of full-length PID were incubated with crude *E.coli* extracts containing Histidine (His)-tagged TCH3, TCH2 or CML10. Protein complexes were pulled down with glutathione beads and separated on gel. Western blot analysis using anti-His antibodies showed that PID interacts most strongly with TCH3, significantly with CML10 and only very weakly with TCH2 (Figure 2H).

These data are in line with our hypothesis that CML10 and other closely related CMLs act redundantly with TCH3 in sequestering PID from the PM through their Ca^{2+}-dependent interaction with this kinase. Based on FRET and *in vitro* pull downs, the more distantly related CML TCH2 does bind to PID, but with insufficient affinity to sequester PID from the PM. This role seems to be reserved for TCH3 and the more closely related CMLs. The results explain why NAA-induced PID internalization is still observed in the *tch3-3* mutant background, and also why the *tch3-3* loss-of-function mutant does not show a strong phenotype.

CaM/CML binding and PM-association are mediated by the PID insertion domain

In Chapter 2 we demonstrated a function for the PID-TCH3 interaction during gravitropic root growth, however, the effect of the *tch3* loss-of-function on root gravitropism was mild, probably because other redundantly interacting CML proteins are also expressed in the root tip. One way to obtain a clearer view on the function of the PID-CML signaling complex in plant development would be to complement the *pid* loss-of-function mutant with a PID mutant version that is fully functional except for its interaction with the CMLs (untouchable PID). We therefore set out to map the CML-binding domain in PID.

A typical characteristic of the plant-specific AGCVIII kinases is that they have an insertion of about 36-90 amino acids in their catalytic domain (Galván-Ampudia and Offringa, 2007; Rademacher and Offringa, 2012) For PID this ID was reported to be involved in its association with the PM (Zegzouti et al., 2006b; Galván-Ampudia and Offringa, 2007; Rademacher and Offringa, 2012). In order to confirm these initial localization studies in yeast, we constructed an ID-YFP fusion and transfected this to *Arabidopsis* protoplasts. Like PID-YFP, also ID-YFP showed predominant PM localisation (Figure 3C, D), confirming that PID associates with the PM through its ID.

Previous analysis showed that TCH3 interacts with the catalytic domain of PID (Chapter 2). As TCH3 binding interfered with the association of PID to the PM, we tested the hypothesis that TCH3 binds to the PID ID. Indeed, TCH3 could be pulled down *in vitro* by GST-PID or even stronger with the GST-ID alone, but not by a GST-PID versions whose ID had been removed (PID minus ID, Figure 3A, B). Placing back the ID in PID minus ID (PID-ID+ID) restored its capacity to pull down TCH3 (Figure 3A, B). Taken together, our results strongly indicated that both the PM association domain and the CaM/CML binding domain are located inside the ID of PID. To further map the CaM/CML binding domain, we replaced the ID with three smaller segments, being 227-253, 240-266, 254-280 (PID-ID+$ID_{227-253}$ etc., Figure 3A). The *in vitro* pull down experiments showed that the $ID_{240-266}$ segment strongly bound to TCH3, whereas the other segments did not (Figure 3G), suggesting that the calmodulin binding domain is located in the middle part of the ID.

When expressed in *Arabidopsis* protoplasts, PID-YFP, PID-ID+ID:YFP and PID-ID+$ID_{240-266}$:YFP localized to the PM (Figure 3H, I, L), whereas the PID-ID:YFP, PID-ID+$ID_{227-253}$:YFP and PID-ID+$ID_{254-280}$:YFP fusions localized to the cytosol (Figure 3E, F, J, K, M). This result suggests that the PM binding domain and the CaM/CML binding domain overlap in the middle segment of the ID. In some protoplasts PID versions with ID deletions localized to cytoskeleton-like stuctures

(Figures 3E and J), suggesting that in the absence of PM association or TCH3 binding PID can be recruited to the cytoskeleton.

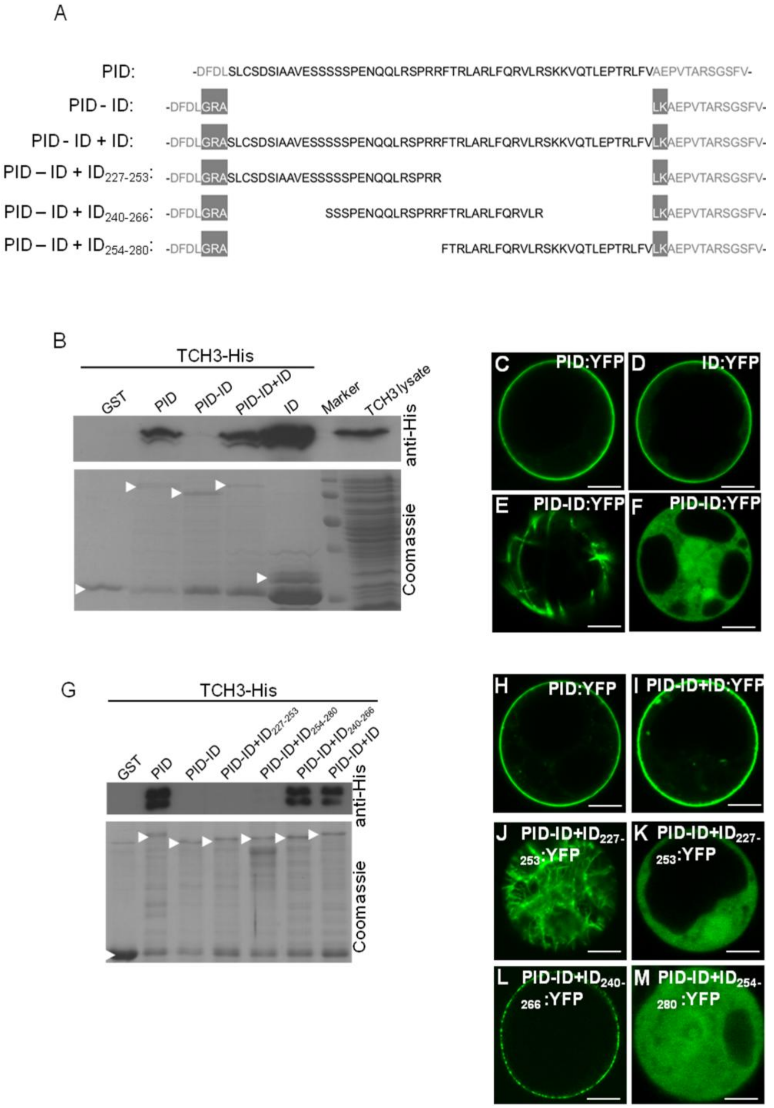
A
PID: -DFDLSLCSDSIAAVESSSSSPENQQLRSPRRFTRLARLFQRVLRSKKVQTLEPTRLFVAEPVTARSGSFV-
PID - ID: -DFDLGRA LKAEPVTARSGSFV-
PID - ID + ID: -DFDLGRASLCSDSIAAVESSSSSPENQQLRSPRRFTRLARLFQRVLRSKKVQTLEPTRLFVLKAEPVTARSGSFV-
PID – ID + ID227-253: -DFDLGRASLCSDSIAAVESSSSSPENQQLRSPRR LKAEPVTARSGSFV-
PID – ID + ID240-266: -DFDLGRA SSSPENQQLRSPRRFTRLARLFQRVLR LKAEPVTARSGSFV-
PID – ID + ID254-280: -DFDLGRA FTRLARLFQRVLRSKKVQTLEPTRLFVLKAEPVTARSGSFV-
B
TCH3-His
GST
PID
PID-ID
PID-ID+ID
ID
Marker
TCH3 lysate
anti-His
Coomassie
C PID:YFP
D ID:YFP
E PID-ID:YFP
F PID-ID:YFP
G
TCH3-His
GST
PID
PID-ID
PID-ID+ID227-253
PID-ID+ID254-280
PID-ID+ID240-266
PID-ID+ID
anti-His
Coomassie
H PID:YFP
I PID-ID+ID:YFP
J PID-ID+ID227-253:YFP
K PID-ID+ID227-253:YFP
L PID-ID+ID240-266:YFP
M PID-ID+ID254-280:YFP

Figure 3 CaM/CML binding and PM association are mediated by the middle part of the PID ID

(A) An overview of the PID ID (black letters) with different PID mutant versions used in the *in vitro* pull down and protoplast expression experiments. The mutant PID versions were generated by creating restriction enzyme sites, which introduced a few additional amino acids at the borders of the ID (boxed in gray).

(B) *In vitro* pull down of His-TCH3 with GST, GST-PID (PID), GST-PID without ID (PID-ID), GST-PID minus ID with the ID placed back (PID-ID+ID) or with GST-ID (ID). Upper panel: Western blot analysis using anti-His antibodies to detect His-tagged TCH3. Lower panel: Coomassie stained gel showing sample loading. The size marker and TCH3 lysate are loaded as reference. White arrowheads indicate the positions of the respective GST-tagged proteins.

(C-F) *Arabidopsis* protoplasts expressing PID-YFP (C), ID-YFP (D) or PID minus ID-YFP (E, F)

(G) *In vitro* pull down of His-TCH3 with GST, GST-PID (PID), GST-PID minus ID (PID-ID), GST-PID minus ID with the ID segments 227-253, 254-280, 240-266 or the complete ID re-inserted (PID-ID+ID$_{227\text{-}253,}$ PID-ID+ID$_{254\text{-}280,}$ PID-ID+ID$_{240\text{-}266,}$ or PID-ID+ID). Upper panel: Western blot analysis using anti-His antibodies to detect His-tagged TCH3. Lower panel: Coomassie stained gel showing sample loading. White arrowheads indicate the positions of the respective GST-tagged proteins.

(H-M) *Arabidopsis* protoplasts expressing a PID-YFP fusion (H), or a PID minus ID-YFP fusion with the ID segments 227-253 (J, K), 240-266 (L), 254-280 (M), or the complete ID (I) re-inserted.

C-F and H-M show confocal YFP channel images. The scale bar indicates 10 µm.

To fine map the PM and TCH3 binding domains, we used alanine scanning to replace stretches of 7 amino acids in the middle part of the ID, being Ala1 (QLRSPRR), Ala2 (FTRLARL), Ala3 (FQRVLRS) (Figure 4A). In general, CaM/CML binding domains are enriched in hydrophobic and positively charged amino acids (Poovaiah et al., 2013), and we therefore ignored the first part of this fragment (SSSPENQ), as it contains no positively charged amino acids and only one hydrophobic residue. Surprisingly, none of the three Ala mutants showed PM localization (Figure 4B-F), nor did they show *in vitro* binding to TCH3 (Figure 4G). This data confirms that the middle part of the ID is both important for CaM/CML binding and for association of the kinase to the PM. Interestingly, besides showing cytoplasmic localization, the PID Ala2-CFP mutant localized to endosomal compartments (Figure 4D), and the PID Ala3-CFP mutant to cytoskeleton-like structures (Figure 4E). These results corroborate our previous findings that PID subcellular localization is dynamically regulated (Chapter 2), and that PID can be recruited to other subcellular compartments, such as endosomes or the cytoskeleton, when PM association or TCH3 binding is disrupted.

An amphipathic alpha helix in the PID insertion domain mediates both CaM/CML binding and PM association

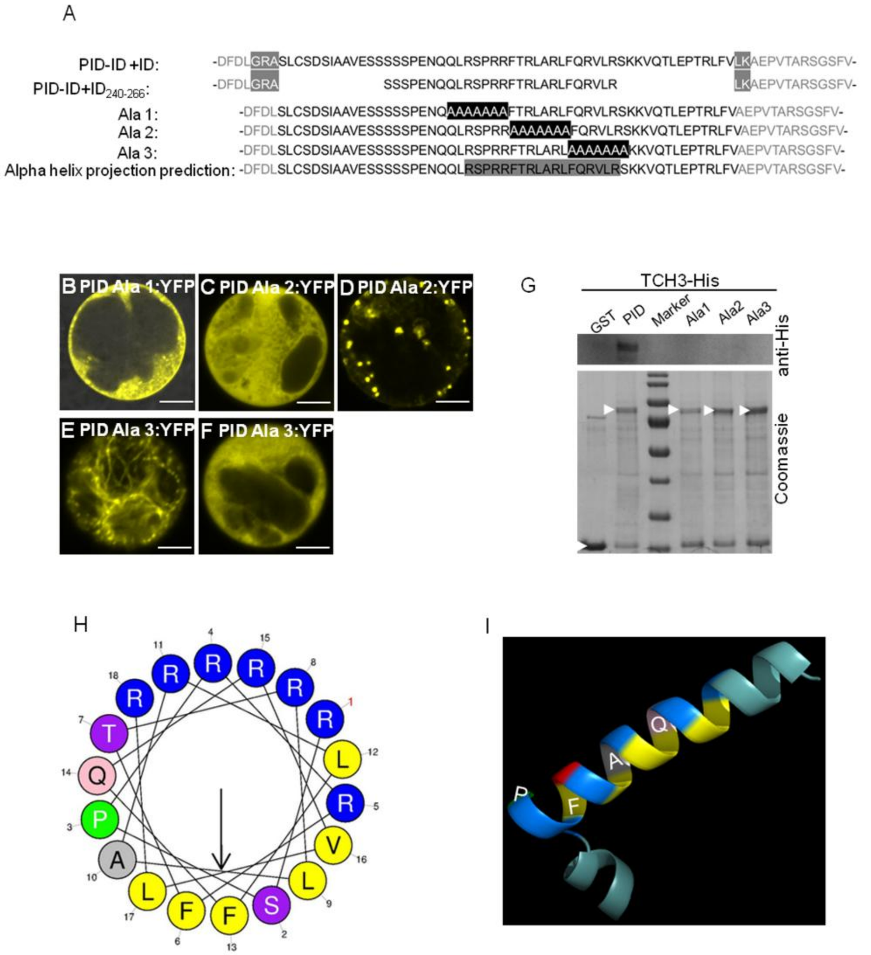
A
PID-ID +ID: -DFDLGRASLCSDSIAAVESSSSSPENQQLRSPRRFTRLARLFQRVLRSKKVQTLEPTRLFVLKAEPVTARSGSFV-
PID-ID+ID240-266: -DFDLGRA SSSPENQQLRSPRRFTRLARLFQRVLR LKAEPVTARSGSFV-
Ala 1: -DFDLSLCSDSIAAVESSSSSPENQAAAAAAAFTRLARLFQRVLRSKKVQTLEPTRLFVAEPVTARSGSFV-
Ala 2: -DFDLSLCSDSIAAVESSSSSPENQQLRSPRRAAAAAAAFQRVLRSKKVQTLEPTRLFVAEPVTARSGSFV-
Ala 3: -DFDLSLCSDSIAAVESSSSSPENQQLRSPRRFTRLARLAAAAAAAKKVQTLEPTRLFVAEPVTARSGSFV-
Alpha helix projection prediction: -DFDLSLCSDSIAAVESSSSSPENQQLRSPRRFTRLARLFQRVLRSKKVQTLEPTRLFVAEPVTARSGSFV-
B PID Ala 1:YFP
C PID Ala 2:YFP
D PID Ala 2:YFP
E PID Ala 3:YFP
F PID Ala 3:YFP
G
TCH3-His
GST
PID
Marker
Ala1
Ala2
Ala3
anti-His
Coomassie
H
R 1
S 2
P 3
R 4
R 5
F 6
T 7
R 8
L 9
A 10
R 11
L 12
F 13
Q 14
R 15
V 16
L 17
R 18
I
P
F
A
Q

Figure 4 Alanine scanning and protein structure prediction suggest that PM association and CaM/CML binding are mediated by an amphipathic alpha helix in the PID ID.

(A) An overview of the amino acid changes in the ID of different PID mutant proteins. The ID is represented by black letters. The white letters in gray background indicate the additional amino acids introduced by the addition of restriction enzyme sites in the construct. The white letters in black background indicate the amino acid stretches substituted by alanines. The black letters in grey background indicate the position of the predicted amphipathic alpha helix. (B-F) *Arabidopsis* protoplasts expressing alanine substitution versions PID Ala1-YFP (B), PID Ala2-YFP (C, D), PID Ala3-YFP (E, F). Scale bars indicate 10 µm.

(G) *In vitro* pull down of His-tagged TCH3 with GST, GST-tagged PID (PID), GST-tagged PID Ala1 (Ala1), GST-tagged PID Ala2 (Ala2) or GST-tagged PID Ala3 (Ala3). Upper panel: Western blot analysis using anti-His antibodies to detect His-tagged TCH3. Lower panel: Coomassie stained gel showing sample loading. White arrowheads indicate the positions of the respective GST-tagged proteins.

(H, I) Alpha helix projection (H) and protein structure prediction indicate that amino acid residues 249 to 266 in PID form a strong amphipathic alpha helix. Positively charged residues are in blue, whereas the hydrophobic residues are in yellow or grey. The numbers 1 to 18 in (H) indicate the order of the amino acids in the sequence. (I) 3D protein structure prediction of the amphipathic alpha helix (residues 249 to 266) with a positively charged face (blue) on one side and a predominantly hydrophobic face (yellow/grey) on the other side. The same color code for the amino acid residues is used in (H) and (I), except that the threonine residue (purple in H) is now red.

Ca^{2+}-dependent CaM binding is generally mediated by a non-conserved domain of around 20 amino acids with multiple basic residues flanking critical hydrophobic residues, and often a propensity to form an amphipathic alpha helix (Poovaiah et al., 2013). Ca^{2+} binding by a CaM results in conformational changes that exposes hydrophobic residues that wrap around the hydrophobic residues in this amphipathic helix, while acidic residues interact with the basic residues in the amphipatic helix (Snedden and Fromm, 2001; Bahler and Rhoads, 2002; Du and Poovaiah, 2005; Poovaiah et al., 2013). Moreover, amphipathic helices have also been reported to mediate interaction of peripheral membrane proteins with phospholipids in the PM (Heximer et al., 2001; Bhardwaj et al., 2013; Lu and Taghbalout, 2013).

In view of the overlapping CaM/CML binding and PM association functionalities in the PID ID, we looked more closely to its 3 dimensional structure. Several protein structure tools predicted the presence of an alpha helix inside of the ID (Figure 4A). Visualization of this alpha helix using helical wheel projection software (http://heliquest.ipmc.cnrs.fr/) indicated that the ID segment comprising amino acid residues 249 to 266 (RSPRRFTRLARLFQRVLR) forms a perfect amphipathic alpha helix with seven positively charged amino acids on one side, and six hydrophobic amino acids on the other side (Figure 4A, H, I).

To confirm that the predicted amphipathic alpha helix is important for CaM/CML binding and PM localization, we generated the PID mutants R249,252,253A,R263,266A, R249,252,253,263,266A in which the amphipathic properties of the helix were disrupted, and used PID mutant S/T250, 255A, which is not changed in the amphipathic properties but has potential phosphorylation sites removed, as a negative control. Transfection of the constructs *35S::PID*$_{R249,252,253A}$*-YFP*, *35S::PID*$_{R263,266A}$*-YFP*, *35S::PID*$_{R249,252,253,263,266A}$*-YFP* and *35S::PID*$_{S/T250,\ 255A}$*-YFP* to

Arabidopsis protoplasts, showed that all arginine to alanine substitutions disrupted PM localization, whereas the serine/threonine to alanine substitutions did not affect PM localization of PID (Figure 5A-E). The *in vitro* pull-down experiments showed that all R to A substitutions also disrupted the interaction with TCH3, whereas the S/T250, 255A substitutions did not. Our results indicate that the amino acid residues 249 to 266 in the ID of PID form an amphipathic alpha helix that mediates both CaM/CML binding and PM association.

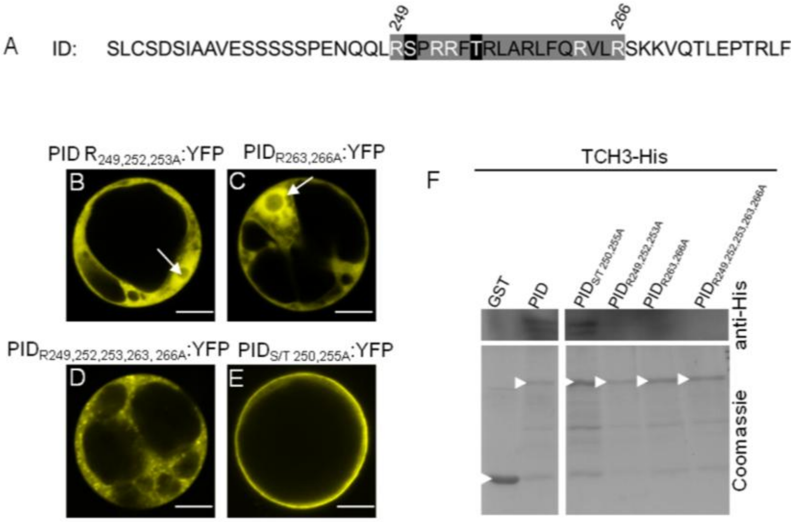
A
ID:
SLCSDSIAAVESSSSSPENQQLRSPRRFTRLARLFQRVLRSKKVQTLEPTRLF
249
266
PID R249,252,253A:YFP
PIDR263,266A:YFP
B
C
PIDR249,252,253,263, 266A:YFP
PIDS/T 250,255A:YFP
D
E
F
TCH3-His
GST
PID
PIDS/T 250,255A
PIDR249,252,253A
PIDR263,266A
PIDR249,252,253,263,266A
anti-His
Coomassie

Figure 5 Amphipathic properties of the alpha helix in the PID ID are important for both PID PM localization and CaM/CML binding.

(A) An overview of the PID ID, with the amino acid residues comprising the predicted amphipathic alpha helix highlighted by a grey box, and the arginines (R) or the serine or threonine (S/T) that were substituted by alanines indicated by white letters. (B-E) *Arabidopsis* cell suspension protoplasts expressing PID$_{R249,252,253A}$-YFP (B), PID$_{R263,266A}$-YFP (C), PID$_{R249,252,253,263,266A}$-YFP (D) or PID$_{S/T\ 250,255A}$-YFP (E). Size bars indicate 10 µm. (F) *In vitro* pull down of His-tagged TCH3 with GST, or GST-tagged PID (PID), -PID$_{R249,252,253A}$, -PID$_{R263,266A}$, -PID $_{R249,252,253,263,266A}$ or -PID$_{S/T\ 250,255A}$. Upper panel: Western blot analysis using anti-His antibodies to detect His-tagged TCH3. Lower panel: Coomassie stained gel showing sample loading. White arrowheads indicate the positions of the respective GST-tagged proteins.

An IQ-like motif overlapping with the amphipathic alpha helix is required for CaM/CML binding *in vivo*

Our previous data showed that the ID$_{240\text{-}266}$ fragment containing the amphipathic alpha helix was sufficient to confer PM localization to the PID-ID+ID$_{240\text{-}266}$ fusion protein (Figure 3L), and also to efficiently pull down TCH3 *in vitro* (Figure 3G). However, co-transfection of *Arabidopsis* protoplasts with *35S::PID-ID+ID*$_{240\text{-}266}$*-CFP* and *35S::TCH3-YFP* showed that this part of the ID cannot be sequestered by TCH3, even in auxin-treated *Arabidopsis* protoplasts (Figure 6A, D, E), whereas the PID-CFP control showed clear auxin-dependent sequestration (Figure 6B, C). These data corroborate that the PM association domain maps to this middle segment of the ID, but also indicate that this segment is not sufficient for efficient binding of TCH3 or related proteins *in vivo.*

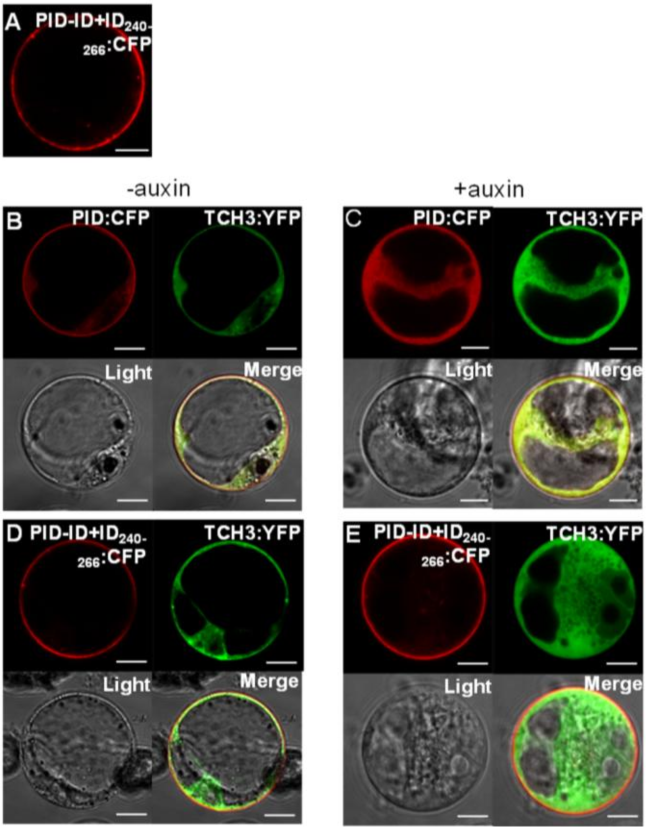
A PID-ID+ID240-266:CFP
-auxin
+auxin
B PID:CFP
TCH3:YFP
Light
Merge
C PID:CFP
TCH3:YFP
Light
Merge
D PID-ID+ID240-266:CFP
TCH3:YFP
Light
Merge
E PID-ID+ID240-266:CFP
TCH3:YFP
Light
Merge

Figure 6 The amphipathic alpha helix in the PID ID is not sufficient for TCH3-mediated sequestration of PID from the PM in *Arabidopsis* protoplasts.

(A) Confocal images (CFP channel) of *Arabidopsis* protoplasts expressing PID-ID+ID$_{240\text{-}266}$-CFP. (B-E) Auxin-starved (B, D) or auxin-cultured (C, E) *Arabidopsis* protoplasts co-expressing TCH3-YFP and

PID-CFP (B,C) or TCH3-YFP and PID-ID+$ID_{240-266}$-CFP (D,E). For each protoplast in B-E the confocal images of the individual CFP-, YFP- and transmitted light channels and of the three channels merged are shown. Scale bar indicates 10 µm.

Further analysis of the PID ID for putative CaM/CML binding domains identified an IQ-like motif that partially overlaps with the amphipathic alpha helix (Figure 7A). IQ motifs can be found in a wide range of CaM target proteins, where they can mediate either Ca^{2+}-dependent or Ca^{2+}-independent interactions with the CaM (Rhoads and Friedberg, 1997; Bahler and Rhoads, 2002). The IQ-like motif identified in PID lacks the central G residue and also the second basic residue that is normally found in Ca^{2+}-independent IQ-motifs, which fits with its Ca^{2+}-dependent action (http://calcium.uhnres.utoronto.ca/ctdb/ctdb/motifs/iq_motif.html; (Houdusse and Cohen, 1995; Munshi et al., 1996)).

To test whether the predicted overlapping amphipathic alpha helix and IQ-like motif together were required for the interaction with TCH3 *in vivo*, a fragment encoding amino acid residues 244 to 275 (ENQQLRSPRRFTRLARLFQRVLRSKKVQTLEP) was translationally fused to YFP. The $ID_{244-275}$-YFP fusion showed PM localization (Figure 7A, B), like PID-YFP and ID-YFP, and the $ID_{244-275}$-YFP fusion protein was sequestered to the cytosol in an auxin-dependent manner when co-expressed with TCH3-CFP (Figure 7C-H). This data suggests that the fragment contains a functional CaM/CML binding and PM association domain, and that the additional amino acids belonging to the predicted IQ-like motif are essential for CaM/CML binding *in vivo* .

Interestingly, we noted that when the ID-YFP and the $ID_{244-275}$-YFP fusion proteins were co-expressed together with TCH3-CFP, they showed significantly more cytoplasmic signal in the auxin-starved protoplasts compared to full length PID-YFP (Figure 7C-H), and also compared to when the fusion proteins were expressed alone (Figure 7A). This suggests that TCH3 has higher affinity for the ID fragments compared to the full length PID protein, which possibly causes TCH3 to interact with these fusion proteins even in the absence of the auxin-induced Ca^{2+} signal. Indeed, the *in vitro* pull down experiments confirmed that the affinity of TCH3 for the $ID_{244-275}$-GST fusion is significantly higher than for the PID-GST fusion (Figure 7I). This result implies that access of TCH3 to the ID is somehow inhibited by the rest of the PID protein, and that an auxin-triggered Ca^{2+} response is required for efficient recruitment of PID by TCH3. Interestingly, in an *in vitro* pull down assay the GST-tagged $ID_{244-275}$ showed interaction with TCH3 and the closely-related CAM2, but not with CML9, and only weakly with the even less-related calmodulin-like protein TCH2 (Figure 7J). In view of the strong amino acid conservation among the seven CAMs in *Arabidopsis* (Figure 9), it is likely that they all interact with PID. Our results suggest that the CAMs and the closely related CMLs TCH3 and CML10 act redundantly in regulating the activity of PID and WAG2, by sequestering these kinases from the PM in response to elevated cytosolic calcium levels ($[Ca^{2+}]_{cyt}$).

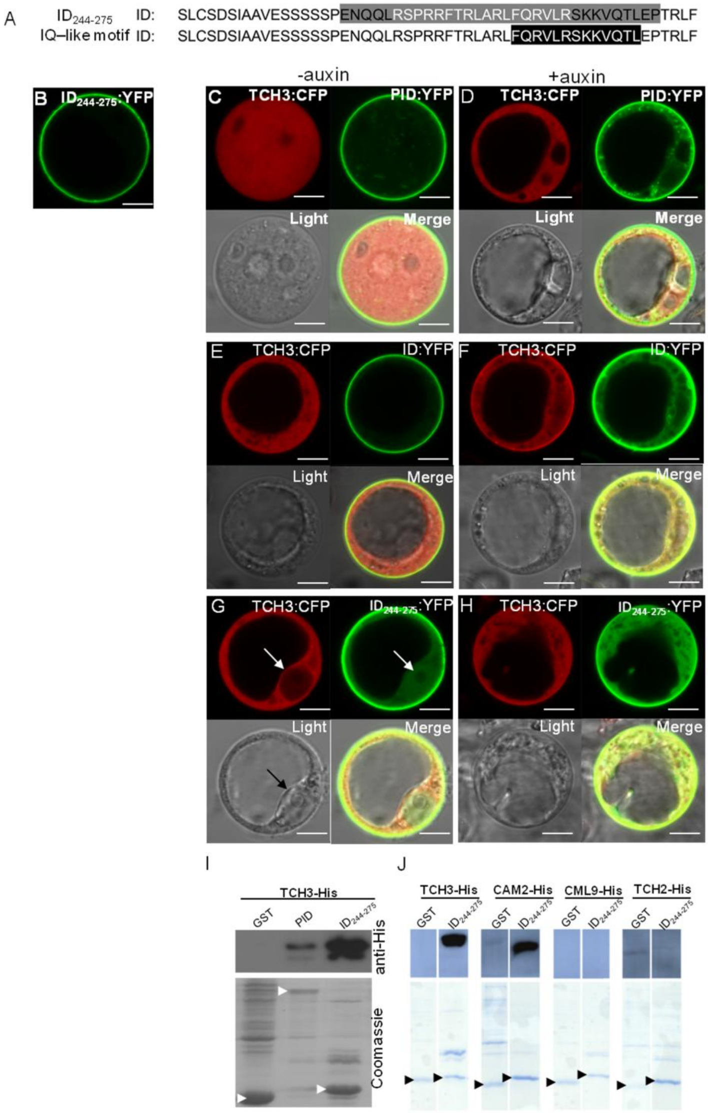
A
ID244-275 ID: SLCSDSIAAVESSSSSPENQQLRSPRRFTRLARLFQRVLRSKKVQTLEPTRLF
IQ–like motif ID: SLCSDSIAAVESSSSSPENQQLRSPRRFTRLARLFQRVLRSKKVQTLEPTRLF
B ID244-275:YFP
-auxin
+auxin
C TCH3:CFP
PID:YFP
D TCH3:CFP
PID:YFP
Light
Merge
E TCH3:CFP
ID:YFP
F TCH3:CFP
ID:YFP
G TCH3:CFP
ID244-275:YFP
H TCH3:CFP
ID244-275:YFP
I
TCH3-His
GST
PID
ID244-275
anti-His
Coomassie
J
TCH3-His
CAM2-His
CML9-His
TCH2-His
GST
ID244-275

Figure 7 A segment of the PID ID comprising the amphipathic alpha helix and the overlapping IQ-like Motif is sufficient for PM association and auxin-triggered CaM/CML-mediated sequestration.

(A) An overview of the PID ID with the amino acid residues of the $ID_{244-275}$ segment highlighted by a grey box, and the IQ-like motif indicated by white letters in a black box. The white letters in the grey box indicate the predicted alpha helix.

(B) Confocal image (YFP channel) of *Arabidopsis* protoplast expressing $ID_{244-275}$-YFP. (C-H) Auxin-starved (C, E, G) or auxin-cultured (D, F, H) *Arabidopsis* protoplasts co-expressing TCH3-CFP and PID-YFP (C,D), TCH3-CFP and ID-YFP (E,F), or TCH3-YFP and $ID_{244-275}$-YFP (G,H). For each protoplast in C-H confocal images are shown of the individual CFP-, YFP- and transmitted light channels and of the three channels merged. Scale bar indicates 10 µm. White arrow in G indicates the nucleus.

(I, J) *In vitro* pull down of His-tagged TCH3 with GST, or GST-tagged PID or -$ID_{244-275}$ (I) or of His-tagged TCH3 , -CAM2, -CML9 or -TCH2 with GST, or GST-tagged $ID_{244-275}$ (J). Upper panel: Western blot analysis using anti-His antibodies to detect His-tagged TCH3. Lower panel: Coomassie stained gel showing sample loading. White (I) or black (J) arrowheads indicate the positions of the respective GST-tagged proteins.

PM association and CaM binding are tightly coupled functionalities in the PID ID

The $ID_{240-266}$ fragment was sufficient for PM association, but sequestration by TCH3 in protoplasts required the $ID_{244-275}$ segment, which included the IQ-like motif. As expected, deletion of the complete IQ-like motif or substitution of the motif for alanines disrupted both PID PM association and its interaction with TCH3 (M3 and M4, Figure 8A,E,F,J). We hypothesized, however, that it should be possible to disrupt the interaction between PID and TCH3 without interfering with PID PM-association by substituting residues in the IQ-like motif that are not part of the predicted amphipathic alpha helix. We focused on positively charged and hydrophobic amino acids, as these are known to be important for the interaction with the CaMs and CMLs (Snedden and Fromm, 2001; Du and Poovaiah, 2005; Du et al., 2009). Unexpectedly, all mutant PID versions (M1, M2, M5, M6 and M7) had lost their capacity to associate to the PM (Figure 8A-I), whereas two IQ-like motif-specific substitutions (M6 and M7) were still able to interact with TCH3 in *in vitro* pull downs (Figure 8A, J). Since the *in vivo* assay for CaM/CML-mediated sequestration requires PID to be at the PM, we cannot exclude that efficient *in vivo* CaM/CML binding does require the complete IQ-like motif (including the VQTL residues).

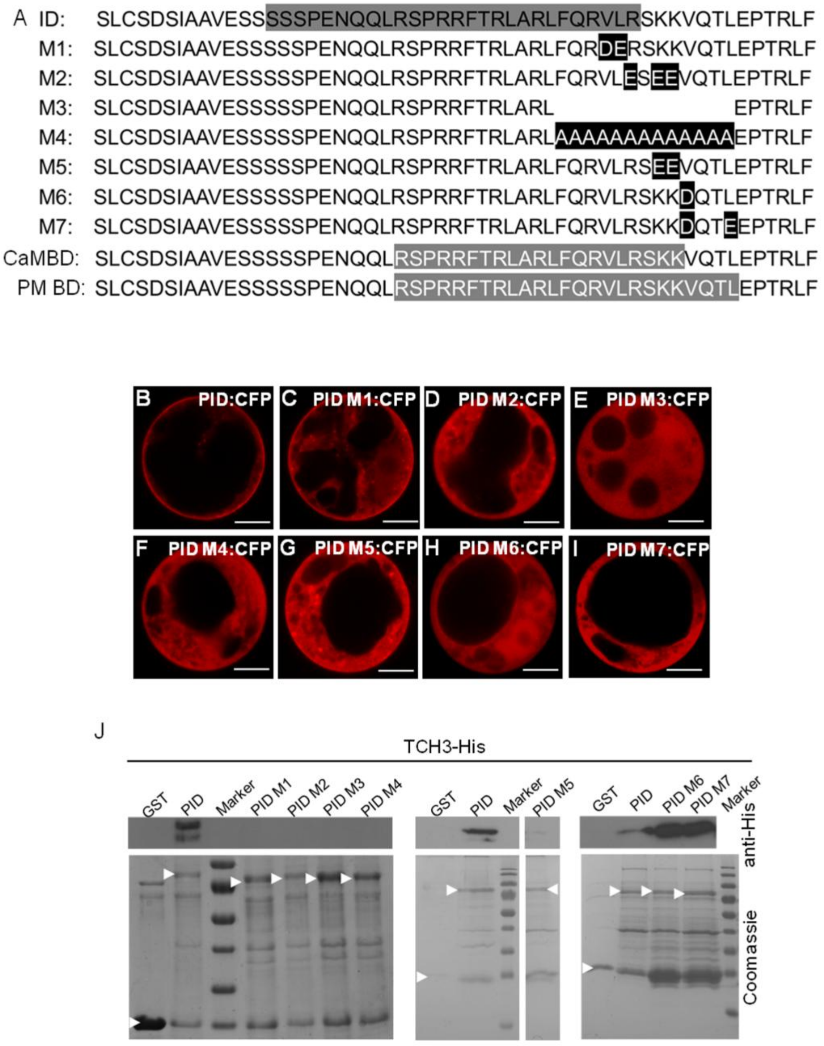
A
ID: SLCSDSIAAVESSSSSPENQQLRSPRRFTRLARLFQRVLRSKKVQTLEPTRLF
M1: SLCSDSIAAVESSSSSPENQQLRSPRRFTRLARLFQRDERSKKVQTLEPTRLF
M2: SLCSDSIAAVESSSSSPENQQLRSPRRFTRLARLFQRVLESEEVQTLEPTRLF
M3: SLCSDSIAAVESSSSSPENQQLRSPRRFTRLARL EPTRLF
M4: SLCSDSIAAVESSSSSPENQQLRSPRRFTRLARLAAAAAAAAAAAAEPTRLF
M5: SLCSDSIAAVESSSSSPENQQLRSPRRFTRLARLFQRVLRSEEVQTLEPTRLF
M6: SLCSDSIAAVESSSSSPENQQLRSPRRFTRLARLFQRVLRSKKDQTLEPTRLF
M7: SLCSDSIAAVESSSSSPENQQLRSPRRFTRLARLFQRVLRSKKDQTEEPTRLF
CaMBD: SLCSDSIAAVESSSSSPENQQLRSPRRFTRLARLFQRVLRSKKVQTLEPTRLF
PM BD: SLCSDSIAAVESSSSSPENQQLRSPRRFTRLARLFQRVLRSKKVQTLEPTRLF
B PID:CFP
C PID M1:CFP
D PID M2:CFP
E PID M3:CFP
F PID M4:CFP
G PID M5:CFP
H PID M6:CFP
I PID M7:CFP
J
TCH3-His
GST
PID
Marker
PID M1
PID M2
PID M3
PID M4
GST
PID
Marker
PID M5
GST
PID
PID M6
PID M7
Marker
anti-His
Coomassie

Figure 8 CaM/CML binding and PM association converge at an overlapping amphipathic alpha helix and IQ-like motif in the PID ID.

(A) An overview of the PID ID and the amino acid deletions or substitutions introduced in the mutant versions M1 to M7. The black letters with a grey background indicate amino acids that are the part of the $\mathrm{ID}_{240\text{-}266}$ segment that seems sufficient for PM localization but not for sequestration by TCH3 binding *in vivo*. The white letters in black background indicate the amino acid substitutions in the PID mutant versions. The white letters with grey background indicate the amino acid region needed for CaM/CML binding (CaM BD) or PM association (PM BD).

(B-I) *Arabidopsis* protoplasts expressing PID-CFP or the mutant versions M1 to M7. The scale bars indicate 10 µm.

(J) *In vitro* pull down of His-tagged TCH3 with GST, or GST-tagged PID or its mutant versions M1 to M7. Upper panel: Western blot analysis using anti-His antibodies to detect His-tagged TCH3. Lower panel: Coomassie stained gel showing sample loading. White arrowheads indicate the positions of the respective GST-tagged proteins.

Based on these data, we concluded that PM association and CaM/CML binding are two tightly associated functionalities present in the ID of PID (PM BD and CaM BD, Figure 8A). Unfortunately, this strong overlap prevents the generation of an untouchable PID, a kinase version that still associates with the PM but cannot be sequestered to the cytosol through the Ca^{2+}-dependent interaction with a CaM or CML. However, our research has identified a novel domain that confers Ca^{2+} responsiveness to the PID kinase by combining the CaM/CML binding and PM association characteristics.

Discussion

The second messenger Ca^{2+} is one of the most elementary signaling molecules in all organisms, that acts through rapid trigger-induced elevation of its cytosolic concentration (Roberts and Harmon, 1992; Trewavas and Malho, 1998; Chin and Means, 2000). In plants, the $[Ca^{2+}]_{cyt}$ is increased in response to diverse stimuli, including the plant hormone auxin (Knight et al., 1991; Polisensky and Braam, 1996; Knight, 2000),. Auxin increases $[Ca^{2+}]_{cyt}$ in root epidermis cells within seconds after application (Monshausen et al., 2011). Ca^{2+} signals are perceived through proteins that recruit Ca^{2+} through specific binding pockets (EF-hands), and subsequently undergo conformational changes that alter their activity (e.g. Ca^{2+}-dependent protein kinases), or allow them to interact with and to (in)activate their target proteins. CaMs are ubiquitous Ca^{2+}-binding proteins that have a double set of two EF hands, and share almost 90% sequence identity across plant, fungal, and vertebrate species (Zielinski, 1998). Based on this high level of sequence conservation, CaMs probably function in a similar way throughout diverse organisms. Next to the seven CAMs, the *Arabidopsis* genome encodes a large family of 50 CMLs that are predicted to act in a similar manner as the CaMs (McCormack and Braam, 2003). After Ca^{2+} binding to the EF-hands, two hydrophobic surfaces in CaM/CMLs surrounded by negative charges will be exposed, and these are able to efficiently interact with a stretch of hydrophobic amino acid residues in the target protein (Snedden and Fromm, 2001). In general, target proteins share very little amino acid sequence similarity in their CaM/CML binding sites (Snedden and Fromm, 2001).

Closely related CaMs and CMLs act redundantly in Ca^{2+}-dependent sequestration of PID from the PM

In Chapter 2 we showed that Ca^{2+} acts downstream of asymmetric distribution of auxin during root gravitropism. Auxin induced elevation of $[Ca^{2+}]_{cyt}$ led to binding of the CML TCH3 to PID, which recruited this kinase to the cytosol, and led to apolar PIN2 distribution in the root epidermis, needed to maximize the root gravitropic response. Based on these initial findings we investigated whether PID interacts with other CMLs or CaMs. Our data indicates that PID interacts with CML10 and CAM2, both closely related to TCH3. In view of the high amino acid identity it is likely that the other 6 *Arabidopsis* CaMs do also interact with PID. Surprisingly, no interaction was observed with CML9, which is closely related to TCH3 and CML10, and we found only a very weak interaction with the more distantly related CML24/TCH2. These results indicate that the Ca^{2+}-dependent sequestration of PID is an activity that is shared by only a few CaMs/CMLs. Moreover, the fact that TCH3 is able to sequester only two of the four AGC3 kinases corroborates the specificity of this interaction, and suggests some structural conservation between PID and WAG2, which is not apparent based on the primary amino acid sequence.

An alignment of the four CML proteins TCH3, CML10, CML9 and CML24/TCH2 tested here, together with the seven CaMs (Figure 9) confirmed the high level of identity among the CaMs, but also showed the increased amino acid sequence variation in the EF hands of the CMLs. The EF hands are enriched in negatively charged amino acids aspartic acid (D) and glutamic acid (E), which provide the electronegative environment for Ca^{2+} binding (Figure 9). Each EF hand also has 1-3 hydrophobic methionines (M) (Figure 9). Ca^{2+} binding induces a conformational change in the EF hands, that exposes the hydrophobic methyl groups from the methionines, which promotes binding to the hydrophobic regions of the amphiphilic helix/IQ motif in the target protein. From the alignment in Figure 9, it is difficult to predict which amino acid residues in the CaMs and CMLs are crucial for the specific interaction with the PID and WAG2 kinases.

Regulation of peripheral kinase localization through a single domain: a novel concept?

To overcome the redundant interaction between CaMs and PID, we tried to generate a PID mutant protein in which CaM binding, but not the PM-association was disrupted (untouchable PID). In order to do this we mapped the PID CaM binding- and PM association domains in PID. Our analysis showed that both functionalities converge to an overlapping amphipathic alpha helix and IQ-like motif in the PID insertion domain. The amphipatic properties of the alpha helix as well as the hydrophopic residues in the IQ motif appeared to be important for both functionalities, and the fact that even single amino acid changes in the C-terminal part of the IQ-like motif did not result in an untouchable PID version, indicates that it will be difficult to separate the two functionalities. The best candidate for an untouchable PID is the version where the middle part of the PID ID was placed back (PID-ID+ID$_{240\text{-}266}$), as it cannot be sequestered by TCH3, but still associates to the PM. This is surprising, since this version lacks the C-terminal part of the IQ motif, which was shown to be required for PM association. Possibly, the amino acid residues downstream of the amphipathic helix in this mutant version (L**K**AEPVT, see Figure 3A) are able to restore PM association but not the function of the IQ motif (S**K**KVQTL in wild-type PID, Figure 3A). Unfortunately, a preliminary test of this mutant version in an *in vitro* phosphorylation assay suggests that it has lost its kinase activity (data not shown).

CaMs/CMLs have numerous target proteins (Yap et al., 2000; Popescu et al., 2007). Among them, CaM-regulated serine/threonine kinases have been best characterized for their mechanism of interaction with CaM (Hoeflich and Ikura, 2002). Either amphipathic alpha helixes or IQ/IQ-like motifs have been identified before as CaM binding sites. In some cases, the IQ motif can form an amphipathic alpha helix, like in scallop myosin (Xie et al., 1994; Houdusse et al., 2006). However, in our case, the IQ-like motif is only half overlapping the clear amphipathic alpha helix that is predicted by our structural analysis. In PID, this amphipathic helix also acts as a membrane binding site, using the hydrophobic face to insert into the lipid acryl chains and the polar face to interact with the polar heads of the lipids and with the solvent (Cornell and Taneva, 2006).

Both protein-PM association and protein-CaMs/CMLs binding are biochemical processes and dependent on the physicochemical properties of protein, PM and CaMs/CMLs. Preliminary data suggest that PID can interact with the negatively charged phosphoinositides PI(3)P, PI(4)P, PI(5)P, PI(3,5)P2 and PI(4,5)P2 ((Zegzouti et al., 2006a);data not shown) that are found in plant cell membranes (Munnik and Nielssen, 2011). Phosphoinositides could produce the negative field needed to attract proteins with a positive patch, which could thus mediate PID localization to the PM (Olivotto et al., 1996). The CaMs/CMLs are also enriched in negative charges especially in EF hands (Figure 9). So both the negatively charged CaMs/CMLs and phosphoinositides may competitively interact with the positive charges on the amphiphitic alpha helix/IQ-like motif, which may be the reason CaMs/CMLs can pull the positive charged amphiphitic alpha helix/IQ-like motif off the PM (McLaughlin and Murray, 2005; Clapham, 2007).

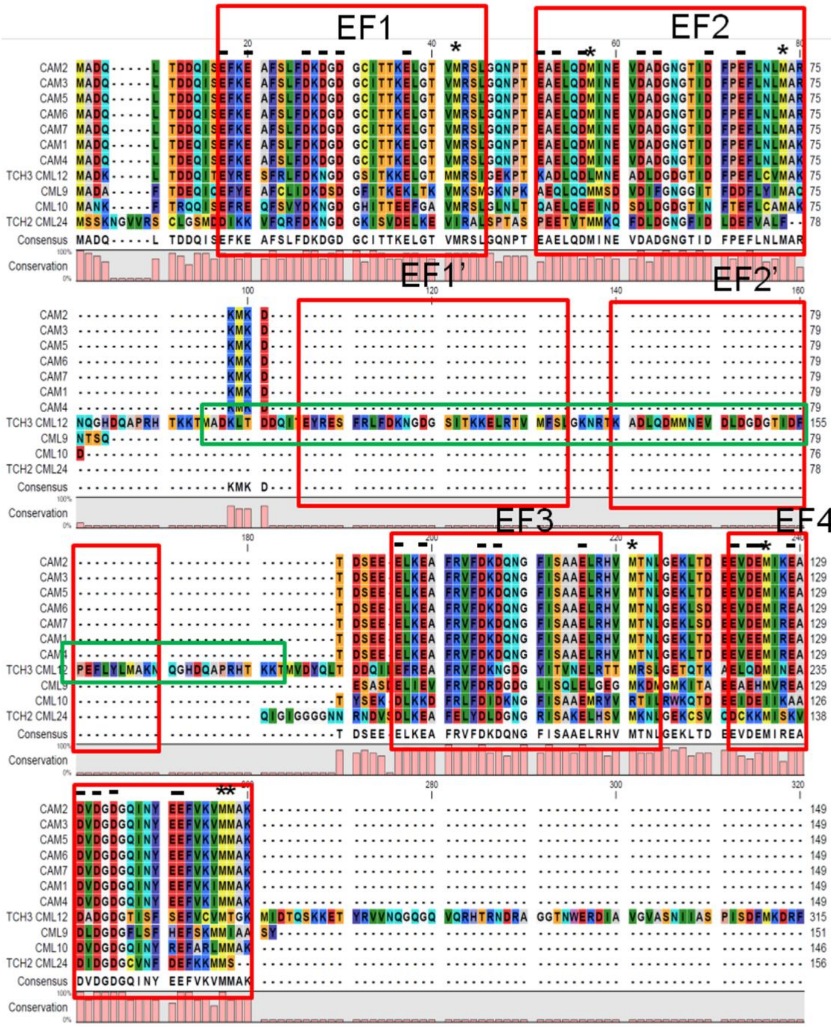
EF1
EF2
EF1'
EF2'
EF3
EF4
CAM2
CAM3
CAM5
CAM6
CAM7
CAM1
CAM4
TCH3 CML12
CML9
CML10
TCH2 CML24
Consensus
Conservation

Figure 9 Alignment of TCH3 with CML9, CML10,TCH2 and CAM1 to CAM7.

The red boxes indicate the positions of the EF-hands. The ‘-’ above the alignment indicates negatively charged amino acids in the EF-hands which may be involved for the ion coordination. The methionine residues are marked with ‘*’.

The dual function of a protein domain in PM association and CaM binding is not a novel concept, as it has been reported for some animal PM associated or transmembrane proteins, but in those cases it just consisted of a cluster of positively charged residues (McLaughlin and Murray, 2005). One example is myristoylated alanine-rich C-kinase substrate (MARCKS), an amorphous protein that besides the basic cluster binds to the PM through a myristylated PM anchor. MARCKS has been shown to specifically associate with PIP2, and its proposed function is to control the level of free PIP2 in the PM dependent on the $[Ca^{2+}]_{cyt}$ through its interaction with CaMs (McLaughlin and Murray, 2005). Other examples are the NMDA and EGF receptors, for which recruitment of the basic cluster by a CaM is used to regulate their activity in a Ca^{2+}-dependent manner (McLaughlin and Murray, 2005).

For PID, the combination of positively charge and the amphipathic helix might be required to guarantee tight binding to the PM, most likely through phosphoinositides, as in contrast to the animal proteins presented above this is the only domain that holds the protein at the PM. Around 14 phosphoinositide binding modules have been identified, most in animal systems (Stahelin et al., 2014), and the combined phosphoinositide binding and CaM/CML binding motif present in PID is certainly a new one. To be able to compete for the tight association of PID with the PM, the CaM/CML requires a high affinity binding site, and this is probably why the combined amphipathic helix /IQ motif in PID has evolved. When expressed in protoplasts, PID is mostly PM associated, whereas the WAG kinases and especially AGC3-4 also show nuclear localization. Further analysis of these kinases should reveal the relevance of this differential localization. At least for PID, and also for WAG2, in view of the redundancy between the CaMs/CMLs and their likely pleitropic function in different signaling pathways, constructing an untouchable version will still be crucial in unraveling the role of the Ca^{2+}-dependent sequestration to the cytosol during plant development.

Experimental procedures

Molecular cloning and constructs

Molecular cloning was performed following standard procedures (Sambrook, 1989).

Bacteria were grown on LC medium containing corresponding antibiotics for *E.coli* strains DH5α, DH10B. Design of molecular cloning, DNA sequence analysis and DNA alignments were performed using the Vector NTI 10 software (Invitrogen).

The constructs *pET16H-TCH3*, *pGEX-PID*, *pART7-TCH3-YFP*, *pART7-PID-CFP, pDONR-PID, 35S::CFP* were described in Chapter 2. The *pART7-PID-YFP* was constructed by LR reaction from *pDONR-PID* to *pART7-Gateway-YFP*. The *pART7-TCH3-CFP* was constructed by LR reaction from *pDONR-TCH3* to *pART7-Gateway-CFP*.

The cDNAs of *TCH2*, *CML10*, *CAM2* and *CML9* were obtained from RIKEN (http://www.brc.riken.jp/lab/epd/Eng/). The entry clones of these genes were constructed by PCR amplication with respectively primers TCH2+attB+F and TCH2+attB+R-stop, CML10+attB+F and CML10+attB+R-stop, CAM2+attB+F and CAM2+attB+R-stop, CML9+attB+F and CML9+attB+R-stop using Phusion High-Fidelity DNA Polymerase (Thermo Scientific). The resulting PCR fragments were recombined into *pDONR207* (BP reaction). All primers used in this study are listed in Table 1. Relevant pDONR sequences of all constructs were checked by sequencing (Macrogen, Amsterdam), and subsequently combined into either pART7- or pET16H-derived destination vectors (LR reaction), containing respectively the YFP- or the His tag coding region in frame with the Gateway cassette (Invitrogen). Gel extraction of PCR products was performed by using the DNA Gel extraction kit from Thermo Scientific.

The PID insertion domain (AA 227 to 280) was exchanged for *Sgs*I and *Bsp*TI restriction sites by amplifying the remaining PID mRNA plus the vector backbone with primer pair ER023/ER024 using *pDONR-PID* as template. This linear PCR product was circularized by ligation of *Bsp*TI restriction site fragments at both termini, yielding *pDONR207-PID –ID*. Fragments of the PID ID were subsequently re-inserted into this construct via the introduced SgsI-BspTI restriction sites. For this purpose DNA fragments coding for the amino acids 227-253, 240-266 and 254-280 of the PID ID with the appropriate restriction site overhangs were generated by annealing oligonucleotides following Sigma-Aldrich's "Protocol for Annealing Oligonucleotides". A 169 bp long DNA fragment, coding for the entire PID ID was obtained by PCR. Following digestion with *Sgs*I and *Bsp*TI and gel purification, this fragment was inserted into the corresponding restriction sites in *pDONR207-PID-ID*. The *pDONR-PID Ala1-3* mutant versions were constructed using the Agilent QuickChange II XL site directed mutagenesis kit, primers ERC064-069, and *pDONR-PID* as template. .

pDONR-PID S/T 250,255A, *pDONR-PID R249,252,253A*, *pDONR-PID R263,266A* were constructed using the Agilent QuickChange II XL site directed mutagenesis kit, primers ER116,117,119, and *pDONR-PID* as template. *pDONR-PID R249,252,253,263,266A* was constructed using Agilent QuickChange II XL site directed mutagenesis kit, primers ER119, and *pDONR-PID R249,252,253A* as template.

The coding regions of M1 to M7 were constructed by PCR amplication using Phusion High-Fidelity DNA Polymerase (Thermo Scientific). The left part of the coding region was PCR amplified with primers PID attB F1 and M1+R+pcr, M2+R+pcr, M3+R+pcr, M4+R+pcr, M5+R+pcr, or M6+R+pcr+9bp using *pDONR-PID* as template. The right part of the coding region was PCR amplified with primers PID attB R1 and M1+F+pcr, M2+F+pcr, M3+F+pcr, M4+F+pcr, M5+F+pcr, or M6+F+pcr also using *pDONR-PID* as template. The complete coding sequences were constructed by PCR amplication using primers PID attB F1 and PID attB R1 and the correct combination of left part and right part PCR products as templates. The resulting PCR fragments were recombined into *pDONR207* (BP reaction, Invitrogen).

All mutant PID versions described above were transferred from the *pDONR* entry vector to expression vectors (*pGEX, pET, pARF7*) by gateway cloning (LR reaction, Invitrogen).The *pART7:ID:YFP* and *pART7:ID*$_{244\text{-}275}$*:YFP* were constructed by first PCR amplifying a fragment containing the ID or ID244-275 by primers SB001-002 or SB003-004, respectively, adding the restriction sites *Bam*HI and *Hind*III. These products were then cloned into *pART7-YFP-HAII* digested with *Bam*HI and *Hind*III. *pGEX:ID* and *pGEX:ID*$_{244\text{-}275}$ were constructed by cloning the above digestion products into *pGEX-KG* digested with *Bam*HI and *Hind*III.

Table 1: Primer list

The attB recombination sites are underlined

TCH3 attB F1	5’GGGGACAAGTTTGTACAAAAAAGCAGGCTTAATGGCGGATAAGCTCACT3’
TCH3 attB R1	5’GGGGACCACTTTGTACAAGAAAGCTGGGTAAGATAACAGCGCTTCGAACA3’
PID attB F1	5’GGGGACAAGTTTGTACAAAAAAGCAGGCTTCAGCATGTTACGAGAATCAGACGGT3’
PID attB R1	5’GGGGACCACTTTGTACAAGAAAGCTGGGTCAAAGTAATCGAACGCCGCTGG3’
PID exon1 F1	5’TCTCTTCCGCCAGGTAAAAA3’
PID exon2 R1	5’CGCAAGACTCGTTGGAAAAG3’
TCH3pr F1	5’AAATGTCCACTCACCCATCC3’

TCH3pr R1	5’GGGAATTCTGAAGATCAGCTTTTGTCG3’
M1+R+pcr:	5’TAAAGTCTGAACCTTTTTAGACCGCTCGTCTCGTTGGAA3’
M1+F+pcr:	5’TTCCAACGAGACGAGCGGTCTAAAAAGGTTCAGACTTTA3’
M2+R+pcr:	5’TAAAGTCTGAACCTCTTCAGACTCCAAGACTCGTTGGAA3’
M2+F+pcr:	5’TTCCAACGAGTCTTGGAGTCTGAAGAGGTTCAGACTTTA3’
PID R1(delete IQ)+M3	5’AGAGACGGGTTGGTTCAAGTCTAGCGAGACGA3’
PID F1(delete IQ)+M3	5’TCGTCTCGCTAGACTTGAACCAACCCGTCTCT3’
PID R2(IQ->A)+M4	5’AGAGACGGGTTGGTTCTCGTCGTCGTCGTCGTCGTCGTCGTCGTCGTCGTCGAAGTCTAGCGAGACGA3’
PID F1(IQ->A)+M4	5’TCGTCTCGCTAGACTTGCTGCTGCTGCTGCTGCTGCTGCTGCTGCTGCTGCTGCTGAACCAACCCGTCTCT3’
M5+R+pcr	5’TAAAGTCTGAACCTCTTCAGACCGCAAGACTCGTTGGAA3’
M5+F+pcr	5’TTCCAACGAGTCTTGCGGTCTGAAGAGGTTCAGACTTTA3’
M6+R+pcr	5’GGTTGGTTCTTCAGTCTGATCCTTTTTAGACCGCAAGACTCGTTGGAA3’
M6+F+pcr	5’TTCCAACGAGTCTTGCGGTCTAAAAAGGATCAGACTGAA3’
CML9+attB+F	5’GGGACAAGTTTGTACAAAAAAGCAGGCTTCATGGCGGATGCTTTCACAGATGAAG3’
CML9+attB+R-stop	5’GGGGACCACTTTGTACAAGAAAGCTGGGTCATAAGAGGCAGCAATCATCA3’
CML10+attB+F	5’GGGGACAAGTTTGTACAAAAAAGCAGGCTTCATGGCGAATAAGTTCACTAG3’
CML10+attB+R-stop	5’GGGGACCACTTTGTACAAGAAAGCTGGGTCAGAAAACAACGCTTCGAACA3’
TCH2+attB+F	5’GGGGACAAGTTTGTACAAAAAAGCAGGCTTCATGTCATCGAAGAACGGAGTTG3’
TCH2+attB+R-stop	5’GGGGACCACTTTGTACAAGAAAGCTGGGTCAGCACCACCACCATTACTCA3’
CAM2+attB+F	5’GGGGACAAGTTTGTACAAAAAAGCAGGCTTCATGGCGGATCAGCTCACAGA3’
CAM2+attB+R-stop	5’GGGGACCACTTTGTACAAGAAAGCTGGGTCCTTAGCCATCATAACCTTCA3’
PID Deletion 2 S (ERC023)	5’AAACTTAAGGGCGCGCCCGAGGTCAAAGTCAGAGAGC3’
PID Deletion 2 AS (ERC024)	5’GACCTTAAGGCTGAACCGGTTACTGC3’
PID InsDom S_1 (ER003)	5’TGGCGCGCCTCTCTATGCTCCGACTCAAT3’
PID InsDom AS_162 (ERC004)	5’CGTCTTAAGAACAAAGAGACGGGTTGG3’
PID InsDom AA227-253 S (ERC005)	5’CGCGCCTCTCTATGCTCCGACTCAATCGCAGCCGTTGAATCTTCCTCGTCTTCGCCGGAGAATCAACAACTCCGTTCACCGCGACGAC3’
PID InsDom AA227-253 AS	5’TTAAGTCGTCGCGGTGAACGGAGTTGTTGATTCTCCGGCGAAGACGAGGAAG

(ERC006)	ATTCAACGGCTGCGATTGAGTCGGAGCATAGAGAGG3’
PID InsDom AA254-280 S (ERC007)	5’CGCGCCTTCACTCGTCTCGCTAGACTTTTCCAACGAGTCTTGCGGTCTAAAAAGGTTCAGACTTTAGAACCAACCCGTCTCTTTGTTC3’
PID InsDom AA254-280 AS (ERC008)	5’TTAAGAACAAAGAGACGGGTTGGTTCTAAAGTCTGAACCTTTTTAGACCGCAAGACTCGTTGGAAAAGTCTAGCGAGACGAGTGAAGG3’
PID InsDom AA240-266 S (ERC009)	5’CGCGCCTCGTCTTCGCCGGAGAATCAACAACTCCGTTCACCGCGACGATTCACTCGTCTCGCTAGACTTTTCCAACGAGTCTTGCGGC3’
PID InsDom AA240-266 AS (ERC010)	5’TTAAGCCGCAAGACTCGTTGGAAAAGTCTAGCGAGACGAGTGAATCGTCGCGGTGAACGGAGTTGTTGATTCTCCGGCGAAGACGAGG3’
PID-ALA1 S (ERC064)	5’GAATCTTCCTCGTCTTCGCCGGAGAATCAAGCAGCCGCTGCAGCGGCAGCATTCACTCGTCTCGCTAGACTTTTCCAACG3’
PID-ALA1 AS (ERC065)	5’CGTTGGAAAAGTCTAGCGAGACGAGTGAATGCTGCCGCTGCAGCGGCTGCTTGATTCTCCGGCGAAGACGAGGAAGATTC3’
PID-ALA2 S (ERC066)	5’GAGAATCAACAACTCCGTTCACCGCGACGAGCCGCTGCTGCCGCTGCAGCTTTCCAACGAGTCTTGCGGTCTAAAAAGGT3’
PID-ALA2 AS (ERC067)	5’ACCTTTTTAGACCGCAAGACTCGTTGGAAAGCTGCAGCGGCAGCAGCGGCTCGTCGCGGTGAACGGAGTTGTTGATTCTC3’
PID-ALA3 S (ERC068)	5’CACCGCGACGATTCACTCGTCTCGCTAGACTTGCCGCAGCAGCCGCGGCGGCTAAAAAGGTTCAGACTTTAGAACCAACCCGT3’
PID-ALA3 AS (ERC069)	5’ACGGGTTGGTTCTAAAGTCTGAACCTTTTTAGCCGCCGCGGCTGCTGCGGCAAGTCTAGCGAGACGAGTGAATCGTCGCGGTG3’
PID InsDom S/T250,255A (ER116)	5’CAACTCCGAGCTCCGCGACGATTCGCTCGTCTCGC3’
PID InsDom R249,252,253A AS (ER117)	5’GTGAATGCTGCAGGTGAAGCGAGTTGTTG 3’
PID InsDom R263,266A (ER119)	5’CTTTTCCAAGCAGTACTGGCGTCTAAAAAGG3’
SB001 attB1 InsDom AA229 S	5’GGGGACAAGTTTGTACAAAAAAGCAGGCTTAATGCTATGCTCCGACTCAATCG3’
SB002 attB2 InsDom AA279 AS	5’GGGGACCACTTTGTACAAGAAAGCTGGGTCAAAGAGACGGGTTGG3’
SB003 attB1 InsDom AA248 S	5’GGGGACAAGTTTGTACAAAAAAGCAGGCTTAATGGAGAATCAACAACTC3’
SB004 attB2 InsDom AA274 AS	5’GGGGACCACTTTGTACAAGAAAGCTGGGTGTTCTAAAGTCTGAACC3’

In vitro pull-down

In vitro pull-down analysis was performed as previously described (Benjamins et al., 2003).

Protoplast transfection and Förster (Fluorescence) Resonance Energy Transfer (FRET) analysis

Protoplasts were obtained from *Arabidopsis thaliana* Col-0 cell suspension cultures that were propagated as described (Schirawski et al., 2000). Protoplast isolation and PEG-mediated transfections with 10 µg plasmid DNA were performed as adapted by Schirawski and coworkers (Schirawski et al., 2000). To obtain auxin-starved protoplasts, auxin (NAA) was removed from the media during protoplast isolation. Following transfection, the protoplasts were incubated for at least 16 hours in the dark prior to observation.

All microscopic analyses were done with a Zeiss LSM5 Exciter (Zeiss, Oberkochen, Germany) using a 63x magnifying objective. The CFP signal was detected using an argon 458 nm laser and a 475-525 nm band pass filter. The YFP signal was detected using an argon 514 nm laser and a 530-600 nm band pass filter. To detect FRET, a 458 nm laser and a 530 nm long pass filter were used, and images were anlysed with a sensitized emission FRET approach by using the Image J plugin *FRET and Colocalization Analyzer*. This plugin allows calculation of a FRET index on a pixel by pixel basis and corrects for donor bleed through, acceptor bleed through and false FRET (by associating FRET with colocalization of the two fluorophores). “Donor only” protoplasts expressing *35S::CFP* and “acceptor only” protoplasts expressing *35S::YFP* were used to determine donor bleed through and acceptor bleed through, respectively. Protoplasts transfected with the *35S::CFP-YFP* construct were used as positive control. The Image J plugin calculated the FRET index. The relative FRET image was obtained by dividing the FRET index by the YFP channel image. For each protoplast three fixed areas (regions of interest, ROIs) were quantified using the ImageJ software. Per sample scanning was performed on ten protoplasts. The obtained intensities of all protoplasts were averaged and used to calculate the standard deviation. The Student’s *t*-test was used to test for significant differences in relative FRET ($p<0.05$ level).

Protein alignment, phylogenetic tree, and helix wheel projection

The PID ID structure was predicted by both http://zhanglab.ccmb.med.umich.edu/QUARK/ and http://bioserv.rpbs.univ-paris-diderot.fr/PEP-FOLD/. Based on the characterization of multiple IQ motifs the following consensus was established for IQ-

([FILV]Qxxx[RK]Gxxx[RK]xx[FILVWY]) or IQ-like motifs ([FILV]Qxxx[RK]xxxxxxxx). The amino acid residues between brackets can substitute for each other at that specific position (http://calcium.uhnres.utoronto.ca/ctdb/ctdb/motifs/iq_motif.html). The helix wheel projection was made by http://heliquest.ipmc.cnrs.fr/.

All calmodulin protein sequences were downloaded from TAIR (http://www.arabidopsis.org/). The phylogenetic tree and calmodulin alignment were constructed with the CLC Main Workbench 6.9.1 software (CLC Bio/Qiagen).

Accession Numbers

The *Arabidopsis* Genome Initiative locus identifiers for the genes mentioned are as follows: *PID* (At2g34650, pda07777), WAG2 (At3g14370), TCH3 (At2g41100, pda09314), TCH2 (AT5g37770, pda17915), CML10(AT2g41090, pda01448), CAM2 (At2g41110, pda02964), CML9 (Atg51920, pda00144).

Acknowledgements

The project was supported by a TOP grant from the Research Council for Chemical Sciences (700.58.301) to R.O., with financial aid from the Netherlands Organization of Scientific Research (NWO). The authors would like to thank Gerda Lamers, Ward de Winter and Jan Vink for their help with the microscopy, tissue culture and plant caretaking, respectively.

Reference

Abas, L., Benjamins, R., Malenica, N., Paciorek, T., Wisniewska, J., Moulinier-Anzola, J.C., Sieberer, T., Friml, J., and Luschnig, C. (2006). Intracellular trafficking and proteolysis of the *Arabidopsis* auxin-efflux facilitator PIN2 are involved in root gravitropism. Nat Cell Biol **8,** 249-256.

Bahler, M., and Rhoads, A. (2002). Calmodulin signaling via the IQ motif. FEBS Lett **513,** 107-113.

Benjamins, R., Ampudia, C.S., Hooykaas, P.J., and Offringa, R. (2003). PINOID-mediated signaling involves calcium-binding proteins. Plant Physiol **132,** 1623-1630.

Bhardwaj, R., Muller, H.M., Nickel, W., and Seedorf, M. (2013). Oligomerization and Ca^{2+}/calmodulin control binding of the ER Ca^{2+}-sensors STIM1 and STIM2 to plasma membrane lipids. Biosci Rep **33**.

Braam, J., and Davis, R.W. (1990). Rain-, wind-, and touch-induced expression of calmodulin and calmodulin-related genes in Arabidopsis. Cell **60,** 357-364.

Chin, D., and Means, A.R. (2000). Calmodulin: a prototypical calcium sensor. Trends Cell Biol **10,** 322-328.

Clapham, D.E. (2007). Calcium signaling. Cell **131,** 1047-1058.

Cornell, R.B., and Taneva, S.G. (2006). Amphipathic helices as mediators of the membrane interaction of amphitropic proteins, and as modulators of bilayer physical properties. Curr Protein Pept Sci **7,** 539-552.

Dhonukshe, P., Huang, F., Galvan-Ampudia, C.S., Mahonen, A.P., Kleine-Vehn, J., Xu, J., Quint, A., Prasad, K., Friml, J., Scheres, B., and Offringa, R. (2010). Plasma membrane-bound AGC3 kinases phosphorylate PIN auxin carriers at TPRXS(N/S) motifs to direct apical PIN recycling. Development **137,** 3245-3255.

Ding, Z., Galvan-Ampudia, C.S., Demarsy, E., Langowski, L., Kleine-Vehn, J., Fan, Y., Morita, M.T., Tasaka, M., Fankhauser, C., Offringa, R., and Friml, J. (2011). Light-mediated polarization of the PIN3 auxin transporter for the phototropic response in *Arabidopsis*. Nat Cell Biol **13,** 447-452.

Du, L., and Poovaiah, B.W. (2005). Ca^{2+}/calmodulin is critical for brassinosteroid biosynthesis and plant growth. Nature **437,** 741-745.

Du, L., Ali, G.S., Simons, K.A., Hou, J., Yang, T., Reddy, A.S., and Poovaiah, B.W. (2009). Ca^{2+}/calmodulin regulates salicylic-acid-mediated plant immunity. Nature **457,** 1154-1158.

Friml, J., Yang, X., Michniewicz, M., Weijers, D., Quint, A., Tietz, O., Benjamins, R., Ouwerkerk, P.B., Ljung, K., Sandberg, G., Hooykaas, P.J., Palme, K., and Offringa, R. (2004). A PINOID-dependent binary switch in apical-basal PIN polar targeting directs auxin efflux. Science **306,** 862-865.

Galván-Ampudia, C.S., and Offringa, R. (2007). Plant evolution: AGC kinases tell the auxin tale. Trends Plant Sci. **12,** 541-547.

Geldner, N., Friml, J., Stierhof, Y.D., Jurgens, G., and Palme, K. (2001). Auxin transport inhibitors block PIN1 cycling and vesicle trafficking. Nature **413,** 425-428.

Heximer, S.P., Lim, H., Bernard, J.L., and Blumer, K.J. (2001). Mechanisms governing subcellular localization and function of human RGS2. J Biol Chem **276,** 14195-14203.

Hoeflich, K.P., and Ikura, M. (2002). Calmodulin in action: diversity in target recognition and activation mechanisms. Cell **108,** 739-742.

Houdusse, A., and Cohen, C. (1995). Target sequence recognition by the calmodulin superfamily: implications from light chain binding to the regulatory domain of scallop myosin. Proc Natl Acad Sci U S A **92,** 10644-10647.

Houdusse, A., Gaucher, J.F., Krementsova, E., Mui, S., Trybus, K.M., and Cohen, C. (2006). Crystal structure of apo-calmodulin bound to the first two IQ motifs of myosin V reveals essential recognition features. Proc Natl Acad Sci U S A **103,** 19326-19331.

Huang, F., Zago, M.K., Abas, L., van Marion, A., Galvan-Ampudia, C.S., and Offringa, R. (2010). Phosphorylation of conserved PIN motifs directs *Arabidopsis* PIN1 polarity and auxin transport. Plant Cell **22,** 1129-1142.

Knight, H. (2000). Calcium signaling during abiotic stress in plants. Int Rev Cytol **195,** 269-324.

Knight, M.R., Campbell, A.K., Smith, S.M., and Trewavas, A.J. (1991). Transgenic plant aequorin reports the effects of touch and cold-shock and elicitors on cytoplasmic calcium. Nature **352,** 524-526.

Lu, F., and Taghbalout, A. (2013). Membrane association via an amino-terminal amphipathic helix is required for the cellular organization and function of RNase II. J Biol Chem **288,** 7241-7251.

McCormack, E., and Braam, J. (2003). Calmodulins and related potential calcium sensors of Arabidopsis. New Phytol. **159,** 585-598.

McCormack, E., Tsai, Y.-C., and Braam, J. (2005). Handling calcium signaling: Arabidopsis CaMs and CMLs. Trends in Plant Science **10,** 383-389.

McLaughlin, S., and Murray, D. (2005). Plasma membrane phosphoinositide organization by protein electrostatics. Nature **438,** 605-611.

Monshausen, G.B., Bibikova, T.N., Weisenseel, M.H., and Gilroy, S. (2009). Ca^{2+} regulates reactive oxygen species production and pH during mechanosensing in *Arabidopsis* roots. Plant Cell **21,** 2341-2356.

Monshausen, G.B., Miller, N.D., Murphy, A.S., and Gilroy, S. (2011). Dynamics of auxin-dependent Ca^{2+} and pH signaling in root growth revealed by integrating high-resolution imaging with automated computer vision-based analysis. Plant J. **65,** 309-318.

Munshi, H.G., Burks, D.J., Joyal, J.L., White, M.F., and Sacks, D.B. (1996). Ca^{2+} regulates calmodulin binding to IQ motifs in IRS-1. Biochemistry **35,** 15883-15889.

Olivotto, M., Arcangeli, A., Carla, M., and Wanke, E. (1996). Electric fields at the plasma membrane level: a neglected element in the mechanisms of cell signalling. Bioessays **18,** 495-504.

Petrasek, J., Mravec, J., Bouchard, R., Blakeslee, J.J., Abas, M., Seifertova, D., Wisniewska, J., Tadele, Z., Kubes, M., Covanova, M., Dhonukshe, P., Skupa, P., Benkova, E., Perry, L., Krecek, P., Lee, O.R., Fink, G.R., Geisler, M., Murphy, A.S., Luschnig, C., Zazimalova, E., and Friml, J. (2006). PIN proteins perform a rate-limiting function in cellular auxin efflux. Science **312,** 914-918.

Polisensky, D.H., and Braam, J. (1996). Cold-shock regulation of the Arabidopsis TCH genes and the effects of modulating intracellular calcium levels. Plant Physiol **111,** 1271-1279.

Poovaiah, B.W., Du, L., Wang, H., and Yang, T. (2013). Recent advances in calcium/calmodulin-mediated signaling with an emphasis on plant-microbe interactions. Plant Physiol **163,** 531-542.

Popescu, S.C., Popescu, G.V., Bachan, S., Zhang, Z., Seay, M., Gerstein, M., Snyder, M., and Dinesh-Kumar, S.P. (2007). Differential binding of calmodulin-related proteins to their targets revealed through high-density *Arabidopsis* protein microarrays. Proc Natl Acad Sci U S A **104,** 4730-4735.

Rademacher, E.H., and Offringa, R. (2012). Evolutionary adaptations of plant AGC Kinases: from light signaling to cell polarity regulation. Front Plant Sci **3,** 250.

Rhoads, A.R., and Friedberg, F. (1997). Sequence motifs for calmodulin recognition. FASEB J **11,** 331-340.

Roberts, D.M., and Harmon, A.C. (1992). Calcium-modulated proteins: targets of intracellular calcium signals in higher plants. Annu. Rev. Plant Physiol. Plant Mol. Biol. **43,** 375-414.

Sambrook, J., Fritsch F. and Maniatis, T. (1989). Molecular cloning-A laboratory mannual. Cold Spring Harbor Laboratory press, NY, USA.

Sauer, M., Balla, J., Luschnig, C., Wisniewska, J., Reinohl, V., Friml, J., and Benkova, E. (2006). Canalization of auxin flow by Aux/IAA-ARF-dependent feedback regulation of PIN polarity. Genes Dev **20,** 2902-2911.

Schirawski, J., Planchais, S., and Haenni, A.L. (2000). An improved protocol for the preparation of protoplasts from an established *Arabidopsis thaliana* cell suspension culture and infection with RNA of turnip yellow mosaic tymovirus: a simple and reliable method. J Virol Methods **86,** 85-94.

Snedden, W.A., and Fromm, H. (2001). Calmodulin as a versatile calcium signal transducer in plants. New Phytol **151,** 35-66.

Stahelin, R.V., Scott, J.L., and Frick, C.T. (2014). Cellular and molecular interactions of phosphoinositides and peripheral proteins. Chem Phys Lipids.

Tanaka, H., Dhonukshe, P., Brewer, P.B., and Friml, J. (2006). Spatiotemporal asymmetric auxin distribution: a means to coordinate plant development. Cell Mol Life Sci **63,** 2738-2754.

Trewavas, A.J., and Malho, R. (1998). Ca^{2+} signalling in plant cells: the big network! Curr Opin Plant Biol **1,** 428-433.

Wisniewska, J., Xu, J., Seifertova, D., Brewer, P.B., Ruzicka, K., Blilou, I., Rouquie, D., Benkova, E., Scheres, B., and Friml, J. (2006). Polar PIN localization directs auxin flow in plants. Science **312,** 883.

Xie, X., Harrison, D.H., Schlichting, I., Sweet, R.M., Kalabokis, V.N., Szent-Gyorgyi, A.G., and Cohen, C. (1994). Structure of the regulatory domain of scallop myosin at 2.8 A resolution. Nature **368,** 306-312.

Yap, K., Kim, J., Truong, K., Sherman, M., Yuan, T., and Ikura, M. (2000). Calmodulin target database. J Struct and Funct Genomics **1,** 8-14.

Zegzouti, H., Anthony, R.G., Jahchan, N., Bogre, L., and Christensen, S.K. (2006a). Phosphorylation and activation of PINOID by the phospholipid signaling kinase 3-phosphoinositide-dependent protein kinase 1 (PDK1) in *Arabidopsis*. Proc Natl Acad Sci U S A **103,** 6404-6409.

Zegzouti, H., Li, W., Lorenz, T.C., Xie, M., Payne, C.T., Smith, K., Glenny, S., Payne, G.S., and Christensen, S.K. (2006b). Structural and functional insights into the regulation of *Arabidopsis* AGC VIIIa kinases. J Biol Chem **281,** 35520-35530.

Zielinski, R.E. (1998). Calmodulin and calmodulin-binding proteins in plants. Annu Rev Plant Physiol Plant Mol Biol **49,** 697-725.

Chapter 4

AGC3 kinase-calmodulin signaling in phyllotaxis

Yuanwei Fan, Jasmijn van der Weide, Remko Offringa

Molecular and Developmental Genetics, Institute Biology Leiden, Leiden University, Sylviusweg 72, 2333 BE Leiden, the Netherlands

Summary

Phyllotaxis, or the arrangement of lateral organs on a plant stem, is determined by the pattern of organ primordium initiation in the shoot apical-, inflorescence- or flower meristem. The position of primordium initiation is in part instructed by the unequal distribution of auxin in the meristem epidermis, which is driven by the asymmetric subcellular localisation of the auxin efflux carrier PIN1. The localization of PIN1 is dependent on phosphorylation of three specific serine residues in its central hydrophilic loop by the AGC3 protein kinases PID, WAG1 and WAG2. Here we show that PIN1 phosphorylation by the three AGC3 kinases is important for maintaining the normal spiral phyllotaxis (137.5 ° angle) in *Arabidopsis*, and that deregulation of PIN1 phosphorylation dynamics leads to irregular phyllotaxis, varying from absence of primordium initiation to a switch from the normal spiral (137.5 ° angle) to a decussate-like (alternating 180 ° and 90 ° angles) pattern. In addition, auxin, mechanical stress and overexpression of the calmodulin-like protein CML12/TCH3 trigger Ca^{2+}-dependent internalization of PID in the inflorescence meristem. The enhanced variation in the divergence angle between flowers in *TCH3* overexpression or *tch3* loss-of-function mutant inflorescences suggests that a dynamic recruitment of the kinase by TCH3 is required for a regular spiral phyllotaxis. Our results suggest the involvement of the AGC3 kinase-CML signalling complex in modulating of the phyllotactic pattern in response to auxin and mechanical stress.

Introduction

A remarkable feature of plant development is the regular arrangement of lateral organs (leaves and flowers) around a plant stem, which is called phyllotaxis. In the developing shoot, existing primordia arising from the shoot apical meristem (SAM) and the inflorescence meristems (IMs) are involved in determining the position where new primordia will be formed (Reinhardt et al., 2005). Auxin produced by the existing primordia is redistributed by polar cell-to-cell transport, which generates a new maximum that serves as initiation point for a new primordium (Reinhardt et al., 2003; Tanaka et al., 2006). This polar auxin transport is mediated by PIN-FORMED (PIN) and AUX1/LAX1 proteins, which function as auxin efflux- and influx carriers, respectively (Tanaka et al., 2006). The direction of auxin transport is determined by the asymmetric subcellular localization of the PIN auxin efflux carriers, which is dependent on phosphorylation of the large central hydrophilic loop by PINOID (PID) and the redundantly functioning WAG1 and WAG2 protein kinases (Friml et al., 2004; Dhonukshe et al., 2010; Huang et al., 2010).

PIN1, the founding member of the PIN protein family, plays an essential role in regulating phyllotaxis. The dynamic subcellular localization of PIN1 in the epidermis of the SAM follows a specific pattern, leading to the transport of auxin towards the sites of organ formation (Reinhardt et al., 2003; Heisler et al., 2005). Proper phosphorylation of PIN1 is essential for the regulation of its subcellular localization and the formation of organs in the IM. In *pin1* mutant IMs expressing non-phosphorylatable PIN1:GFP, with the serine phosphorylation targets substituted for alanines, the mutant PIN1 is localized at the basal instead of the apical membrane of epidermis cells and the meristem is defective in lateral organ formation (Huang et al., 2010). Based on the apparent role of auxin and PIN1 in the formation of organs at the SAM, Reinhardt and coworkers proposed that as a consequence of auxin transport to the primordia, the concentration of auxin in tissues surrounding the primordia will be low and thus, no organs will be formed there; only at a certain distance from existing primordia, new auxin maxima can arise, leading to new primordia (Reinhardt et al., 2003). Using mathematical modelling, it was shown that these simple assumptions can generate patterns similar to the phyllotactic patterns occurring in nature (Jonsson et al., 2006; Smith et al., 2006).

Although models based only on biochemical processes can explain phyllotactic patterns, several lines of evidence suggest that cells in the meristem that constantly produces new organs experience mechanical stress, and that mechanical stress might also be directing phyllotactic patterns (Besnard et al., 2011; Mirabet et al., 2011). Mathematical models indicate that mechanical and biochemical mechanisms can reinforce each other (Newell et al., 2008). A link between mechanical forces and plant development has been described by Hamant and co-workers (Hamant et al., 2008). Microtubules are well known to determine the direction of cell growth. In cells of the SAM the orientation of microtubules is altered in response to changes in stress patterns or to externally applied mechanical constraints (Hamant et al., 2008). Recently, it has been shown that the polar localization of PIN1 proteins also responds to changes in mechanical stress patterns and that PIN1 localization and microtubule orientation are highly correlated in the SAM. A likely role for PID in mechanical stress signalling was suggested based on the absence of PIN1 re-polarization following mechanical stress in *pid* loss-of-function mutants (Heisler et al., 2010). The question now arises how PIN1 orientation is regulated by mechanical stress. Since the subcellular localization of PIN1 depends on phosphorylation by PID, molecules that regulate PID function can be involved in regulating PIN1 orientation in response to mechanical stress.

One of the first responses in cells that are under mechanical stress is a rapid increase in the cytosolic Ca^{2+} levels (Monshausen et al., 2009). Based on the results in Chapters 2 and 3, elevated Ca^{2+} levels can be translated into changes in PIN localisation by calmodulin-mediated sequestration of PID and WAG2 from the plasma membrane to the cytosol. The AGC3 kinase-calmodulin signalling complex is therefore a strong candidate to couple mechanical stress to PIN1 orientation during phyllotaxis.

The first calmodulin-like protein identified as PID binding protein was TOUCH3 (Benjamins et al., 2003). The *TCH3* gene was originally identified as a gene whose transcription is induced by several stimuli, including rain, touch and wind (Braam and Davis, 1990). *TCH3* expression can be induced by auxin (Antosiewicz et al., 1995) and increased Ca^{2+} concentrations (Braam, 1992). Since TCH3 seems to regulate PID activity in a Ca^{2+}-dependent manner (Benjamins et al., 2003)(Chapters 2 and 3), and mechanical stimuli can result in increased cytoplasmic Ca^{2+} levels (Trewavas and Knight, 1994; Haley et al., 1995), TCH3 is the perfect candidate to couple mechanical signals to reorientation of PIN polarity. In this chapter, we studied the possible involvement of the AGC3 kinases in phyllotaxis, and we also tested the possibility that *TCH3* is involved in regulating phyllotaxis. Our results show that the AGC3 kinases PID, WAG1 and WAG2 are involved in maintaining the normal spiral phyllotaxis (137.5 ° angle) in *Arabidopsis*, and that deregulation of PIN1 phosphorylation dynamics leads to irregularities, and frequently results in switches from spiral to decussate (alternating 180 ° and 90 ° angles) phyllotaxis. *tch3-3* loss-of-function mutants showed a distichous phyllotaxis pattern and changes in its activity led to enhanced variation in the divergence angle between primordia in the IM. Our results suggest the involvement of the AGC3 kinase-TCH3 signalling complex in controlling the phyllotactic pattern, in response to auxin and mechanical stress dynamics in the *Arabidopsis* SAM and IM.

Results

AGC3 kinases play a role in phyllotaxis

To investigate the role of PID and its close homologs WAG1 and WAG2 in phyllotactic patterning, the divergence angles between subsequent lateral organs of rosette leaves were measured in wild-type *Arabidopsis* (Col-0), the *pid-14*, *wag1 wag2*, *pid wag1*, *pid wag2* and *pid wag1 wag2* loss-of-function mutants and in *35S::PID* overexpression plants. In addition, we performed measurements on *pin1* mutant plants expressing the complementing *PIN1::PIN1-GFP* fusion gene, or the *PIN1::PIN1-GFP S123A* loss-of-phosphorylation or *PIN1::PIN1-GFP S123E* phosphomimic version (Table 1).

Table 1. AGC3 kinases reduce the variation in divergence angle in *Arabidopsis* rosette leaf phyllotaxis

Plant line	Mean	SD	p1	#plants	#angles	Angle>180 °	p2
Col-0	138.0	13.3		8	66	0	-
Col-0 (II)	138.8	17.1		11	75	0	-
pid (II)	137.2	17.5	0.88	9	81	1	0.97
wag1 wag2	139.0	19.3	0.001	12	111	1	0.79
pid wag1	125.4	33.6	$< 10^{-3}$	3	29	1	0.67
pid wag2	148.8	40.3	$< 10^{-3}$	5	41	3	0.10
pid wag2 (II)	154.3	50.2	$< 10^{-3}$	8	50	9	0,005
pid wag1	137.7	26.8	$< 10^{-3}$	7	51	1	0.90
35S::PID	140.0	25.1	$< 10^{-3}$	10	83	1	0.91
PIN1-GFP	136.3	17.6	0.82	11	76	0	1
PIN1-GFP	146.0	42.2	$< 10^{-3}$	13	64	6	0.02
PIN1-GFP	135.7	21.2	$< 10^{-3}$	12	84	0	1
tch3-3	138.4	16.6	0.052	12	112	1	0.79
35S::TCH3-2	137.1	17.3	0.025	11	88	0	1

Per plant line the mean divergence angle and the standard deviation are given. (II) indicates plant lines that were tested in a second experiment. Number of plants and the total number of angles on which the mean values are based are provided. Also the number of divergence angles that are larger than 180 degrees is indicated. p1 indicates the significance level given by an F test of equality of the variance of divergence angles in a specific line compared to wild-type (Col-0). p2 indicates the probability value for the Pearson's Chi squared test ($P < 0.05$ for significant difference with Col-0) for the fraction of angles that is larger than 180 degrees as compared to that in wild-type plants.

We focused our analysis on rosettes, as the inflorescence phyllotaxis is too much disturbed in those mutants that form pin-like structures. The mean divergence angle in Col-0 rosettes approximated the 'golden angle' of 137.5 ° for spiral phyllotaxis (Mitchison, 1977; Kuhlemeier, 2007) (Table 1). However, the variation in values as indicated by standard deviation was quite high (Table 1). The rosette phyllotaxis of the *pid* mutant was comparable to that of wild type, but all double and triple mutant combinations of *pid*, *wag1* and *wag2* showed a significantly increased variation in the divergence angles, which is in line with the functional redundancy between these kinases. The fact that the variation in the *pid wag1 wag2* triple mutant plants was significantly higher compared to the *wag1 wag2* double mutants (p = 0.0047), confirmed the relative importance of *PID* for the maintenance of the spiral phyllotactic pattern.

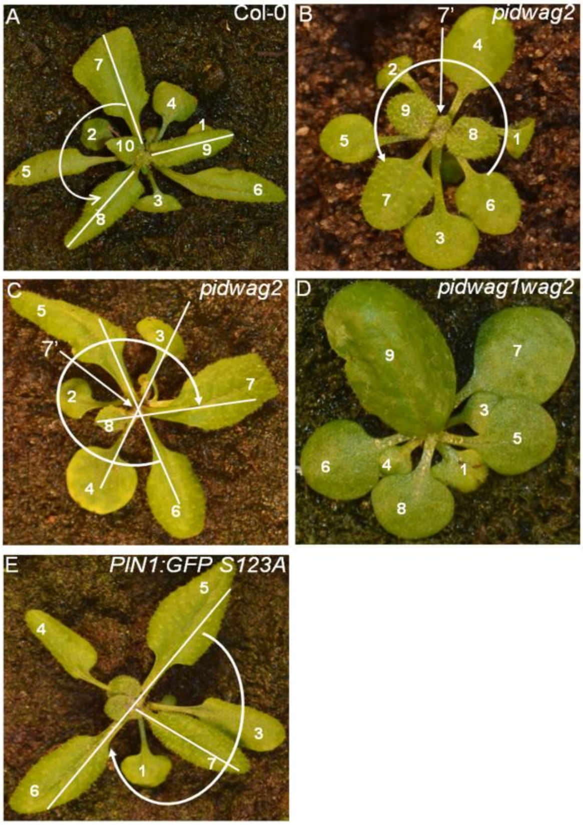
A
Col-0
7
4
1
2
10
9
5
6
3
8
B
7'
pidwag2
4
2
9
8
1
5
7
6
3
C
pidwag2
5
3
7'
7
2
8
4
6
D
pidwag1wag2
9
7
3
5
6
4
1
8
E
PIN1:GFP S123A
5
4
3
7
1
6

Figure 1. The phenotypes of AGC3 kinase mutants

(A) Normal phyllotaxis in a rosette of wild-type *Arabidopsis* (Col-0), with divergence angles approaching the 'golden angle' of 137.5°. (B-E) irregular phyllotaxis in *pid wag2*, *pid wag1 wag2* and *pin1 PIN1::PIN1:GFP S123A* mutant rosettes. The divergence angles in *pid wag2* mutant rosettes (B, C) vary significantly compared to wild-type rosettes. An angle of 270° observed in some rosettes suggests failure of primordium initiation (white straight arrow in B and C), whereas the rosette in (C) also has a decussate appearance (subsequent angles of 180° and 90°).*pid wag1 wag2* rosettes have a dwarf appearance with a relatively normal spiral phyllotaxis, except for the 270° angle between leaves 4 and 5 (D). *pin1 PIN1::PIN1:GFP S123A* plants occasionally show a decussate phyllotaxis. The white curved arrow indicates the turn of the phyllotaxis.

Unexpectedly, the standard deviation in *pid wag1 wag2* triple mutants was lower than in *pid wag2* double mutants (p=0.0067), suggesting that the *wag1* mutation somehow counteracts the effect of *wag2*. The mean value for the divergence angle of the *pid wag1* double mutant was lower than that of wild type, whereas it was higher for the *pid wag2* mutant combination. This together with the fact that the value of *pid wag1 wag2* is closer to the angle in wild-type (Col-0) *Arabidopsis*, suggests that *WAG1* and *WAG2* antagonistically contribute to maintaining the 137.5° divergence angle. However, the strong dwarf phenotype of the *pid wag1 wag2* triple mutant rosette compared to all other mutants (Figure 1D) corroborates the previously shown redundant activity of the three kinase genes (Dhonukshe et al., 2010).

The involvement of the three AGC3 kinases in phyllotaxis was confirmed by the results of the *PIN1::PIN1:GFP S123A* loss-of-phosphorylation or *PIN1::PIN1:GFP S123E* phosphomimic lines. In both cases a significant increase in the variation in the divergence angle was observed, with loss-of-phosphorylation having a more severe effect, indicating that for proper phyllotaxis the PIN1 phosphorylation dynamics is important.

For those mutant lines that did not form pin-like inflorescences we also determined the divergence angles between subsequent flower petioles on inflorescence stems. All mutant lines tested (*35S:PID*, *wag1 wag2* and *PIN1-GFP S123E*) showed a significantly higher standard deviation in the divergence angle compared to wild-type (Table 2). These results confirm the involvement of AGC3 kinase-mediated PIN1 phosphorylation in the stability of the phyllotactic pattern.

Table 2. AGC3 kinases reduce the variation in the divergence angle in inflorescence phyllotaxis

Plant line	Mean	SD	P1	#Angles	angles > 180 °	P2
Col-0	142.1	26.8	-	74	2	-
Col-0 (II)	139.6	19.7	-	123	9	-
tch3-3	138.1	44.0	$< 10^{-3}$	151	13	0.17
35S::TCH3	142.9	35.8	0.006	163	11	0.34
35S::PID	133.5	53.5	$< 10^{-3}$	111	8	0.32
wag1 wag2	129.8	37.7	0.002	118	5	0.88
PIN1-GFP (II)	139.8	19.3	0.82	123	7	0.80
PIN1-GFP S123E	128.7	51.9	$< 10^{-3}$	106	11	0.10

Mean divergence angle and standard deviation (SD) of divergence angles between subsequent rosette leaves and pedicels in Col-0 and mutant inflorescences. P1 indicates the significance level given by an F test of equality of the variance of divergence angles in a specific line compared to wild-type. P2 indicates the probability value for the Pearson's Chi squared test ($P < 0.05$ for significant difference with Col-0) for the fraction of angles that is larger than 180 ° as compared to the fraction in wild-type plants.

AGC3 kinase-mediated PIN1 phosphorylation is required for spiral phyllotaxis

For wild-type *Arabidopsis*, the divergence angle between rosette leaves was approximately 137.5 ° and, as reported before, the phyllotactic spiral was either clockwise or anticlockwise (Figure 1A;(Landrein et al., 2013)). Divergence angles of more than 180 ° were occasionally observed in *pid*, *pid wag1*, *pid wag1 wag2*, *wag1 wag2* and *35S::PID* rosettes, and significantly more frequent in *pin1 PIN1::PIN1:GFP S123A* and *pid wag2* mutant rosettes (Table 1). When we carefully studied *pid wag2* rosettes containing these larger divergence angles, in several cases such angles appeared to be two times the normal angle (275 °), and to be followed by a normal wild-type angle (Figure 1B). Such a large angle can be explained by the failure of primordium initiation at one position, followed by a successful initiation event at the subsequent position (Figure 1B, C).

Further detailed analysis of the rosettes with strongly deviated angles showed that angles of around 180 ° were frequently observed, which is typical for a distichous rather than a spiral phyllotaxis (Figure 1C, D, E). Considering the variation in phenotypes, we classified the observed divergence angles in 5 groups: 1) 135 ± 25 ° typical for a spiral phyllotaxis, 2) 90±20 ° typical for a two opposite leaves per node decussate phyllotaxis and 3) 180±20 ° typical for a distichous phyllotaxis, and 4) smaller than 70 ° than or 5) larger than 200 °, typical for respectively additional- or lack of primordium initiation. Interestingly, angles of 70 ° or smaller were only observed in *wag1 wag2* or *pid wag1* mutant rosettes, whereas angles larger than 200 ° were observed significantly more in *pid wag2* mutant rosettes, and a few times in *pin1 PIN1::PIN1:GFP S123A*. In *pid wag1 wag2* triple mutant rosettes a 270 ° angle was observed only once, confirming the antagonistic action between WAG1 and WAG2, and that their dual activity is needed for correct spacing of organ initiation during spiral phyllotaxis. We found that *35S::PID*, *pin1 PIN1::PIN1:GFP S123E* and *wag1 wag2* rosettes showed significantly more 90±20 ° angles compared to wild type (Figure 2). In *pid wag1*, *pid wag2*, *pid wag1 wag2* and *pin1 PIN1::PIN1:GFP S123A* rosettes both 90±20 ° and 180±20 ° angles were significantly increased. The results indicate that proper regulation of PIN1 phosphorylation by the AGC3 kinases is important for maintaining the spiral phyllotaxis, and that loss-of-phosphorylation, and in a milder version also enhanced phosphorylation results in a switch from spiral to a decussate-like phyllotaxis.

TCH3 regulates inflorescence phyllotaxis

Several recent publications have reported on the involvement of mechanical stress in the SAM or IM as an important determinant of phyllotaxis (Dumais and Steele, 2000; Hamant et al., 2008; Uyttewaal et al., 2012). One way mechanical stress links to PAT is by reorientation of the microtubule cytoskeleton, which was found to show co-alignment with the polar distribution of PIN1, suggesting a role for the microtubules in directing PIN1 polarity (Heisler et al., 2010). Another way mechanical stress could link to the direction of PAT is by regulating the activity of the AGC3 kinases. An interesting candidate for this regulation is the CML TCH3, as *TCH3* was initially identified as a mechanical stress-induced gene (Braam and Davis, 1990), and we previously found that TCH3 negatively regulates PID and WAG2 activity by sequestering these protein kinases from the PM, thereby affecting PIN polarity (Chapter 2).

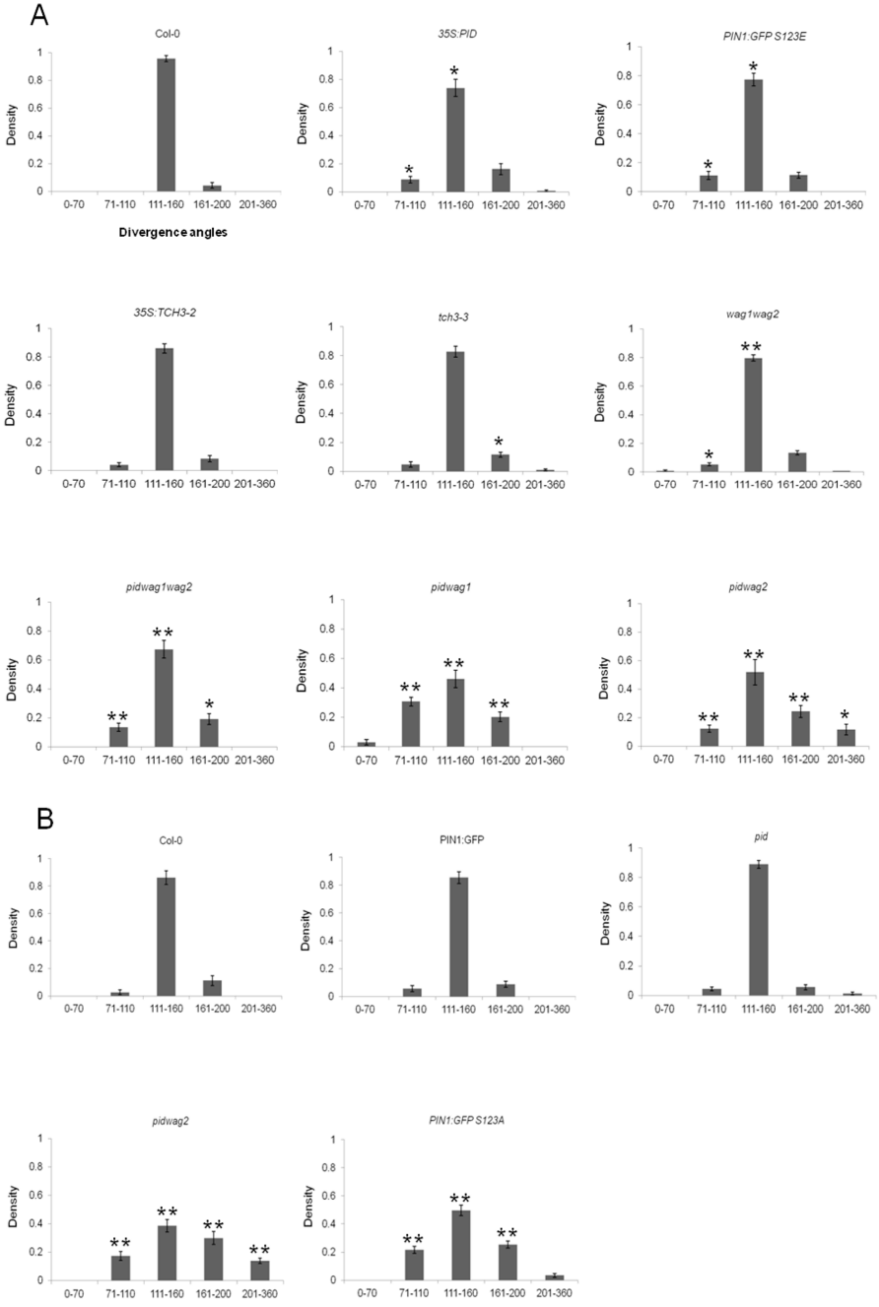

Figure 2. Divergence angle distribution in rosettes of (**A**, **B**) wild-type *Arabidopsis* (Col-0) or of the indicated

mutant plants

A and B represent two independent experiments. Asterisks indicate group values that are significantly different between mutant and Col-0 rosettes: *$p<0.05$; **$p<0.01$ (Student's *t*-test).

Both *tch3-3* loss-of-function mutant and *35S::TCH3-2* overexpression rosettes showed mild differences compared to wild-type. For *tch3-3* rosettes significantly more divergence angles around 180 ° were observed, whereas for *35S::TCH3-2* plants, the variation in the divergence angle was significantly higher compared to wild-type (Table 1, Figure 2A). In inflorescences, however, both *tch3-3* loss-of-function and *35S::TCH3-2* overexpression resulted in a significant increase in the variation of the divergence angle (Table 2), suggesting that TCH3 might be more actively involved in controlling inflorescence phyllotaxis, or that other redundantly acting CaMs of CML proteins act more predominantly in the SAM (Chapter 3). Earlier studies reported the expression of *TCH3* in the SAM (Antosiewicz et al., 1995; McCormack et al., 2005). However, in our hands the *TCH3pro::TCH3-GUS* (Sistrunk et al., 1994) or *TCH3pro::TCH3-mRFP* (Chapter 2) reporter lines only showed a very weak signal in either the SAM or IM, so the exact location of *TCH3* expression in these tissues remains to be investigated (results not shown).

As phyllotaxis is determined by PIN-driven auxin maxima that initiate lateral organ formation, we investigated the quality of the *DR5::GFP*-reported auxin maxima in *TCH3* overexpression or *tch3* loss-of-function IMs. In the *tch3-3* IMs, *DR5:GFP* was clearly expressed in the incipient primordia, and compared to a wild-type IM, the signal was slightly stronger (Figure 3A, C, D). In the *35S:TCH3-2* background, the *DR5::GFP* signal was much stronger than in wild-type IMs (Figure 3A, B, D). These results suggest that a balanced level of *TCH3* expression is required for proper phyllotaxis, and that possibly *TCH3* expression in the boundary regions, which are regions of mechanical stress [26], and exclusion of *TCH3* expression from the incipient primoridia is important in positioning and confining the auxin maxima, leading to regular spiral phyllotaxis.

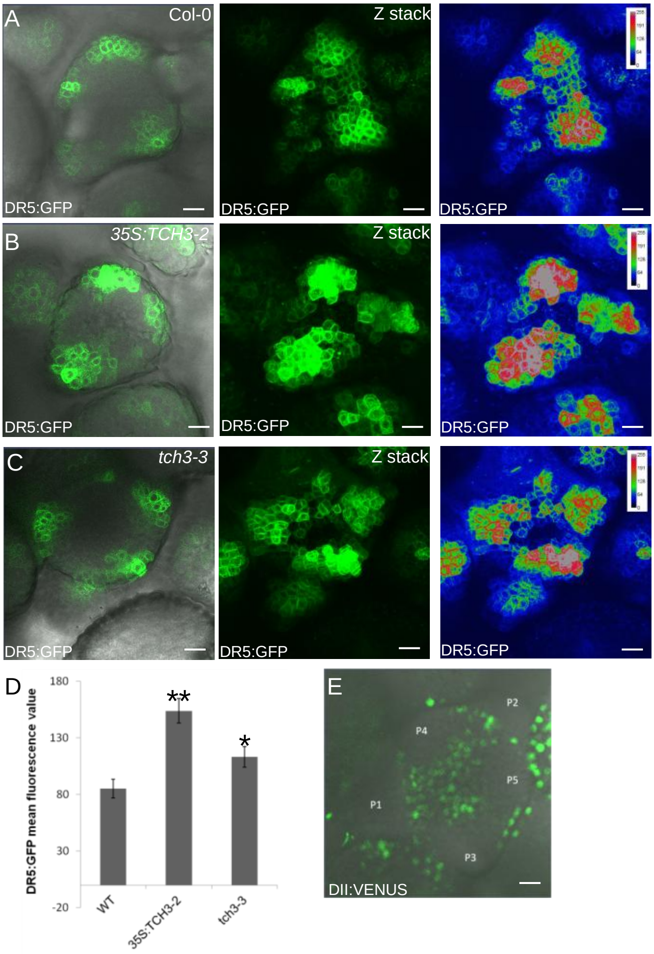
A
Col-0
Z stack
DR5:GFP
DR5:GFP
DR5:GFP
B
35S:TCH3-2
Z stack
DR5:GFP
DR5:GFP
DR5:GFP
C
tch3-3
Z stack
DR5:GFP
DR5:GFP
DR5:GFP
D
DR5:GFP mean fluorescence value
180
130
80
30
-20
**
*
WT
35S:TCH3-2
tch3-3
E
P1
P2
P3
P4
P5
DII:VENUS

Figure 3. *TCH3* functions in inflorescence meristems (IMs). (A-C) Confocal images of the expression pattern of the *DR5::GFP* auxin response reporter in IMs of wild-type (Col-0, A), *tch3-3* (B) and *35S:TCH3-2* (C) plants. From left to right: overlay of GFP and transmitted light signal at a single focal plane, reconstructed Z-stack showing GFP signal, and reconstructed Z-stack after changing to the look up table to color-code signal intensity (low to high = blue to red). (D) Quantification of the *DR5::GFP* signal in organ primordia. $*p<0.05$; $**p<0.01$ (*t*-test). (E) Confocal image of *35S::DII-VENUS* expression in the IM. Numbered from oldest (P1) to youngest (P5) primordium. The scale bars indicate 10 µm.

Auxin and mechanical stress induce TCH3-mediated PID internalization in the inflorescence meristem

In Chapter 2 we showed that TCH3 sequesters PID from the plasma membrane (PM) to the cytoplasm in the presence of auxin, as auxin triggers elevation of $[Ca^{2+}]_{cyt}$. Mechanical stress has also been reported to cause rapid elevation of $[Ca^{2+}]_{cyt}$ (Monshausen et al., 2009), and TCH3 (and other redundant CaMs or CMLs) might play a role in translating mechanical stress into a phyllotactic pattern by internalizing PID in regions of mechanical stress, resulting in relocalization of PIN1 auxin efflux carriers.

Analysis of *PID::PID-VENUS* IMs by confocal microscopy confirmed previous observations that *PID* expression is highest in the boundaries between the meristem and the newly formed primordia (Christensen et al., 2000; Furutani et al., 2004).

In untreated meristems, PID was mainly localized at the PM, and only a few cells showed clear PID internalization (Figure 4A-C). Predominant expression of the auxin minimum reporter *35S::DII-VENUS* in the boundaries (Figure 3E), and restriction of *DR5::GFP* reporter expression to the primordia (Figure 3A) indicated that auxin levels in the boundaries are low, making it unlikely that auxin would contribute to the elevation in $[Ca^{2+}]_{cyt}$ in these regions. PID internalization was mostly observed in boundary cells between adjacent primordia, initially suggesting that these are regions of higher mechanical stress (Fig. 4B, C). However, when studying the *DR5::GFP* and *35S::DII-VENUS* images more carefully, we discovered that the boundaries between specific primordia showed a significant auxin response (Fig. 3A, E), suggesting that the observed PID internalization could be caused by both auxin and mechanical stress.

To test whether the PID internalization response to auxin observed before in *Arabidopsis* protoplasts and roots (Chapter 2) could also be observed in the IM, 5 µM NAA was applied to the meristem. Only after 2 hours treatment (and not after 5, 10, 20 or 30 minutes), PID internalization could be observed in the entire NAA treated meristem (Fig. 4E), whereas control treatments with DMSO did not result in internalization of PID (Fig. 4D). Pretreatment with the Ca^{2+} channel blocker lanthanum chloride prior to auxin application prevented PID internalization (Fig. 4F), indicating that Ca^{2+} is necessary for auxin-triggered PID internalization. In the *tch3-3* mutant background, clear PID internalization could only be observed after 4 hours of auxin application (Fig. 4H), but not after 2 hours (Fig.4G), indicating that PID internalization is delayed in this mutant background, and that like in the root tip, TCH3 is also involved in the auxin-triggered PID internalization in the IM.

In order to investigate whether mechanical stress could lead to changes in PID subcellular localization, a cover glass was placed on the IM. This resulted in rapid internalization of PID after 30 minutes (Fig. 4I). However, when the IM was pretreated with lanthanum chloride before placing the cover glass, PID remained at the plasma membrane as in untreated samples (Fig. 4J). In the *tch3-3* mutant background, we did not observe a clear delay in mechanical stress-induced PID internalization (Fig. 4K). The results can be explained in two ways, one is TCH3 itself is not involved in mechanical stress-induced PID internalization in the meristem, which is in line with its low expression in these tissues (data not shown, (McCormack et al., 2005)). Alternatively, the CaMs and CMLs interacting with PID are acting redundantly in the SAM/IM, which fits with our observations in the root tip (Chapter 2).

In IMs of *TCH3* overexpression lines we observed PID internalization even without any treatment (Figure 4N), which is similar to what was observed in the root tip (Chapter 2). The lack of a strong phenotype in this line suggests that PID is not constitutively internalized, but rather that due to *TCH3* overexpression this line is hypersensitive to mechanical stimuli, and that internalization is due to manipulation of the IM during microscopy. Although the effects of *tch3-3* loss-of-function on phyllotaxis are mild, and the expression of *TCH3* in the SAM/IM is not detectable, the TCH3-induced internalization of PID and the observed effect of TCH3 overexpression on phyllotaxis, indicates that et least some CaM/CML proteins act redundantly in the SAM and IM to translate mechanical/auxin signals into phyllotactic patterns, by modulating PAT through internalization of PID.

Discussion

The regular pattern of organ formation in the SAM and IM, or phyllotaxis is in part determined by the unequal distribution of auxin in the L1 layer of the meristem, which is generated by the asymmetric subcellular distribution of PIN1 auxin efflux carriers (Reinhardt et al., 2003; Guenot et al., 2012; Kierzkowski et al., 2012). The polar localization of PIN1 in epidermis cells of these meristems is very dynamic (Heisler et al., 2005) and is directed by the phosphorylation status of its large central hydrophilic loop through the antagonistic action of PP2A/PP6 phosphatases on the one hand, and the AGC3 protein kinases PID, WAG1 and WAG2 on the other (Friml et al., 2004; Michniewicz et al., 2007; Dhonukshe et al., 2010; Huang et al., 2010). Moreover, PIN1 polar localization has been shown to correlate with the direction of mechanical stress (Heisler et al., 2010) and to respond to osmo-mechanical stress treatments (Nakayama et al., 2012). In Chapters 2 and 3 we showed that the activity of the AGC3 kinases PID and WAG2 is regulated by sequestration of these kinases from the PM to the cytosol by the Ca^{2+}-dependent interaction with the CML TCH3 and closely related CaMs/CMLs. Since mechanical stress is known to induce *TCH3* expression (Braam and Davis, 1990), and at the same time leads to a rapid increase in the $[Ca^{2+}]_{cyt}$ (Monshausen et al., 2009), the AGC3 kinase–CML/CaM signaling complex is a candidate module that might be involved in translating mechanical signals into changes in PIN polarity during phyllotaxis.

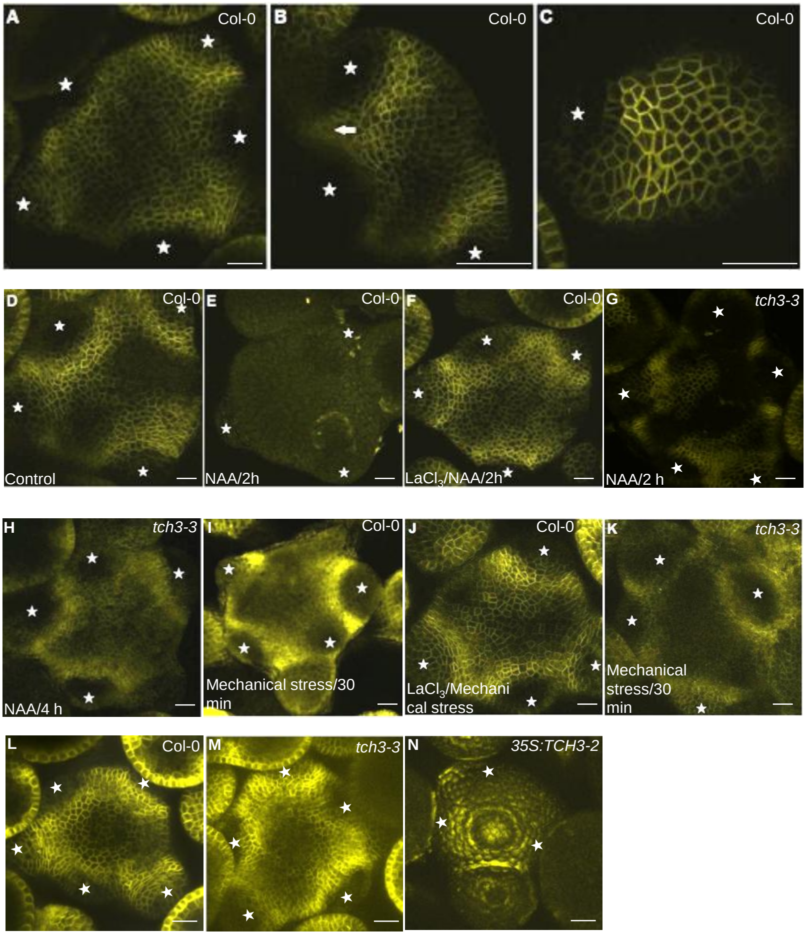
A
Col-0
B
Col-0
C
Col-0
D
Col-0
Control
E
Col-0
NAA/2h
F
Col-0
LaCl3/NAA/2h
G
tch3-3
NAA/2 h
H
tch3-3
NAA/4 h
I
Col-0
Mechanical stress/30 min
J
Col-0
LaCl3/Mechanical stress
K
tch3-3
Mechanical stress/30 min
L
Col-0
M
tch3-3
N
35S:TCH3-2

Figure 4. Ca^{2+}-dependent internalization of PID:VENUS in IMs following auxin and mechanical stress treatment. (**A-C**) PID is mostly plasma membrane localized in untreated wild-type *Arabidopsis* (Col-0) IMs.

Between primordia, PID is internalized (**B**, arrow). (**D-K**) Subcellular localization of PID-VENUS in wild–type (Col-0) (D-F,I,J,L), *tch3*-3 (G,H,K) IMs following 2 hours control treatment (D), 2 hours treatment with 5 μM NAA (E,G), 4 hours treatment with 5 μM NAA (H), 30 minutes pretreatment with 1.25 mM of the Ca^{2+} channel blocker $LaCL_3$ followed by 2 hours treatment with 5 μM NAA (F),30 minutes mechanical stress (covering with a cover glass, I,K), or pretreatment with 1.25 mM $LaCL_3$ followed by 30 minutes mechanical stress (**J**). (**L-N**) PID-VENUS is predominantly at the plasmamembrane in wild-type (Col-0, **L**) or *tch3-3* (**M**) IMs, but is mostly internalized in the *35S:TCH3-2* overexpression background (N). Primoridium tips are marked with asterisks. The scale bar indicates 10 µm.

Here we studied the possible involvement of the AGC3 kinases and the CML TCH3 in phyllotaxis. Our results show that the AGC3 kinases PID, WAG1 and WAG2 are redundantly involved in maintaining the normal spiral phyllotaxis in *Arabidopsis*, and that deregulation of PIN1 phosphorylation dynamics leads to irregularities, such as defective initiation, resulting in a 270 ° divergence angle, and in switches from the spiral (137.5 °) to a decussate-like (90/180 °) phyllotaxis. These defects were most apparent in the *pid wag2* loss-of-function mutant and in *pin1* mutant plants expressing the PIN1-GFP S>A loss-of-phosphorylation version. A defective primordium initiation can be explained by the inability to sufficiently focus PIN1-driven auxin transport in order to accumulate auxin at the next position in the L1 layer of the meristem. Based on the mutant studies, this seems to specifically require PIN1 phosphorylation by PID and WAG2.

Remarkably, in the *pid wag1 wag2* triple mutant these major phyllotaxis defects seemed to be restored, which points to the opposite effect of the *wag1* and the *wag2* mutation on the divergence angle, and suggests that, besides their redundant function in controlling spiral phyllotaxis, WAG1 and WAG2 also act antagonistically. On the one hand, their opposite effect might relate to a difference in their tissue-specific expression, and on the other it may relate to the fact that WAG2 activity is sensitive to auxin and mechanical stress through its interaction with CaM/CMLs, whereas WAG1 is not (Chapter 3).

The exact role of the CML TCH3 in the rosette phyllotaxis is not clear, as *tch3-3* loss-of-function only had mild effects on phyllotaxis, but changes in its activity led to enhanced variation in the divergence angle between primordia in the IM. Our results suggest the involvement of the AGC3 kinase-calmodulin signalling complex in controlling the phyllotactic pattern, in response to auxin and mechanical stress dynamics in the *Arabidopsis* SAM and IMs.

The switch from spiral to decussate-like phyllotaxis that we observed in the *pid wag2* double mutant and in the *PIN1-GFP S>A* line was previously also reported for the first few rosette leaves of *pin1* mutant plants, for plants grown on the PAT inhibitor NPA and for plants mutated in *PLETHORA* genes (Prasad et al., 2011). For the *pin1* mutant plants it was suggested that this aberrant pattern was induced by the absence of one of the cotyledons (Guenot et al., 2012). In fact, in the *pid wag1 wag2* triple mutant seedlings, which lack cotyledons, we observed that the first two sets of true leaves showed a distichous phyllotaxis that is normally observed for the cotyledons and first true leaves in wild-type seedlings. This suggests that the process of cotyledon initiation during *Arabidopsis* embryogenesis is important for the subsequent onset of the spiral phyllotaxis. Apparently, the first true leaves initiated in *pid wag1 wag2* triple mutant can replace the cotyledons, so that the phyllotaxis of subsequent leaves is relatively normal, except for the larger variation in the divergence angle, which was observed for most of the mutant plants analysed (Table 1). The shift from spiral to decussate-like phyllotaxis might be explained by a higher or lower auxin amount pointing the location of the new primordium, resulting in a higher or lower inhibitory field around the primordium, and causing the new primordium to be formed respectively closer (90°) or further away (180°) from the last primordium.

To further investigate the involvement of mechanical stress in regulation of phyllotaxis by influencing polar auxin transport, the PID subcellular localization in IMs was studied. It has been previously shown that external auxin application leads to rapid TCH3-mediated PID internalization in a Ca^{2+}-dependent manner in protoplasts and roots (Chapter 2). The present study showed that external application of auxin or mechanical stress also leads to PID internalization in IMs. Mechanical stress, as well as auxin, can lead to an increase in the $[Ca^{2+}]_{cyt}$ within seconds (Trewavas and Knight, 1994; Haley et al., 1995). However, much more time was needed for PID internalization to occur; PID internalization in meristems was only visible after two hours treatment with auxin, while in roots internalization was observed within five minutes of auxin treatment. Despite this difference in time requirement, the finding that PID is not internalized in control meristems and in lanthanum pretreated meristems indicates that the observed internalization is caused by auxin-mediated Ca^{2+} signaling. The 2 hour time frame needed might relate to the general insensitivity of the IM to auxin or stress treatment. At the same time, in view of our problems to detect *TCH3* expression in the SAM or IM, the amount of TCH3 protein present in IM cells might be insufficient for efficient PID internalization, and an auxin- or mechanical stress-induced increase in *TCH3* expression levels (Antosiewicz et al., 1995) might be needed.

If intrinsic mechanical stress influences PIN1 localization via TCH3, it is expected that PID would be internalized in regions of the meristem experiencing high levels of mechanical stress. In the present study it was shown that PID is internalized between neighboring primordia, where mechanical stress might indeed be high due to the turgor pressure. Models predict mechanical stress to be high in the boundary between the primordia and the meristem (Hamant et al., 2008), and a switch in PIN1 polarity has been predicted there (Heisler et al., 2005), which could be caused by a change in PID activity and localization. However, at this position PID was found to be localized mainly at the plasma membrane of boundary cells, as in the centre of the meristem, where the auxin minimum localized. These data suggest that PID is not internalized as a result of intrinsic mechanical stress in this region.

Beside intrinsic mechanical stress, the meristem can experience external mechanical stress. The present study indicates that external application of mechanical stress leads to PID internalization. The prevention of mechanical stress induced PID internalization by treatment with a Ca^{2+} channel blocker implies that Ca^{2+} is involved in the signaling pathway. Since 30 minutes stress treatment was sufficient to inducePID internalization, and *TCH3* transcription is known to be upregulated by mechanical stress within this time span by touch stimulation (Braam and Davis, 1990) and increased $[Ca^{2+}]_{cyt}$ (Braam, 1992), the observed PID internalization could be caused by TCH3. In the *35S:TCH3-2* line, PID-VENUS was strongly internalized, suggesting that TCH3 and/or redundantly acting CaM/CMLs (Chapter 3) could be involved in the mechanical stress-regulated phyllotaxis.

Our analysis has shown that some CaMs and CMLs can interact with PID and lead to PID internalization (Chapter 3). Possibly, one or more of these proteins is involved in the observed PID internalization in the IM in response to auxin or touch. It has been reported that *CAM1-7* and several *CML* genes are strongly expressed in the inflorescence (McCormack et al., 2005). Moreover, besides *TCH3*, 11 other genes encoding CAM/CMLs were shown to be upregulated by touch (Lee et al., 2005), indicating that these proteins are important for the plant’s response to mechanical stress. Based on the results presented in Chapter 3, especially the touch-inducible *CAM2/TCH1* and *CML10* genes are of interest here. It would be interesting to investigate if plants mutated in these *CAM/CML* genes show irregularities in phyllotaxis and to study the expression of these genes in undisturbed and touch stimulated meristems.

Finally, it is well established now that PID, WAG1 and WAG2 act redundantly in directing PIN polar localization (Dhonukshe et al., 2010), but the phenotypic analysis presented here indicates that WAG1 and WAG2 act antagonistically in the establishment of the phyllotactic pattern. For a deeper insight into the antagonistic behavior of these kinases it will be necessary to study their expression and subcellular localization in the meristem in more detail.

Experimental Procedures

Arabidopsis lines and plant growth

The *Arabidopsis thaliana* (col-0) *35S::PID-21*, *DR5rev::GFP*, *35S::DII-VENUS*, *TCH3::TCH3-GUS*, *PID::PID-VENUS*, *PIN::PIN1-GFP*, *PIN1::PIN1-GFP S123A* and *PIN1::PIN1-GFP S123E* lines and *pid-14*, *wag1* and *wag2* single, double and triple mutants have been described previously (Sistrunk et al., 1994; Benjamins et al., 2001; Benkova et al., 2003; Michniewicz et al., 2007; Dhonukshe et al., 2010; Huang et al., 2010; Brunoud et al., 2012). The *TCH3::TCH3-mRFP* and *35S::TCH3-2* lines and the *tch3-3* mutant, have been described in Chapter 2.

Arabidopsis seeds were surface sterilized by washing in 70% ethanol, incubating for 8 minutes in 50% commercial bleach, and washing six times with sterile water. Seeds were stored at 4 ℃ for two to three days and germinated on solid MA medium (Masson and Paszkowski, 1992) at 21 ℃ and 16 hours photoperiod. Plants were transferred to soil 10-14 days after germination and grown at 21 ℃, 70% relative humidity and 16 hours photoperiod.

Phenotypic analysis

For the phenotypic analysis of Col-0, *tch3-3*, *35S::TCH3*, *35S::PID-21*, *pid-14 wag1*, *pid-14 wag2*, *pid-14 wag1 wag2*, *wag1 wag2* and *PIN::PIN1-GFP S123E* plant lines, pictures of rosettes were taken when the plants were 14-, 19- and 26-day-old. The pictures of 14- and 19-day-old plants were used to determine the order of initiation of rosette leaves in the 26-day-old plants. Angles between subsequent leaves were measured from the pictures of 26-day-old plants. Angles between subsequent pedicels in inflorescences were determined from pictures of inflorescences of six to eight week old plants. For the phenotypic analysis of Col-0, *pid-14*, *pid-14 wag2*, *PIN1:GFP* and *PIN1:GFP S123A* plant lines, pictures of rosettes were taken when plants were 19- and 27-days-old and pictures of 27-day-old plants were used to measure divergence angles. Divergence angles in primary inflorescences of Col-0 and *PIN1:GFP* plants were measured from pictures of inflorescences of 5-week-old plants and divergence angles of secondary inflorescences were determined using pictures of inflorescences of 6-week-old plants.

Statistical analysis

The F-test was used for comparing variances between plant lines and the Pearson's Chi squared test was used for comparing the number of divergence angles bigger than 180 º per line. The Student's *t*-test was used to compare the divergence angle distribution and *DR5::GFP* fluorescence intensities between mutant lines and wild-type *Arabidopsis*.

Histochemical staining and microscopy

Seedlings were stained for GUS activity as described (Benjamins et al., 2001) and analyzed using a Zeiss Axioplan II microscope with DIC optics. Images were recorded with a ZEISS AxioCam MRc5 camera. IMs of *PID::PID-VENUS* and *tch3-3/PID::PID-VENUS* plants were dissected and put in a drop of 1% low melting point agarose. Chemical and mechanical treatments were performed after dissection. To apply mechanical stress a cover glass was put on the meristem and the sample was observed after removal of the cover glass or with the cover glass remaining on the meristem. As a control, meristems were left untreated after dissection before observation. Auxin or control treatments were performed by putting a drop of liquid MA medium containing 5 µM NAA (dissolved in DMSO) or DMSO only on the meristem. When indicated, meristems were pretreated with 1.25 mM lanthanum chloride (125 mM stock in H_2O; Sigma) for 30-40 minutes before mechanical or auxin treatment. Samples were observed with a ZEISS LSM5 confocal microscope using a 40x long working distance water dipping objective or a 20x objective. PID-VENUS fluorescence was visualized with an argon laser for excitation at 514 nm and a 530-600 nm band pass emission filter. DII-VENUS fluorescence was monitored with an argon laser for excitation at 514 nm and a 530-600 nm band pass emission filter. *DR5::GFP* fluorescence was monitored using an argon laser for excitation at 488 nm and a 505-530 nm band pass emission filter. TCH3-mRFP fluorescence was monitored using an argon laser for excitation at 543 nm excitation and a 560nm long pass emission filter. Images were processed using Image J and assembled in Adobe Photoshop (http://rsb.info.nih.gov/ij/).

Acknowledgements

The authors would like to thank J.Braam for sharing her unpublished data on the *tch3-3* allele, Teva Vernoux for sharing *35S::DII-VENUS*, Gerda Lamers, Ward de Winter and Jan Vink for their help with the microscopy, tissue culture and plant caretaking, respectively.

References

Antosiewicz, D.M., Polisensky, D.H., and Braam, J. (1995). Cellular localization of the Ca^{2+} binding TCH3 protein of *Arabidopsis*. Plant J **8,** 623-636.

Benjamins, R., Ampudia, C.S., Hooykaas, P.J., and Offringa, R. (2003). PINOID-mediated signaling involves calcium-binding proteins. Plant Physiol **132,** 1623-1630.

Benjamins, R., Quint, A., Weijers, D., Hooykaas, P., and Offringa, R. (2001). The PINOID protein kinase regulates organ development in *Arabidopsis* by enhancing polar auxin transport. Development **128,** 4057-4067.

Benkova, E., Michniewicz, M., Sauer, M., Teichmann, T., Seifertova, D., Jurgens, G., and Friml, J. (2003). Local, efflux-dependent auxin gradients as a common module for plant organ formation. Cell **115,** 591-602.

Besnard, F., Vernoux, T., and Hamant, O. (2011). Organogenesis from stem cells in planta: multiple feedback loops integrating molecular and mechanical signals. Cell Mol Life Sci **68,** 2885-2906.

Braam, J. (1992). Regulated expression of the calmodulin-related *TCH* genes in cultured *Arabidopsis* cells: induction by calcium and heat shock. Proc Natl Acad Sci U S A **89,** 3213-3216.

Braam, J., and Davis, R.W. (1990). Rain-, wind-, and touch-induced expression of calmodulin and calmodulin-related genes in Arabidopsis. Cell **60,** 357-364.

Brunoud, G., Wells, D.M., Oliva, M., Larrieu, A., Mirabet, V., Burrow, A.H., Beeckman, T., Kepinski, S., Traas, J., Bennett, M.J., and Vernoux, T. (2012). A novel sensor to map auxin response and distribution at high spatio-temporal resolution. Nature **482,** 103-106.

Christensen, S.K., Dagenais, N., Chory, J., and Weigel, D. (2000). Regulation of auxin response by the protein kinase PINOID. Cell **100,** 469-478.

Dhonukshe, P., Huang, F., Galvan-Ampudia, C.S., Mahonen, A.P., Kleine-Vehn, J., Xu, J., Quint, A., Prasad, K., Friml, J., Scheres, B., and Offringa, R. (2010). Plasma membrane-bound AGC3 kinases phosphorylate PIN auxin carriers at TPRXS(N/S) motifs to direct apical PIN recycling. Development **137,** 3245-3255.

Dumais, J., and Steele, C.R. (2000). New evidence for the role of mechanical forces in the shoot apical meristem. J Plant Growth Regul **19,** 7-18.

Friml, J., Yang, X., Michniewicz, M., Weijers, D., Quint, A., Tietz, O., Benjamins, R., Ouwerkerk, P.B., Ljung, K., Sandberg, G., Hooykaas, P.J., Palme, K., and Offringa, R. (2004). A PINOID-dependent binary switch in apical-basal PIN polar targeting directs auxin efflux. Science **306,** 862-865.

Furutani, M., Vernoux, T., Traas, J., Kato, T., Tasaka, M., and Aida, M. (2004). *PIN-FORMED1* and *PINOID* regulate boundary formation and cotyledon development in *Arabidopsis* embryogenesis. Development **131,** 5021-5030.

Guenot, B., Bayer, E., Kierzkowski, D., Smith, R.S., Mandel, T., Zadnikova, P., Benkova, E., and Kuhlemeier, C. (2012). Pin1-independent leaf initiation in Arabidopsis. Plant Physiol **159,** 1501-1510.

Haley, A., Russell, A.J., Wood, N., Allan, A.C., Knight, M., Campbell, A.K., and Trewavas, A.J. (1995). Effects of mechanical signaling on plant cell cytosolic calcium. Proc Natl Acad Sci U S A **92,** 4124-4128.

Hamant, O., Heisler, M.G., Jonsson, H., Krupinski, P., Uyttewaal, M., Bokov, P., Corson, F., Sahlin, P., Boudaoud, A., Meyerowitz, E.M., Couder, Y., and Traas, J. (2008). Developmental patterning by mechanical signals in *Arabidopsis*. Science **322,** 1650-1655.

Heisler, M.G., Ohno, C., Das, P., Sieber, P., Reddy, G.V., Long, J.A., and Meyerowitz, E.M. (2005). Patterns of auxin transport and gene expression during primordium development revealed by live imaging of the *Arabidopsis* inflorescence meristem. Curr Biol **15,** 1899-1911.

Heisler, M.G., Hamant, O., Krupinski, P., Uyttewaal, M., Ohno, C., Jonsson, H., Traas, J., and Meyerowitz, E.M. (2010). Alignment between PIN1 polarity and microtubule orientation in the shoot apical meristem reveals a tight coupling between morphogenesis and auxin transport. PLoS Biol **8,** e1000516.

Huang, F., Zago, M.K., Abas, L., van Marion, A., Galvan-Ampudia, C.S., and Offringa, R. (2010). Phosphorylation of conserved PIN motifs directs *Arabidopsis* PIN1 polarity and auxin transport. Plant Cell **22,** 1129-1142.

Jonsson, H., Heisler, M.G., Shapiro, B.E., Meyerowitz, E.M., and Mjolsness, E. (2006). An auxin-driven polarized transport model for phyllotaxis. Proc Natl Acad Sci U S A **103,** 1633-1638.

Kierzkowski, D., Nakayama, N., Routier-Kierzkowska, A.L., Weber, A., Bayer, E.,

Schorderet, M., Reinhardt, D., Kuhlemeier, C., and Smith, R.S. (2012). Elastic domains regulate growth and organogenesis in the plant shoot apical meristem. Science **335,** 1096-1099.

Kuhlemeier, C. (2007). Phyllotaxis. Trends Plant Sci **12,** 143-150.

Landrein, B., Lathe, R., Bringmann, M., Vouillot, C., Ivakov, A., Boudaoud, A., Persson, S., and Hamant, O. (2013). Impaired cellulose synthase guidance leads to stem torsion and twists phyllotactic patterns in *Arabidopsis*. Curr Biol **23,** 895-900.

Lee, D., Polisensky, D.H., and Braam, J. (2005). Genome-wide identification of touch- and darkness-regulated Arabidopsis genes: a focus on calmodulin-like and *XTH* genes. New Phytol. **165,** 429-444.

McCormack, E., Tsai, Y.C., and Braam, J. (2005). Handling calcium signaling: *Arabidopsis* CaMs and CMLs. Trends Plant Sci **10,** 383-389.

Michniewicz, M., Zago, M.K., Abas, L., Weijers, D., Schweighofer, A., Meskiene, I., Heisler, M.G., Ohno, C., Zhang, J., Huang, F., Schwab, R., Weigel, D., Meyerowitz, E.M., Luschnig, C., Offringa, R., and Friml, J. (2007). Antagonistic regulation of PIN phosphorylation by PP2A and PINOID directs auxin flux. Cell **130,** 1044-1056.

Mirabet, V., Das, P., Boudaoud, A., and Hamant, O. (2011). The role of mechanical forces in plant morphogenesis. Annu Rev Plant Biol **62,** 365-385.

Mitchison, G.J. (1977). Phyllotaxis and the fibonacci series. Science **196,** 270-275.

Monshausen, G.B., Bibikova, T.N., Weisenseel, M.H., and Gilroy, S. (2009). Ca^{2+} regulates reactive oxygen species production and pH during mechanosensing in *Arabidopsis* roots. Plant Cell **21,** 2341-2356.

Nakayama, N., Smith, R.S., Mandel, T., Robinson, S., Kimura, S., Boudaoud, A., and Kuhlemeier, C. (2012). Mechanical regulation of auxin-mediated growth. Curr Biol **22,** 1468-1476.

Newell, A.C., Shipman, P.D., and Sun, Z. (2008). Phyllotaxis: cooperation and competition between mechanical and biochemical processes. J Theor Biol **251,** 421-439.

Prasad, K., Grigg, S.P., Barkoulas, M., Yadav, R.K., Sanchez-Perez, G.F., Pinon, V., Blilou, I., Hofhuis, H., Dhonukshe, P., Galinha, C., Mahonen, A.P., Muller, W.H., Raman, S., Verkleij, A.J., Snel, B., Reddy, G.V., Tsiantis, M., and Scheres, B. (2011). *Arabidopsis* PLETHORA transcription factors control phyllotaxis. Curr Biol **21,** 1123-1128.

Reinhardt, D., Frenz, M., Mandel, T., and Kuhlemeier, C. (2005). Microsurgical and laser ablation analysis of leaf positioning and dorsoventral patterning in tomato.

Development **132,** 15-26.

Reinhardt, D., Pesce, E.R., Stieger, P., Mandel, T., Baltensperger, K., Bennett, M., Traas, J., Friml, J., and Kuhlemeier, C. (2003). Regulation of phyllotaxis by polar auxin transport. Nature **426,** 255-260.

Sistrunk, M.L., Antosiewicz, D.M., Purugganan, M.M., and Braam, J. (1994). Arabidopsis *TCH3* encodes a novel Ca^{2+} binding protein and shows environmentally induced and tissue-specific regulation. Plant Cell **6,** 1553-1565.

Smith, R.S., Guyomarc'h, S., Mandel, T., Reinhardt, D., Kuhlemeier, C., and Prusinkiewicz, P. (2006). A plausible model of phyllotaxis. Proc Natl Acad Sci U S A **103,** 1301-1306.

Tanaka, H., Dhonukshe, P., Brewer, P.B., and Friml, J. (2006). Spatiotemporal asymmetric auxin distribution: a means to coordinate plant development. Cell Mol Life Sci **63,** 2738-2754.

Trewavas, A., and Knight, M. (1994). Mechanical signalling, calcium and plant form. Plant Mol Biol **26,** 1329-1341.

Uyttewaal, M., Burian, A., Alim, K., Landrein, B., Borowska-Wykret, D., Dedieu, A., Peaucelle, A., Ludynia, M., Traas, J., Boudaoud, A., Kwiatkowska, D., and Hamant, O. (2012). Mechanical stress acts via katanin to amplify differences in growth rate between adjacent cells in *Arabidopsis*. Cell **149,** 439-451.

Summary

As sessile organisms, plants respond to changes in their environment by adjusting their growth and development through a highly dynamic combination of signal perception and transduction systems. The plant hormone auxin is a central regulator in these adaptive responses to environmental cues. Polar cell-to-cell transport of the hormone results in its local accumulation or depletion in tissues and organs, which controls plant growth and development by regulating basic processes such as cell division, -differentiation and -elongation. Polar auxin transport (PAT) is driven by PIN FORMED (PIN) auxin efflux carriers that through their asymmetric localisation at the plasma membrane (PM) determine the direction of transport. PIN subcellular localisation is dynamic and established by clathrin-dependent endocytosis and ARF-GEF-(guanine-nucleotide exchange factors for ADP-ribosylation factor GTPases)-dependent recycling (Tanaka et al., 2006).

The *Arabidopsis* PINOID (PID) serine/threonine protein kinase has been identified as a key determinant in the polar distribution of PIN proteins. The *PID* gene is named after the pin-like phenotype of loss-of-function mutant inflorescences, a phenotype that is shared with the *pin1* mutant. The *pid* mutant defects in embryo bilateral symmetry and inflorescence organogenesis are caused by an apical to basal (shootward to rootward) shift in PIN1 polarity in epidermis cells in embryos and inflorescence meristems. In contrast, *PID* gain-of-function results in an opposite basal to apical PIN polarity shift, leading to auxin depletion from the root meristem, and ultimately resulting in its collapse (Benjamins et al., 2001; Friml et al., 2004). PID is a member of the AGC3 clade of plant-specific *Arabidopsis* AGCVIII protein kinases, together with WAG1, WAG2 and AGC3-4. PID, WAG1 and WAG2 act redundantly in regulating the polarity of the PM-localized ('long') PINs by phosphorylating the serine in three conserved TPRXS motifs present in their large PIN central hydrophilic loop (Michniewicz et al., 2007; Huang et al., 2010). Phosphorylation recruits these PINs for GNOM ARF-GEF-independent (apical-, outer lateral-, indentation-specific) recycling, directing auxin flow and regulating cotyledon development, root meristem size and tropic growth responses (Michniewicz et al., 2007; Kleine-Vehn et al., 2009; Dhonukshe et al., 2010; Huang et al., 2010; Ding et al., 2011).

Previously, a six EF-hand calmodulin-like protein CML12/TOUCH3 (TCH3) has been identified by a yeast two-hybrid screen as a PID-interacting protein (Benjamins et al., 2003). TCH3 appeared not to be a phosphorylation target of PID, but instead to regulate the *in vitro* activity of this kinase through its Ca^{2+}-dependent binding (Benjamins et al., 2003). *TCH3* expression is induced by auxin and mechanical stress (Braam and Davis,

1990), and at the same time auxin and environmental signals such as touch and light can induce a rapid increase in the cytosolic Ca^{2+} levels ($[Ca^{2+}]_{cyt}$) (Monshausen et al., 2011). TCH3 therefore seems an ideal candidate to regulate PID activity and thereby induce changes in PIN polarity in response to both endogenous and environmental signals.

The two key objectives of the research described in this thesis were 1) to demonstrate the role of TCH3 as negative regulator of PID activity *in vivo*, and 2) to investigate in which developmental processes in *Arabidopsis* the kinase-CML interaction plays a role, and whether other AGC3 kinases and CMLs or calmodulins (CaMs) act redundantly in these processes.

Chapter 2 follows up on the initial finding of the PID-TCH3 interaction by confirming that TCH3 negatively regulates PID activity by interacting with the catalytic domain of the protein kinase. Furthermore, protoplast transfection experiments combined with Fluorescence Resonance Energy Transfer (FRET) measurements showed that TCH3 interacts with PID and WAG2 *in vivo*, but not with WAG1 or AGC3-4, and that this interaction is auxin dependent. PID and WAG2 are both PM associated kinases, and previous studies suggested that they phosphorylate PINs at the PM (Michniewicz et al., 2007; Dhonukshe et al., 2010). Interestingly, we observed that TCH3 through its interaction was able to sequester the PID and WAG2 kinases from the PM to the cytoplasm. Moreover, in root epidermis cells expressing the complementing *PID::PID-VENUS* fusion construct, PID-VENUS was released from the PM to the cytosol as early as 5 minutes after auxin treatment, and this internalization could be inhibited by pretreatment with the Ca^{2+} channel inhibitor lanthanum, and was delayed in the *tch3-3* loss-of-function and enhanced in the *TCH3* overexpression background, indicating that this internalization is dependent on Ca^{2+} and at least in part mediated by TCH3. In line with its function as negative regulator of the PID and WAG2 kinases, *TCH3* overexpression delayed root meristem collapse by PID overexpression, and seedlings developed short roots, a phenotype also observed for *pid/wag1/wag2* triple mutant seedlings. Moreover, *TCH3* overexpression seedlings and *tch3-3* loss-of-function mutant lines showed a delay in root gravitropism, suggesting the involvement of the TCH3-kinase interaction in root gravitropism. Root gravitropic growth is mediated by PIN-driven redirection of auxin flow to the lower side of the root tip (Tanaka et al., 2006), coinciding with $[Ca^{2+}]_{cyt}$ peaks in cells at this side of the root tip (Monshausen et al., 2011). We could show that Ca^{2+} acts downstream of auxin during root gravitropism. The auxin-induced $[Ca^{2+}]_{cyt}$- and *TCH3* expression levels promote the kinase-CML interaction, through internalization of the kinase, and depolarisation (and enhanced degradation) of PIN2. This enhances the asymmetric auxin distribution, and thereby root gravitropic growth.

Chapter 3 describes a study to identify the function of the PID-CML interaction throughout plant development. The mild effects of *tch3-3* loss-of-function suggested that some of the 7 CaMs and 50 CMLs in *Arabidopsis* act redundantly with TCH3. Indeed we could show that PID interacts with, and is sequestered by the closely related CML10, but not by the more distantly related CML24/TCH2. This result confirmed that there is redundancy among the CMLs, but it also showed some level of specificity, especially with respect to the ability of CMLs to recruit PID from the PM. In view of this redundancy, and the likely pleiotropic function of CMLs, we decided to unravel this process from the kinase side, by generating 'untouchable PID': a kinase that does not interact with TCH3, but is still fully functional as a PM associated, PIN phosphorylating kinase. AGCVIII kinases are characterised by an insertion of 36 to 90 amino acids in the kinase catalytic domain (Galván-Ampudia and Offringa, 2007), and it has been shown that the PM association function of PID localises to this insertion domain (ID) (Zegzouti et al., 2006). By generating mutant versions of PID having deletions or specific amino acid substitutions in this ID we could show that PM association and TCH3 binding functions overlapped to a region in the middle of this ID. Careful amino acid sequence and 3D structure analysis revealed that this part contains a partially overlapping amphipathic alpha-helix and IQ-motif. Both structures are known to interact with CaMs in animal cells (Snedden and Fromm, 2001; Bahler and Rhoads, 2002; Lu and Taghbalout, 2013), and through *in vitro* pull downs we could show that this specific region does not only interact with TCH3 and CML10, but also with an *Arabidopsis* CaM. Moreover, the amphipathic alpha helix is also known as a high affinity PM association domain (Lu and Taghbalout, 2013). Fusion of the amphipathic alpha helix/IQ-motif to GFP resulted in a PM associated fusion protein that could be sequestered to the cytosol by TCH3 binding. Amino acid substitution of residues that were part of the IQ-motif but outside the alpha helix still resulted in loss of PM association, indicating that the two functions tightly overlap. Although this has prevented us from generating an 'untouchable' PID version, our studies have provided valuable information on the function of the PID kinase. Its tight association with the PM, possibly enhanced through the interaction with phospholipids, takes care that it stays close to the PIN phosphorylation targets. However, the two overlapping CaM/CML binding domains that are located in the heart of the kinase catalytic domain will allow TCH3 to recruit and inactivate PID when both the $[Ca^{2+}]_{cyt}$ and TCH3 levels are sufficient. This may explain the relatively late occurrence of PID internalization during root gravitropism, which was observed only a few hours after gravistimulation (Chapter 2).

The *pid* loss-of-function mutant phenotypes suggest that the kinase is important for the initiation and positioning of new aerial organs. In fact, preliminary results by Reinhardt and coworkers (Reinhardt et al., 2003) suggested that PID is involved in maintaining the regular spiral phyllotaxis in *Arabidopsis* rosettes and inflorescences. In addition, mechanical stress in the shoot apical and inflorescence meristems was reported as a key determinant in generating phyllotactic patterns (Heisler et al., 2010). As *TCH3* transcription is induced by auxin and mechanical stress (Braam and Davis, 1990), and the same signals also elevate $[Ca^{2+}]_{cyt}$, the TCH3-PID interaction could be an important signalling event in phyllotactic patterning.

Chapter 4 describes studies that further investigate the role of the AGC3 kinases and their interaction with CaMs and CMLs in phyllotaxis. By using AGC3 kinase loss-of-function mutants or *pin1* mutants plants expressing non-phosphorylatable or phosphomimic versions of PIN1-GFP we could show that reversable PIN1 phosphorylation by these kinases is important to maintain the spiral phyllotaxis in *Arabidospsis* with a 'golden' divergence angle of 137.5 °. In general, mutants showed an increased variation in the divergence angle. Especially PID and WAG2 appeared important, as their loss-of-function regularly led to a shift from spiral to decussate (alternating 90 ° and 180 ° divergence angles) phyllotaxis. In some cases we found angles around 270 °, suggesting that the organ initiation event in between had been unsuccessful, and implying that kinase activity is important for focussing the auxin maximum required for organ initiation. Plants overexpressing TCH3 or *tch3* loss-of-function mutants only showed weak irregularities in phyllotactic patterns, and the expression of TCH3 in shoot and inflorescence meristems was weak. However, by using the *PID::PID-VENUS* reporter line we could show that both auxin and mechanical stress induce Ca^{2+}-dependent internalization of PID-VENUS in inflorescence meristems. A role for TCH3 in this process is unlikely, however, based on results in Chapter 3 possibly CML10 or one of the CaMs are involved in modulating the phyllotactic pattern by recruiting PID and WAG2 from the PM in response to auxin and mechanical stress signals.

In conclusion, based on the functional analysis of PID, and its interaction with TCH3 *in vivo* described in this thesis, we propose a new model in which the PID-CaM/CML module translates both endogenous and external signals into changes in development and growth by modulating the subcellular localisation of PINs. But there are still some unanswered questions that need further investigation. For example, it would still be desirable to generate an untouchable PID to study the function of the PID-CaM/CML interaction throughout development. This would require further fine mapping of the PM association and CaM/CML binding domains in PID, possibly through high throughput amino acid substitution analysis. Such studies will provide important new insights into the capacity of plants to change their growth and development in response to both internal and environmental signals.

References

Bahler, M., and Rhoads, A. (2002). Calmodulin signaling via the IQ motif. FEBS Lett **513,** 107-113.

Benjamins, R., Ampudia, C.S., Hooykaas, P.J., and Offringa, R. (2003). PINOID-mediated signaling involves calcium-binding proteins. Plant Physiol **132,** 1623-1630.

Benjamins, R., Quint, A., Weijers, D., Hooykaas, P., and Offringa, R. (2001). The PINOID protein kinase regulates organ development in *Arabidopsis* by enhancing polar auxin transport. Development **128,** 4057-4067.

Braam, J., and Davis, R.W. (1990). Rain-, wind-, and touch-induced expression of calmodulin and calmodulin-related genes in Arabidopsis. Cell **60,** 357-364.

Dhonukshe, P., Huang, F., Galvan-Ampudia, C.S., Mahonen, A.P., Kleine-Vehn, J., Xu, J., Quint, A., Prasad, K., Friml, J., Scheres, B., and Offringa, R. (2010). Plasma membrane-bound AGC3 kinases phosphorylate PIN auxin carriers at TPRXS(N/S) motifs to direct apical PIN recycling. Development **137,** 3245-3255.

Ding, Z., Galvan-Ampudia, C.S., Demarsy, E., Langowski, L., Kleine-Vehn, J., Fan, Y., Morita, M.T., Tasaka, M., Fankhauser, C., Offringa, R., and Friml, J. (2011). Light-mediated polarization of the PIN3 auxin transporter for the phototropic response in *Arabidopsis*. Nat Cell Biol **13,** 447-452.

Friml, J., Yang, X., Michniewicz, M., Weijers, D., Quint, A., Tietz, O., Benjamins, R., Ouwerkerk, P.B., Ljung, K., Sandberg, G., Hooykaas, P.J., Palme, K., and Offringa, R. (2004). A PINOID-dependent binary switch in apical-basal PIN polar targeting directs auxin efflux. Science **306,** 862-865.

Galván-Ampudia, C.S., and Offringa, R. (2007). Plant evolution: AGC kinases tell the auxin tale. Trends Plant Sci. **12,** 541-547.

Heisler, M.G., Hamant, O., Krupinski, P., Uyttewaal, M., Ohno, C., Jonsson, H., Traas, J., and Meyerowitz, E.M. (2010). Alignment between PIN1 polarity and microtubule orientation in the shoot apical meristem reveals a tight coupling between morphogenesis and auxin transport. PLoS Biol **8,** e1000516.

Huang, F., Zago, M.K., Abas, L., van Marion, A., Galvan-Ampudia, C.S., and Offringa, R. (2010). Phosphorylation of conserved PIN motifs directs *Arabidopsis* PIN1 polarity and auxin transport. Plant Cell **22,** 1129-1142.

Kleine-Vehn, J., Huang, F., Naramoto, S., Zhang, J., Michniewicz, M., Offringa, R., and Friml, J. (2009). PIN auxin efflux carrier polarity is regulated by PINOID kinase-mediated recruitment into GNOM-independent trafficking in *Arabidopsis*. Plant Cell **21,** 3839-3849.

Lu, F., and Taghbalout, A. (2013). Membrane association via an amino-terminal amphipathic helix is required for the cellular organization and function of RNase II. J Biol Chem **288,** 7241-7251.

Michniewicz, M., Zago, M.K., Abas, L., Weijers, D., Schweighofer, A., Meskiene, I., Heisler, M.G., Ohno, C., Zhang, J., Huang, F., Schwab, R., Weigel, D., Meyerowitz, E.M., Luschnig, C., Offringa, R., and Friml, J. (2007). Antagonistic regulation of PIN phosphorylation by PP2A and PINOID directs auxin flux. Cell **130,** 1044-1056.

Monshausen, G.B., Miller, N.D., Murphy, A.S., and Gilroy, S. (2011). Dynamics of auxin-dependent Ca^{2+} and pH signaling in root growth revealed by integrating high-resolution imaging with automated computer vision-based analysis. Plant J. **65,** 309-318.

Reinhardt, D., Pesce, E.R., Stieger, P., Mandel, T., Baltensperger, K., Bennett, M., Traas, J., Friml, J., and Kuhlemeier, C. (2003). Regulation of phyllotaxis by polar auxin transport. Nature **426,** 255-260.

Snedden, W.A., and Fromm, H. (2001). Calmodulin as a versatile calcium signal transducer in plants. New Phytol **151,** 35-66.

Tanaka, H., Dhonukshe, P., Brewer, P.B., and Friml, J. (2006). Spatiotemporal asymmetric auxin distribution: a means to coordinate plant development. Cell Mol Life Sci **63,** 2738-2754.

Zegzouti, H., Anthony, R.G., Jahchan, N., Bogre, L., and Christensen, S.K. (2006). Phosphorylation and activation of PINOID by the phospholipid signaling kinase 3-phosphoinositide-dependent protein kinase 1 (PDK1) in *Arabidopsis*. Proc Natl Acad Sci U S A **103,** 6404-6409.

Samenvatting

Planten zijn sessiele organismen die reageren op veranderingen in hun omgeving door hun groei en ontwikkeling aan te passen via een dynamisch complex van signaalperceptie- en transductiesystemen. Het plantenhormoon auxine is een centrale regulator in deze adaptieve responsen op omgevingsfactoren. Auxine wordt polair van cel naar cel getransporteerd, en dit resulteert in lokale accumulatie of depletie van het hormoon in weefsels en organen. Door op een concentratie-afhankelijke manier basale processen zoals celdeling, -differentiatie, en –elongatie te reguleren, controleert auxine de groei en ontwikkeling van een plant.

De PIN FORMED (PIN) auxine efflux carriers zijn de drijvende kracht achter polair auxine transport (PAT). Zij bepalen de richting van transport door hun asymmetrische lokalisatie op het plasmamembraan (PM). De subcellulaire lokalisatie van de PIN eiwitten is zeer dynamisch, en wordt mede gegenereerd en in stand gehouden door clathrine-afhankelijke endocytose en ARF-GEF (Guanine-nucleotide Exchange Factor van de ADP-Ribosylating Factor GTPase) -afhankelijke recycling naar het PM [1].

Het *Arabidopsis* PINOID (PID) serine/threonine proteïne kinase is geïdentificeerd als een bepalende factor in de polaire distributie van PIN eiwitten. De naam van het *PID* gen is afgeleid van de pin-achtige bloeiwijzen van de *pid* verlies-van-functie mutant, een fenotype dat vergelijkbaar is met dat van de verlies-van-functie mutant in the PIN1 auxine transporter. De defecten van de *pid* mutant in de vorming van zaadlobben in het embryo en in de orgaanvorming in de bloeiwijze worden veroorzaakt door een verschuiving in PIN1 polariteit van apicaal naar basaal (van scheut- naar wortel-gericht) in epidermis cellen in embryos en bloeimeristemen. Overexpressie van *PID* zorgt daarentegen voor de tegenovergestelde basale naar apicale verschuiving in PIN polariteit, wat leidt tot het onttrekken van auxine uit het wortelmeristeem, en uiteindelijk tot de desintegratie van het meristeem [2,3]. PID behoort samen met WAG1, WAG2 en AGC3-4 tot de AGC3 subgroep van de plant-specifieke AGCVIII proteïne kinases. PID, WAG1 en WAG2 reguleren alle drie de polariteit van de PM gelocaliseerde (“lange”) PINs, door serines in drie geconserveerde TPRXS motieven in hun lange centrale hydrofiele lus te fosforyleren [4, 5]. Gefosforyleerde PIN eiwitten worden gerecruteerd door GNOM ARF-GEF-onafhankelijke (apicale, buiten-laterale, indentatie-specifieke) recycling, en dit bepaald de richting van auxine transport en reguleert onder andere de ontwikkeling van bloemen, de grootte van het wortelmeristeem, en de richting van groei ten opzichte van omgevingssignalen [4-8].

In een eerdere gist twee-hybride screen was het calmoduline-achtige eiwit CML12/TOUCH3 (TCH3) als PID-interacterend eiwit geïdentificeerd [9]. TCH3 bleek geen fosforylatietarget van PID te zijn, maar juist de activiteit van dit kinase te reguleren door zijn Ca^{2+}-afhankelijke binding [9]. *TCH3* expressie wordt geïnduceerd door auxine en mechanische stress [10], en tegelijkertijd leiden auxine en omgevingssignalen tot een snelle verhoging van de cytoplasmatische Ca^{2+} niveaus ($[Ca^{2+}]_{cyt}$) [11]. Het TCH3 eiwit was daarom een kandidaat bij uitstek om de activiteit van PID, en daarmee de PIN polariteit, te reguleren in response op zowel endogene als externe signalen.

De twee hoofddoelen van het in dit proefschrift beschreven onderzoek waren 1) om de rol van TCH3 als negatieve regulator van PID *in planta* aan te tonen, en 2) om te onderzoeken bij welke ontwikkelingsprocessen in *Arabidopsis* de kinase-CML interactie een rol speelt, en of andere AGC3 kinases en calmodulines (CaMs) of calmoduline-achtige eiwitten (CMLs) redundant werken in deze processen.

Het onderzoek beschreven in **Hoofdstuk 2** bevestigde dat TCH3 de activiteit van PID onderdrukt door te binden aan het katalytische domein van het proteïne kinase. Fluorescence Resonance Energy Transfer (FRET) metingen in getransfecteeerde protoplasten lieten vervolgens zien dat TCH3 interacteert met PID en WAG2, maar niet met WAG1 en AGC3-4, en dat deze interactie auxine afhankelijk is. PID en WAG2 zijn beiden PM geassocieerde kinases, en een vorige studie suggereerde dat zij de PINs op het PM fosforyleren [7]. Interessant genoeg bleek TCH3 door zijn interactie met PID en WAG2 de kinases van het PM naar het cytosol te verplaatsen. De internalisatie van PID werd ook waargenomen in wortelepidermiscellen en bleek afhankelijk van de auxine geïnduceerde verhoging van de cytosolisch Ca^{2+} concentratie ($[Ca^{2+}]_{cyt}$) en de *TCH3* expressieniveaus. In overeenstemming met de functie als repressor van de PID en WAG2, verminderde *TCH3* overexpressie het effect van *PID* overexpressie op het wortelmeristeem, en ontwikkelden *TCH3* overexpressie zaailingen een korte wortel, een fenotype dat ook gevonden was voor *pid/wag1/wag2* triple mutante zaailingen [7]. Zowel *TCH3* overexpressie als *tch3* verlies-van-functie mutante lijnen lieten een vertraging in de wortel geotropie zien, wat een rol suggereerde voor de TCH3-kinase interactie in deze groeiresponse. Wortelgeotropie wordt gemedieerd door PIN-gedreven herverdeling van auxine naar de onderkant van de wortelpunt [1]. In overeenstemming met eerder geobserveerde $[Ca^{2+}]_{cyt}$ pieken in de cellen aan deze kant van de wortel [11], bleek Ca^{2+} downstream van auxine te werken gedurende de geotrope response van de wortel. De auxine-geïnduceerde verhoging in $[Ca^{2+}]_{cyt}$ en *TCH3* expressieniveaus resulteerden in internalisatie van het kinase en depolarisatie (en verhoogde afbraak) van PIN2. Dit bleek de asymmetrische verdeling van auxine te versterken, en uiteindelijk de gravitrope groei van de wortel te versnellen.

De studie beschreven in **Hoofdstuk 3** had tot doel de functie van de kinase-CML interactie door de ontwikkeling van de plant heen te ontrafelen. Het milde effecten van *TCH3* verlies-van-functie suggereerde dat sommige van de 7 CAMs en 50 CMLs in *Arabidopsis* dezelfde functie vervullen. Inderdaad bleek PID te interacteren met, en van het PM gehaald te worden door de zeer verwante CML10, maar niet door de minder gerelateerde CML24/TCH2. Dit resultaat bevestigde enerzijds dat er functionele redundantie is tussen bepaalde CMLs, maar anderzijds liet het ook een niveau van specificiteit zien. Met het oog op deze redundantie, en de waarschijnlijke pleiotrope functie van CMLs, werd besloten om de rol van de kinase-CML interactie vanuit het PID kinase te bestuderen. Dit door te pogen een “untouchable PID” te generen, een kinase dat niet meer interacteert met TCH3, maar nog wel volledig functioneel is met betrekking tot PM associatie en PIN fosforylering. Eerder was aangetoond dat de PM associatie functie van PID is gelokaliseerd in een insertiedomein (ID) in het katalytische domein van het kinase [13]. Dit ID is karakteristiek voor de AGCVIII kinases [12]. Door mutanten versies van PID te maken met deleties of specifieke aminozuurvervangingen in het ID kon worden aangetoond dat de PM associatie- en TCH3 bindingsfuncties overlappen in een regio in het midden van dit ID. Nauwkeurige aminozuursequentie en 3D structuuranalyse brachten aan het licht dat het ID een amfipatische alfa helix en een IQ motief bevat die deels overlappen. Van beide eiwitdomeinen is bekend dat ze interacteren met CAMs [14-16]. *In vitro* interactiestudies toonden inderdaad aan dat TCH3, CML10 en ook *Arabidopsis* CAM2 de regio binden die de amfipatische alfa helix en het IQ motief omvat. Voor een amfipatische alfa helix is ook bekend dat het met het PM kan associeren [16]. Fusie van het gecombineerde amfipatische alpha helix/IQ motief met GFP resulteerde in een PM geassocieerd fusie-eiwit dat naar het cytosol gehaald kon worden door binding met TCH3. Aminozuurveranderingen in het IQ motief, maar buiten de amfipatische alfa helix, resulteerden nog steeds in verlies van PM associatie, wat een sterke koppeling tussen deze functie en TCH3 binding aangaf. De hechte assocatie van het kinase met het PM, mogelijk versterkt door binding aan fosfolipiden, zorgt ervoor dat het kinase dicht bij zijn PIN fosforylatietargets blijft. Echter, de twee overlappende CAM/CML bindingsdomeinen die zich bevinden in het hart van het katalytische kinase domein, maken het mogelijk voor CMLs zoals TCH3 om het kinase te rekruteren en te inactiveren als de $[Ca^{2+}]_{cyt}$ en de CAM/CML expressie voldoende zijn. Dit verklaart mogelijk het relatief late optreden van PID internalisatie, wat pas enkele uren na de start van de geotrope respons kon worden waargenomen (Hoofdstuk 2).

De fenotypes van de *pid* verlies-van-functie mutant en resultaten van Reinhardt en collega's [17] suggereren dat het PID kinase betrokken is bij het in stand houden van de spiraalsgewijze fyllotaxis van de rozet en de bloeiwijzen van *Arabidopsis*. Tevens is gerapporteerd dat mechanische stress in het scheut apicale- en bloeimeristeem een sleutelrol heeft bij de fyllotactische patroonvorming [18]. Omdat *TCH3* expressie door auxine en mechanische stress wordt geïnduceerd, en dezelfde signalen ook leiden tot verhoogde $[Ca^{2+}]_{cyt}$, zou de TCH3-PID interactie een belangrijke signaaltransductiemodule kunnen zijn is bij het sturen van fyllotaxis.

Het in **Hoofdstuk 4** beschreven onderzoek bestudeerde de rol van de AGC3 kinases en hun regulatie door CaMs/CMLs in fyllotaxis. De resultaten laten zien dat omkeerbare PIN1 fosforylatie door deze kinases belangrijk is voor het in stand houden van de spiraalsgewijze fyllotaxis in *Arabidopsis* (spreidingshoek van 137.5°). Vooral PID en WAG2 bleken belangrijk in dit proces, omdat hun verlies-van-functie regelmatig leidde tot een verschuiving van een spiraalsgewijze naar een decussate fyllotaxis (afwisselende spreidingshoeken van 90° en 180°). Regelmatig werd een spreidingshoek van circa 270° gemeten, wat suggereerde dat de ertussen gelegen orgaaninitiatie niet had plaats gevonden. TCH3 overexpressie planten of *tch3* mutante lijnen vertoonden slechts geringe onregelmatigheden in het fyllotaxis patroon, en *TCH3* bleek laag tot niet in het scheut- en bloeimeristeem tot expressie te komen. Echter, met behulp van de *PID::PID-VENUS* reporterlijn kon worden aangetoond dat auxine en mechanische stress leiden tot Ca^{2+}-afhankelijke internalisatie van PID-VENUS in het bloeimeristeem. Een rol van TCH3 in dit proces in onwaarschijnlijk, maar mede gebaseerd op resultaten in Hoofdstuk 3 is mogelijk CML10 of een van de CAMs betrokken zijn bij het moduleren van het fyllotaxispatroon, door PID (en WAG2) van het PM af te halen in respons op verhoogde auxine niveaus of mechanische stress signalen.

Op basis van de in dit proefschrift beschreven functionele analyse van PID en de analyse van de *in vivo* interactie met TCH3 komen we tot een nieuw model, waarin de PID/WAG2-CaM/CML module zowel endogene als externe signalen vertaalt in groei en ontwikkeling van de plant door de subcellulaire lokalisatie van PINs te sturen. Zoals met al het onderzoek blijven er vragen onbeantwoord die verder onderzoek behoeven. Zo blijft het nog steeds wenselijk om middels het creëren van een "untouchable" PID de functie van de PID-CaM/CML interactie verder in kaart te brengen. Mogelijk kan dit bereikt worden door de PM associatie- en CaM/CML bindingsdomeinen verder in kaart te brengen via een "high throughput" aminozuursubstitutie benadering. Een dergelijke studie zal belangrijke nieuwe inzichten opleveren met betrekking tot de capaciteit van planten om hun groei en ontwikkeling aan te passen in respons op zowel interne- als omgevingssignalen.

Curriculum Vitae

Yuanwei Fan was born on January 29th, 1984 in Weifang, Shandong Province, China. In 2002 she completed her high school education at the Weifang No.4 Middle School in Shandong, China. In the same year, she started her BSc studies in Biology Science and was involved as research trainee in ongoing projects under the supervision of Prof. Shupeng Gai. After her graduation in 2006, she started her MSc study with the research project on transformation of *Populus euphratica* in Prof. Huafang Wang's group at the Beijing Forestry University. She obtained her MSc degree in Biochemistry and Molecular Biology in 2009. In October 2009, she started her PhD project on calcium signaling and polar auxin transport in *Arabidopsis thaliana* under supervision of Dr. Remko Offringa and Prof. Paul Hooykaas at Leiden University, The Netherlands.